

**A MACHINE LEARNING APPROACH TO PREDICT THE
MECHANICAL PROPERTIES OF ZEOLITIC IMIDAZOLATE
FRAMEWORKS (ZIFS)**

By

Sarmin Akter Rima

A Thesis Submitted in Partial Fulfillment of the Requirements for the Degree of
Master of Engineering in Bio-Nano Material Science and Engineering

Examination Committee: Dr. Raffaele Ricco (Chairperson)
Dr. Tanujjal Bora
Dr. Chaklam Silpasuwanchai

Nationality: Bangladeshi

Previous Degree: Bachelor of Science in Electrical and
Electronic Engineering in Power
Green University of Bangladesh
Dhaka, Bangladesh

Scholarship Donor: His Majesty the King's Scholarship
(Thailand)

Asian Institute of Technology
School of Engineering and Technology

Thailand

July 2024

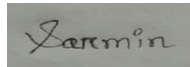
AUTHOR'S DECLARATION

I, Sarmin Akter Rima, declare that the research work carried out for this thesis was by the regulations of the Asian Institute of Technology. The work presented in it is my own and has been generated by me as the result of my original research, and if external sources were used, such sources have been cited. It is original and has not been submitted to any other institution to obtain another degree or qualification. This is a true copy of the thesis, including final revisions.

Date: 19-July-2024

Name: SARMIN AKTER RIMA

Signature:

A rectangular box containing a handwritten signature in cursive script that reads "Sarmin".

ACKNOWLEDGEMENTS

I am very thankful to Dr Raffaele Ricco from the Asian Institute of Technology, Thailand for supervising my thesis and guiding me toward excellence. He has been a great source of inspiration for my core electronics and nanotechnology field. Moreover, a bundle of gratitude to Dr. Tanujjal Bora and Dr Chaklam Silpasuwanchai for being on my thesis committee and for the better selection of courses due to which I was able to grab core knowledge implemented in the thesis.

I would like to acknowledge the generous contribution of the H.M. KINGs scholarship to making my dream come true. AIT offered the best education and opportunities, making it possible to complete my research.

I am grateful to my parents, advisor, and friends for always encouraging me to achieve something bigger.

ABSTRACT

Zeolitic imidazolate frameworks (ZIFs), which are porous crystalline materials composed of metal centers (mostly Zn (II) or Co (II)) and imidazole-based ligands, have garnered significant attention due to their versatile applications in gas separation and catalysis. In this regard, the mechanical properties of ZIFs are relevant to study, to obtain information on their flexibility and the effect on species adsorption and release. Traditional methods for predicting the properties of ZIFs are time-consuming and computationally intensive. This research explores the application of machine learning techniques to predict the mechanical properties of a set of ZIFs with sufficient accuracy and computational efficiency. By leveraging a dataset of ZIF structures and their corresponding mechanical properties, machine learning was trained and used to predict key mechanical attributes such as shear modulus (G) and bulk modulus (K). The results will be used not only to assess the potential of machine learning as a valuable tool for calculating and predicting the mechanical performance of ZIF materials but also to enable the design of novel ZIF-based materials with tailored mechanical characteristics for various applications. This research can offer valuable insights into the synergy between traditional computational chemistry and machine learning, opening new avenues for the efficient exploration and development of ZIFs with desired mechanical properties.

Keywords: ZIFs, Machine learning, Molecular dynamics.

CONTENTS

	Page
AUTHOR'S DECLARATION	ii
ACKNOWLEDGEMENTS	iii
ABSTRACT	iv
LIST OF TABLES	viii
LIST OF FIGURES	ix
LIST OF ABBREVIATIONS	xi
CHAPTER 1 INTRODUCTION	1
1.1 Background of the Study	1
1.2 Statement of the Problem	3
1.3 Objectives of the Study	5
1.4 Scope of the Study	5
1.5 Limitations of the Study	5
1.6 Organizations of the Report	6
CHAPTER 2 LITERATURE REVIEW	7
2.1 Introduction of ZIFs	7
2.2 Topological Equivalents of ZIFs	7
2.3 Correlation Between Mechanical Properties, Porosity, and Bond Structure	10
2.3.1 Bond Structure of ZIFs	11
2.4 Investigating Mechanical Properties of ZIFs	12
2.4.1 Size-Dependent Mechanical Properties	13
2.4.2 Mechanical Instability of ZIFs Due to Pressure	13
2.4.3 Adaptable Force Fields for Structural and Mechanical Properties	14
2.4.4 Mechanically and Chemically Robust ZIF	14
2.4.5 Identical Composition and Distinct Performance ZIF	14
2.4.6 Defects in Crystallization and Their Impact on Mechanical Properties	15
2.4.7 Structural and Mechanical Insights into Zeolitic Metal- Organic Frameworks	15
2.5 Artificial Intelligence Applications in Predicting Mechanical Characteristics	16
2.6 Conclusions and Future Perspectives in ZIF Research	17

CHAPTER 3 METHODOLOGY	18
3.1 Flowchart of Methodology	18
3.2 Specific Mechanical Properties	18
3.3 Collecting Data Through Designed ZIF Structure	22
3.4 Computational Representation	23
3.5 Data Preprocessing	24
3.6 Gradient-Boosting Regression Algorithm (GBR)	26
3.7 Machine Learning Method And GBR Model	27
3.8 Process of Prediction	28
CHAPTER 4 RESULT AND DISCUSSION	30
4.1 Design of MOF	30
4.2 Design of ZIF With Three Metals and Their Composition with Seven Ligands	30
4.2.1 2-Methylimidazole (Hmim) with Zn, Cu, and Co	30
4.2.2 2-Ethylimidazole (EtHim) with Zn, Cu and Co	31
4.2.3 2-Nitroimidazole (NIz) with Zn, Cu and Co	33
4.2.4 2-Methyl-4-nitroimidazole (MNIz) with Zn, Cu and Co	35
4.2.5 Benzimidazole (BIm) with Zn, Cu and Co	37
4.2.6 Imidazole-2-carbaldehyde (IC) with Zn, Cu and Co	39
4.2.7 3-Methyl-1,2,4-triazole (3-MTZ) with Zn, Cu and Co	41
4.3 Model Accuracy	43
4.3.1 Evaluation of RMSE Value for Shear Modulus (G)	44
4.3.2 Evaluation of RMSE Value for Bulk Modulus (K)	48
4.4 Without Validation the Test Data	52
4.5 Model Feature	53
4.5.1 Descriptors And Their Importance to Predict Shear Modulus Accurately	54
4.5.2 Descriptors and Their Importance to Predict Bulk Modulus Accurately	56
4.5.3 Correlation Between K and N–M–N Min in The MD Training Set	57
4.5.4 Correlation Between G and Pore Limiting Diameter in the Data Training Set	58
4.6 Discussion	59

CHAPTER 5 CONCLUSION	61
5.1 Future Suggestion	62
REFERENCES	63
APPENDICES	69
APPENDIX A : SEVEN LIGANDS,THREE TOPOLOGY AND THREE METALS WITH THEIR COMPOSITION	70
APPENDIX B : GITHUB LINK FOR THE MACHINE MODEL	89

LIST OF TABLES

Tables	Page
Table 2.1 DFT Topology Of ZIF-3	8
Table 2.2 CAG Topology Of ZIF-4	9
Table 2.3 SOD Topology Of ZIF-8	10
Table 4.1 Connectivity Of Three Metals with 2-Methylimidazole Ligand	31
Table 4.2 Connectivity Of Three Metals with 2-Ethyl Imidazole Ligand	32
Table 4.3 Connectivity Of Three Metals with 2-Nitroimidazole Ligand	34
Table 4.4 Connectivity Of Three Metals with 2-Methyl-4-Nitroimidazole Ligand	36
Table 4.5 Connectivity Of Three Metals with Benzimidazole Ligand	38
Table 4.6 Connectivity Of Three Metals with Imidazole-2-Carbaldehyde Ligand	40
Table 4.7 Connectivity Of Three Metals with 3-Methyl-1,2,4-Triazole Ligand	42
Table 4.8 Hyperparameters Of The Model	44

LIST OF FIGURES

Figures	Page
Figure 1.1 Contrasted Traditional (Based On Trial-And-Error)And Data-Driven (Based On ML) Approaches To MOF Synthesis	2
Figure 3.1 Methodology Process Map	18
Figure 3.2 Basic Properties of Engineering Materials	19
Figure 3.3 Data Type Process Map	21
Figure 3.4 Crystal Structure Modification Process Flow	22
Figure 3.5 Computational Representation of Crystal Structure And Selective Descriptor	24
Figure 3.6 Data Processing Process Map	25
Figure 3.7 General Schematic of Decision Tree Models	26
Figure 3.8 GBR Model	27
Figure 3.9 Standard Prediction Workflow for AI-Based Methods	28
Figure 4.1 Evaluating GBR Predictions Against Cross-Validated MD Training Data	45
Figure 4.2 Best-Fitted Line for Shear Modulus G (Fold-1)	45
Figure 4.3 Best-Fitted Line for Shear Modulus G (Fold-2)	46
Figure 4.4 Best-Fitted Line for Shear Modulus G (Fold-3)	47
Figure 4.5 Best-Fitted Line for Shear Modulus G (Fold-4)	47
Figure 4.6 Best-Fitted Line for Shear Modulus G (Fold-5)	48
Figure 4.7 Evaluating GBR Predictions Against Cross-Validated MD Training Data for K	48
Figure 4.8 Best-Fitted Line for Bulk Modulus K (Fold-1)	49
Figure 4.9 Best-Fitted Line for Bulk Modulus K (Fold-2)	49

Figure 4.10 Best-Fitted Line for Bulk Modulus K (Fold-3)	50
Figure 4.11 Best-Fitted Line for Bulk Modulus K (Fold-4)	50
Figure 4.12 Best-Fitted Line for Bulk Modulus K (Fold-5)	51
Figure 4.13 Best-Fitted Line of Test Data Set For Shear Modulus (K) For Fold	52
Figure 4.14 Best-Fitted Line of Test Data Set For Shear Modulus (K) For Fold	52
Figure 4.15 Relative Importance of The Descriptors Used To Produce The GBR Model for G	54
Figure 4.16 Relative Importance of The Descriptors Used to Produce The GBR Model For Bulk Modulus (K)	56
Figure 4.17 Correlation Between K And N–M–N Min	58
Figure 4.18 Correlation Between G And Pore Limiting Diameter	58

LIST OF ABBREVIATIONS

MD	= Molecular Dynamics
ML	= Machine Learning
GBR	= Gradient-Boosting Regression
MOFs	= Metal-Organic Frameworks
ZIFs	= Zeolitic Imidazolate Frameworks
DFT	= Density Functional Theory
NMR	= Nuclear Magnetic Resonance

CHAPTER 1

INTRODUCTION

1.1 Background of the Study

Recently, there has been a growing focus on creating new materials with tailored properties for diverse technological applications. Computational research plays a crucial role in examining and comprehending the mechanical characteristics of these materials. Metal-organic frameworks (MOFs), discovered three decades ago, stand out as an exceptional class of materials that have garnered significant attention. MOFs are composed of metal ions or clusters (nodes) that are interconnected with organic molecules (ligands) through self-assembly processes. Zeolitic imidazolate frameworks (ZIFs) are a notable subset of these materials that have sparked considerable interest. ZIFs are a family of metal-organic frameworks composed of imidazole-based organic ligands and zinc tetrahedra, which result in the formation of porous frameworks that mimic the topology of zeolites (Bennett et al., 2010). ZIFs have a unique structure that combines the properties of zeolites and MOFs, including high surface area, high crystallinity, and unimodal micropores (M. R. Ryder & Tan, 2016a).

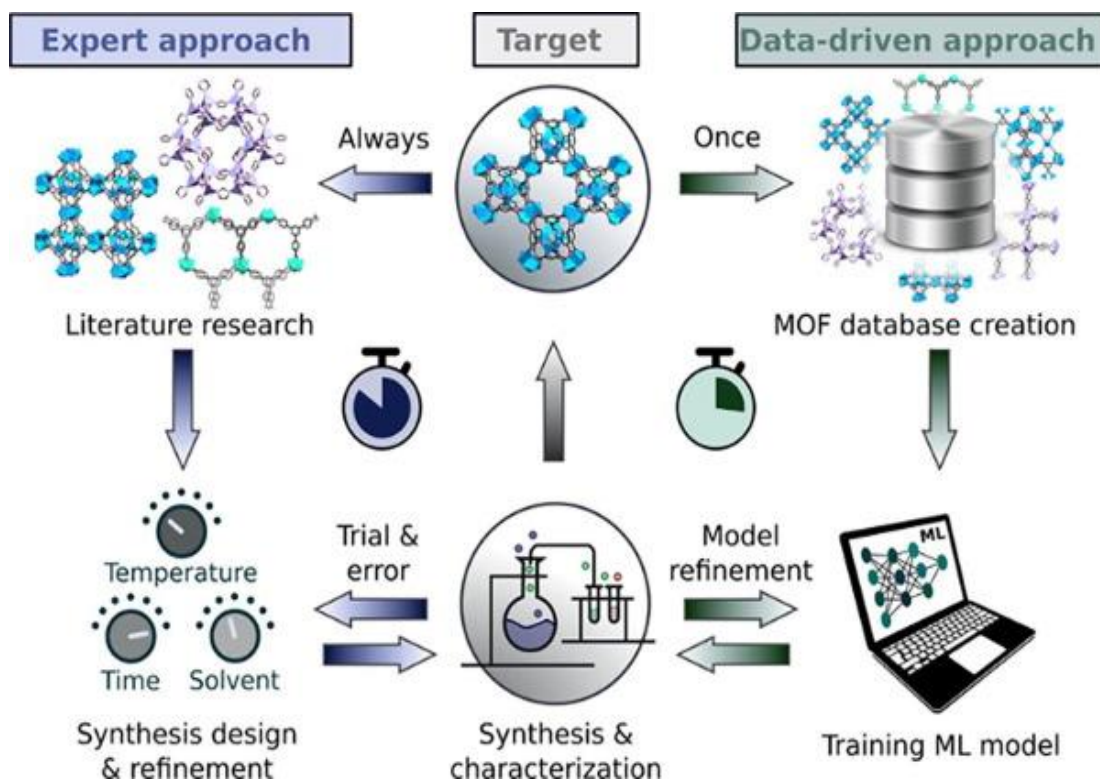
Understanding ZIFs mechanical characteristics is essential for assessing their suitability in real applications. These properties encompass elastic moduli, hardness, fracture toughness, and resistance to deformation under varying conditions. (Burtch et al., 2018) An inclusive investigation of the mechanical behavior of ZIFs can offer insights into their structural integrity, stability, and robustness during industrial processes or environmental changes (Gao et al., 2017).

Due to the need for precise information about structural stability during material use, many studies are currently focused on the mechanical properties of MOFs. Although experimental studies of ZIFs' mechanical properties offer useful information, they are frequently hindered by issues like sample availability and the difficulties of carrying out experiments under adverse circumstances. Computational simulations, specifically molecular dynamics (MD) and density functional theory (DFT), offer a complementary approach to elucidating the mechanical behavior of ZIFs (Zheng et al., 2012). The timeline of major milestones in computational Metal-Organic Framework (MOF) research has witnessed a fascinating evolution over the years. In the early 2000s,

computational techniques began to gain traction in MOF research, aiding in the prediction of MOF structures and properties.

Figure 1.1

Contrasted Traditional (Based on Trial-and-Error) and Data-Driven (Based on ML) Approaches to MOF Synthesis.



By the mid-2000s, density functional theory (DFT) advancements allowed for more accurate calculations of MOF properties, such as adsorption capacities and mechanical stability. The 2010s marked a significant turning point, with the development of high-throughput screening methods, enabling the rapid discovery of novel MOFs with tailored properties. In recent years, machine learning and artificial intelligence have been integrated into MOF research, accelerating materials discovery and property prediction. Today, computational MOF research continues to expand its horizons, with the promise of designing custom-made MOFs for various applications, from gas storage and separation to catalysis and drug delivery. This timeline underscores the transformative role of computational tools in advancing our understanding and utilization of MOFs as versatile materials.

1.2 Statement of the Problem

With the increasing demand for materials, there has been a significant focus on enhancing material properties to ensure their suitability across various applications. This has led to extensive research into improving the mechanical and electronic properties of ceramics, as they have garnered considerable attention for their potential benefits. Precisely forecasting the mechanical properties of materials, such as strength, stiffness, elasticity, plasticity, ductility, brittleness, toughness, and hardness, is crucial for their effective use in diverse engineering disciplines. (Song, Wang, Liu, Yin, & Long, 2023). Traditionally, the assessment of materials' mechanical properties has depended on extensive and costly experimental procedures, including tensile, compression, and impact tests. However, these experiments are time-intensive, expensive due to the necessary equipment, and susceptible to errors caused by testing inaccuracies, equipment malfunctions, or inconsistencies among different manufacturers.(Yu et al., 2021).

This paper (H. Li et al., 2023) used solvent synthesis method where the method requires the use of CO₂, which may contribute to greenhouse gas emissions if not properly managed as well as the method relies on the use of ZnO instead of Zn(NO₃)₂, which may limit the applicability of the method to specific ZIFs synthesis. The procedural steps necessitate the application of either heat or vacuum procedures to facilitate the removal of CO₂, thereby potentially introducing supplementary energy consumption to the overall process. Furthermore, the method's feasibility for mass production may necessitate the deployment of specialized equipment or adherence to specific operational conditions, thereby potentially constraining its accessibility and implementation for smaller-scale operations.

The conventional approaches involve the washing of filter cake, which can be time-consuming and inefficient(M. Li et al., 2022). Additionally, these methods may not be environmentally friendly as they rely on the use of solvents that can be harmful to both the environment and human health(Pérez-Miana et al., 2021). Furthermore, the traditional methods may not be cost-effective for large-scale production of ZIFs(Yin et al., 2015). Near-field infrared nano-spectroscopy and density function theory calculations are used to examine local defects, such as missing ligands or metal vacancies, in ZIF-8 nano- and micro-crystals(Fan et al., 2023) which is costly.

The mechanical properties optimization of ZIF using solvothermal and solution techniques has been proven for ZIF-8 that shrinking crystals to nanoscale dimensions causes a 40% decrease in crystal stiffness, which could be utilized to explain previously documented variations in gas adsorption that are size-dependent.(A. Tiba et al., 2019).The Rietveld technique was employed to enhance the mechanical characteristics of ZIF. A solvothermal method employing methanol or dimethylformamide (DMF) as solvents was utilized to synthesize the cobalt 2-methyl imidazolate framework (ZIF-67) with an SOD topology, resulting in a yield of 2.5 grams of the material.(Ethiraj et al., 2020).

Research on amorphous ZIFs is limited due to nanoindentation testing providing only isotropic mechanical properties (Tan & Cheetham, 2011). This restricts the ability to fully understand the anisotropic mechanical behavior of amorphous ZIFs. The symmetry of metal nodes in amorphous ZIFs is difficult to explore and identify using experimental techniques. Utilizing high-field nuclear magnetic resonance (NMR) can provide insights into the microstructural characterization, but this is still a challenging task. Structural order and complexity: The intricate nature and uncertain configuration of chemical bonds in non-crystalline ZIF formulations present heightened difficulties for theoretical simulations. Accurately depicting the structural development of ZIF glasses necessitates employing ab initio molecular dynamics or reactive force field dynamics to simulate melt-quenched ZIF glasses.(Shi et al., 2023).

There is a noticeable absence of systematic comparisons and evaluations of classical force fields in addressing the guess of mechanical properties. (Acuna-Yeomans et al., 2023).Studying the mechanical properties of MOFs is challenging due to the vast structural diversity, batch-to-batch variance, and the need for advanced techniques. Computational simulations are essential for studying these properties.(Redfern & Farha, 2019). Modifying the primary network of ZIF-4 by adding extra ligands is challenging but possible with computational study.(Moosavi et al., 2018).

A time- and money-efficient technique to study and evaluate complex structures and phenomena is through computational investigations. Investigation of traits and behaviors that may be challenging or impossible to see experimentally can be done using computational studies. The atomic structure and mechanical characteristics of materials under various situations, such as high pressure, can be gleaned from

computational analyses. The design of novel materials with particular and adjustable physical properties is made possible by the application of computational research to anticipate and optimize the properties of materials.

1.3 Objectives of the Study

Understanding the mechanical properties of ZIF is crucial for harnessing their full potential and for the development of novel materials with tailored mechanical characteristics. The objective of the study is to optimize the topology, bond length, and angle between the node and ligand of ZIFs changing the ligands a mechanism using an MD-based FORCITE module. After collecting the required data of the new composition process the data as a descriptor to train an ML model so that mechanical properties of the new ZIF can be predicted by the machine. The specific objectives are as follows:

1. Designed crystal structure and optimized the structure to evaluate the crystal elastic constants to find out the mechanical properties, specially, the shear modulus and bulk modulus.
2. Feed data into the machine model to train the model and predict the mechanical properties of ZIF.

1.4 Scope of the Study

For improving the mechanical characteristics of materials, machine learning offers a number of advantages. First of all, it enables the identification of new materials with improved properties by allowing researchers to analyze vast amounts of material data gathered through simulations and tests. Additionally, machine learning is suited for comprehending the physics behind materials processing and behavior since it can model complicated non-linear interactions and behaviors. Additionally, it makes it easier to construct data-driven techniques for identifying trends and structure-property connections across a range of length and time scales. Additionally, machine learning can forecast material characteristics including tensile strength, fatigue behavior, and viscoelastic research, obviating the need for time-consuming and expensive testing.

1.5 Limitations of the Study

1. Small data sets may degrade the machine model accuracy.
2. Studying the anisotropy of elastic properties or directional characteristics like Young's modulus and Poisson's ratio can be effectively predicted via

simulation, whereas achieving the same through machine learning poses significant challenges.

1.6 Organizations of the Report

This thesis comprises five chapters organized as outlined below:

Chapter 1: The first chapter covers the study's background, problem statement, objectives, scope, thesis limitations, and organizational structure.

Chapter 2: Various literature was reviewed in this chapter to gain knowledge of data collection and how to process them for train the machine model as well as for better understanding the effect of changes between the ligand bond length, angle, ZIF topology, and geometry.

Chapter 3: Represent the computational mechanism and method for collecting data and elaborated discussion on the preprocessing of data. Machine model algorithm also discussed on which the model will be train and test.

Chapter 4: This chapter provides a comprehensive overview of the results and discussion achieved from the molecular dynamics simulation and machine model.

Chapter 5: The application and potentials of machine learning are discussed in this chapter and possible future work is also suggested.

CHAPTER 2

LITERATURE REVIEW

2.1 Introduction of ZIFs

Metal-organic frameworks (MOFs) are formed by the self-assembly of metal ion nodes bridged by coordination bonds to multidentate ligands. Tetrahedrally-coordinated metal cations linked by imidazolate organic ligands create a structurally distinctive family of MOFs (Furukawa et al., 2013) known as zeolitic imidazolate frameworks (ZIFs), which come together to form porous crystalline solids (Y. Q. Tian et al., 2007). Similar to the connection of silicon and oxygen in zeolites, they take on porous crystalline structures made of metal ions and organic ligands. In particular, at the M-Im-M center [typically M= Zn (II) or Co (II)], tetrahedral metal centers subtend a 145° angle that is exclusively coordinated by nitrogen atoms in the 1,3-positions of the imidazolate bridging ligand (Im =C₃N₂H₃). Because of their ability to adapt synthetically, a wide range of structures can be synthesized by combining metal nodes with organic ligands in numerous combinations. Their adaptability enables them to be used in numerous industrially significant applications, including gas separation(W. Wang & Yuan, 2014)(Zhang et al., 2013) and storage(Wu et al., 2007), catalysis(Gascon et al., 2014), drug delivery(Miller et al., 2010) and sensors(Chen et al., 2018).

2.2 Topological Equivalents of ZIFs

Computational analysis has played a crucial role in comprehending the mechanisms and consequences of high pressure on MOFs, complementing experimental research efforts. Ryder and Tan aimed to determine how topology affected a set of MOFs with the same chemical composition's mechanical characteristics. The extraordinarily low shear and Young's moduli of ZIF-3 [Zn(imidazolate)₂] showed in their discoveries can significantly influence the stability of MOFs due to the spatial orientation of nodes and ligands.

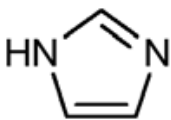
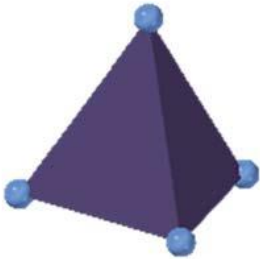
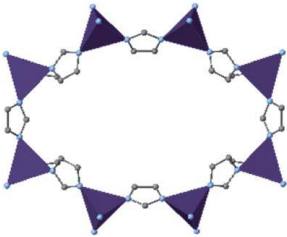
The bond structure of ZIF-1, which has a network topology called CRB and an orthorhombic crystal symmetry, plays a crucial role in determining its porosity. Different modifications to the bond structure can lead to changes in the adsorptive properties and mechanical properties of ZIFs. This is significant for applications like

gas storage or encapsulation of guests. Furthermore, although ZIF-1 has the same chemical composition as ZIF-2 and ZIF-4, the way it is packed affects its porosity. The storage behavior of ZIF-1 as anode materials for lithium-ion batteries can also be influenced by the bond structure, with ZIFs containing more vertexes and edges exhibiting superior electrochemical performance.

Researchers have discovered that ZIF-3 exhibits a negative Poisson's ratio, which gives it its unique auxetic behavior. This is due to its distinct DFT network topology, which contributes to its mechanical properties. ZIF-3 has a low shear resistance ($G_{\min} = 0.1$ GPa) compared to other frameworks and is extremely prone to shear strain, making it more anisotropic. The presence of 8-membered rings (8MRs) in ZIF-3 is believed to play a role in its mechanical response. However, ZIF-3's structural shear instability, characterized by easy plane slippage, may limit its form to powder and hinder the growth of sizable crystals. Furthermore, different modifications to the bond structure can lead to changes in the mechanical properties, adsorptive properties, and electrochemical performance of ZIFs. Additionally, the storage behavior of ZIFs as anode materials for lithium-ion batteries can also be influenced by the bond structure, with ZIFs containing more vertexes and edges exhibiting superior electrochemical performance. (M. R. Ryder & Tan, 2016b).

Table 2.1

DFT Topology of ZIF-3

MOF	Organic linker	Inorganic node	Structure	Topology
ZIF-3				DFT

The mechanical properties of ZIF-4 are intrinsically related to its framework bonding topology. The unique DIA network of ZIF-4 results in a robust and mechanically stable framework due to the spatial configuration of its constituent nodes and ligands. This

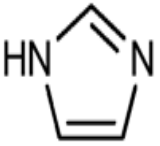
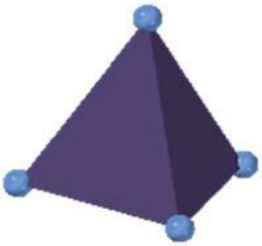
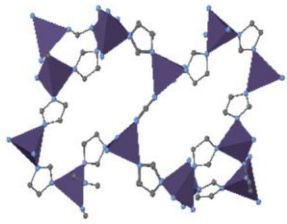
topology, dominated by bond bending rather than bond stretching, contributes to the distinctive mechanical resilience of ZIF-4.

The cohesive interactions in the ZIF-4 framework, particularly the durable bonds among the metal center and the organic ligands, provide mechanical robustness to the material. These bonds form a three-dimensional framework, which gives rise to unique mechanical attributes. The high shear modulus of ZIF-4, for instance, is a result of its CAG topology and the associated strong bond interactions within the network.

Further, the isostructural nature of the ZIF-4 framework, wherein the structure remains unchanged under various chemical compositions, provides evidence of the link between framework bonding topology and mechanical performance. By selecting different organic ligands and metal ions, the mechanical characteristics of ZIF-4 can be adjusted while preserving its fundamental topological structure. In essence, the mechanical properties of ZIF-4 are intricately linked to its framework bonding topology. By understanding this relationship, one could potentially manipulate the mechanical performance of ZIF-4 and other similar MOFs through careful control of their synthesis and design (Moosavi et al., 2018).

Table 2.2

CAG Topology of ZIF-4

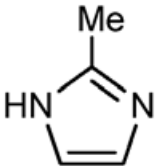
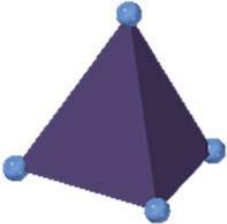
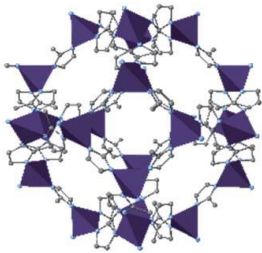
MOF	Organic linker	Inorganic node	Structure	Topology
ZIF-4				CAG

ZIF-8, a zeolitic imidazolate framework (ZIFs), stands out for its cubic symmetry and impressive porosity, characterized by Zn (II) ions coordinated with 2-methylimidazolate (mIm) ligands. This framework's network topology aligns with the zeolite net known as gmelinite (GME), contributing to its structural stability. ZIF-8's high porosity is particularly noteworthy, providing it with a substantial surface area for

various applications. When considering its mechanical properties, ZIF-8 exhibits an elastic modulus ranging from 2.973 to 3.199 GPa and a hardness ranging from 0.501 to 0.531 GPa, indicative of its mechanical robustness. When compared to existing metal-organic frameworks (MOFs), like MOF-5, ZIF-8 exhibits better mechanical properties. The interplay between structure and mechanical properties is underscored, with the framework density and porosity emerging as influential factors in determining the mechanical characteristics of ZIFs, including ZIF-8. Furthermore, the study highlights the role of the rigidity and bulkiness of organic linkages in substituted imidazolate frameworks as additional contributors to their mechanical behavior, providing insights that are vital for tailoring these materials for specific applications.(Tan et al., 2010).

Table 2.3

SOD Topology of ZIF-8

MOF	Organic linker	Inorganic node	Structure	Topology
ZIF-8				SOD

Also, several studies give information about chemical structure and the physical data which helps to conduct the computational study that play a vital role to design a functional material.

2.3 Correlation Between Mechanical Properties, Porosity, and Bond Structure

Understanding the correlation between the bond structure, porosity, and mechanical properties of zeolitic imidazolate frameworks is essential for the design and development of efficient and functional materials. Several studies have focused on investigating the bond structure of ZIFs and its influence on their porosity and mechanical properties. This research(Tan et al., 2010) demonstrates a strong correlation among the elastic properties of ZIF crystal structures and the framework density and porosity.

The elastic behavior of ZIFs is directly related to their mechanical characteristics, showing a strong association with the density and porosity of the framework. As a result, ZIFs have elastic moduli values ranging from 3 to 10 GPa and hardness values ranging from 300 MPa to 1.1 GPa. In particular, ZIFs show superior mechanical properties over other metal-organic frameworks (MOFs), including MOF-5. The bulkiness and rigidity of the substituted organic links, which can be tailored for particular purposes, play a key role in the elastic properties of substituted imidazolate frameworks. Additionally, the complex pore morphology and general framework topology of ZIFs may introduce mechanical anisotropy, which will affect their adaptability and mechanical characteristics. Local order, which includes bond lengths and bond angles, within amorphous ZIFs further shapes this adaptability.

Amorphous zeolite imidazolate frameworks (a-ZIFs) and their topological counterparts are studied in (Shi et al., 2023) for their bond structure, porosity, and mechanical characteristics. The study explores how short-range and mid-range local order impact the mechanical properties of a-ZIFs. The porosity of a-ZIFs can be altered, resulting in differences in Young's modulus and shear modulus. Various metal nodes can be combined with organic ligands to achieve this. The document emphasizes the relationship between structural order and mechanical properties of a-ZIFs. The local structures of various a-ZIF compositions are also compared, and their effects on the mechanical characteristics are discussed. The a-ZIFs' porosity structures are also studied, demonstrating variations in the ability of the pores to hold gas molecules.

2.3.1 Bond Structure of ZIFs

In recent years, ZIFs have arisen as an innovative subclass of MOF materials with unique structural and physicochemical properties. The bond structure of ZIFs plays a crucial role in determining their properties. There are several options for separation because of ZIFs' high structural diversity.

ZIFs can change the spatial rearrangement of the construction basis (such as the Zn-MeIm-Zn angle or network topology) (Liu et al., 2018) (Widmer et al., 2019) to exhibit amusing polymorphism for a specific chemical formula, in addition to changing the configuration of metals or ligands (Lu et al., 2014; Ban et al., 2016).

By manipulating the bond structure of ZIFs, their mechanical, adsorptive, and electrochemical performance can be effectively altered and optimized according to specific applications and requirements. In addition, a stiffer framework may arise from the inclusion of additional groups that reinforce the ZnN₄ tetrahedron (Zheng et al., 2017). The storage behavior of ZIFs as anode materials for lithium-ion batteries can also be influenced by the bond structure, with ZIFs containing more vertexes and edges exhibiting superior electrochemical performance (H. Wang et al., 2020). Moreover, the CO₂ uptake capacity of ZIFs can be enhanced by tuning the bond structure, such as varying the Co/Zn ratio in bimetallic Co-Zn ZIFs (Imawaka et al., 2019). Overall, the bond structure of ZIFs plays a critical role in determining their mechanical, adsorptive, and electrochemical properties. (H. Baur & X. Fischer, 2019)

In this extensive study, an analysis encompassing more than 7000 crystal structures of zeolites focused on critical parameters such as bond lengths (T–O, where T represents Si, Al, P, Zn, Be, Ge, B, As, Ga, Co) and the flexibility of bond angles (O–T–O). The average tetrahedral bond lengths were found to be 1.603(11) Å for Si–O, 1.736(8) Å for Al–O, and 1.522(9) Å for P–O, showing slight variations of approximately 0.07 Å across the studied samples. Remarkably, the study uncovered distinct differences in bond lengths between zeolites and non-zeolitic compounds, emphasizing that T–O distances exhibit variability across different inorganic compounds. This variance in bond lengths was attributed to diverse atomic displacement parameters of oxygen atoms within distinct zeolite framework types, indicating that mean bond lengths are inherently characteristic of specific framework configurations. Additionally, the research unveiled that O–T–O angles in zeolites ranged from 94.5° to 129.1°, centered around the tetrahedral angle of 109.5°, with larger deviations observed for tetrahedra featuring longer mean T–O distances. Notably, bond lengths in zeolites were consistently shorter compared to those in non-framework compounds, with differences ranging from 0.014 Å to 0.031 Å, underscoring the unique structural attributes of zeolitic materials.

2.4 Investigating Mechanical Properties of ZIFs

The bulk and elastic moduli of ZIFs have been experimentally determined with great effort. (Su et al., 2015);(Bennett et al., 2016);(Bennett et al., 2015). Nevertheless, the small number of reports represent that it is much more challenging to experimentally

determine the corresponding shear modulus(Tan et al., 2012) .Hence, the theoretical computation of the mechanical properties of ZIFs has become an imperative substitute (Tan et al., 2015)(Ortiz et al., 2013)even though it remains challenging to gain precise values over computational methods(M. R. Ryder et al., 2016) .Until now an assessment of the mechanical modulus values attained for different ZIFs might yield significant insights. Tan et al. carried out single-crystal nanoindentation experiments as part of a study on the mechanical stability of ZIFs (Gómez-Gualdrón et al., 2016). The stiffness and bulkiness of the substituted imidazolate ligands were discovered to be the primary determinants of ZIFs' mechanical properties, which they found to be superior to those of other MOFs.

2.4.1 Size-Dependent Mechanical Properties

ZIF-8 crystals of various sizes were subjected to atomic force microscopy (AFM) nanoindentation to evaluate their mechanical characteristics. Smaller crystals of ZIF-8 have more flexible and less rigid mechanical characteristics than larger crystals. Crystal downsizing, which can be regulated by changing the synthesis conditions, can make ZIF-8 more flexible. Defects and impurities in the crystal structure have an impact on ZIF-8's mechanical properties. By understanding the size-dependent mechanical properties of MOFs, researchers can design materials with specific and tunable physical properties.(A. Tiba et al., 2019).

2.4.2 Mechanical Instability of ZIFs Due to Pressure

First molecular dynamics study on the softening under the shear mode of the mechanical instability responsible for the pressure-induced amorphization of the ZIF-8. As the study reports, the presence of the shearing mode is the reason that ZIF-8 starts to turn from crystal to amorphous under the compression leading to the loss of mechanical stability. Based on the lack of evidence for amorphization upon heating of ZIF-8, this further accounts for why no softening was detected with an increase in temperature in this study. It was discovered that having adsorbate in the pores made the framework more shear stable, which in turn affected how compressible and mechanically stable it was. It was found that the crystalline porous ZIF phases to maintain the zeolite-like framework topologies are mechanically unstable due to the weak Zn-imidazolate coordinative bonds in contrast to the stabilizing Si-O link in zeolites. The very high porosity leads to low shear resistance, which uniquely causes

the low-pressure shear softening and leads to the third effect i.e., the mechanical instability at low pressure.(Ortiz et al., 2013).

2.4.3 Adaptable Force Fields for Structural and Mechanical Properties

The article investigates five established flexible force fields for ZIF-8 through molecular dynamics simulations in the isothermal-isobaric ensemble. The authors analyze the relationship between elastic constants at 0 K and how they vary with temperature and pressure with the lattice parameters of the framework. They compare their findings with current experimental data and quantum-mechanical simulations to elucidate the relationship between structural and elastic properties under the chosen parameterization. In conclusion, the article offers useful perspectives on the mechanical stability of MOFs and the importance of elastic constants in defining their structural stability in this Esteemed Contribution.(Acuna-Yeomans et al., 2023).

2.4.4 Mechanically and Chemically Robust ZIF

The experiment, involving a simple synthetic procedure and without the need of binders or high pressure, matched ZIF-8 to develop big, crystalline rigid monolithic structures. The elasticity of these structures is at least two orders of magnitude larger compared to the material's single crystals, while they preserve the outstanding and ultra-porous architectural space of ZIF-8 without destroying the micropore system. It additionally emerges that the volumetric adsorption capacity is more than twice the single crystal's predicted value, whereas the bulk solidities and volumetric BET areas are three times larger than those measured on the partially deactivated powder material. The article states that these findings have a dramatic impact in the quest for potential practical applications of ZIFs and MOF for gas adsorption, separation, and catalysis and that being able to shape ZIFs and MOFs is essential to reduce to a minimum the pressure drops of an incoming gas flow in columns due to the powders' dispersion.(T. Tian et al., 2015).

2.4.5 Identical Composition and Distinct Performance ZIF

The paper offers insightful knowledge into how ZIFs' chemical structure influences their olefin/paraffin adsorption behavior and could contribute to the development of nano-porous materials that have improved separation abilities. The study investigates the effects of ZIF-8 polymorph structures on ethane and ethene adsorption and

separation. From large Monte Carlo and ideal adsorbed solution theory simulations, the authors investigate the adsorption of the two molecules of ethane and ethene to several different types of ZIF-8 polymorphs, finding that the ethane or ethene adsorption behavior is very much dependent on the geometric characteristics of ZIF-8 polymorphs, and that adsorption mechanism may be fundamentally different under extreme pressure and near to the ground pressure. They find that high-pressure uptake depends closely on geometrical features (e.g., porosity or surface area) of the ZIFs, whereas low-pressure uptake depends more directly upon ZIF-gas interaction. Along similar lines, the authors also compared the adsorption and separation of ethane/ethene and propane/propene.(Ke et al., 2021).

2.4.6 Defects in Crystallization and Their Impact on Mechanical Properties

The direct investigation of local flaws in ZIF-8 nano- and microcrystals and their impact on Young's modulus are covered in this article. The authors discovered that defects degrade the stability of the material by introducing local disorder into the otherwise highly structured 3-D framework, though their effects on the material properties may go even further. It was discovered that the mechanical characteristics of ZIF-8 considerably changed in the presence of flaws, with a reduced stiffness and a higher local anisotropy. The authors conclude that creating and improving ZIF-8-based materials requires an understanding of the link between flaws and their effect on material performance.(Möslein et al., n.d.).

2.4.7 Structural and Mechanical Insights into Zeolitic Metal-Organic Frameworks

In this study, the authors explore the extensive elastic properties of ZIFs using density functional theory (DFT) calculations, providing a surprising insight into their mechanical behavior. Notably, their investigation reveals fascinating traits in particular ZIF variations. For instance, ZIF-3 stands out due to its extraordinarily low shear resistance and even negative Poisson's ratio, which indicate the existence of a flexible mechanism behind auxetic activity. Furthermore, for particular crystal orientations, ZIF-1, ZIF-2, and ZIF-4 show an intriguing phenomenon where they can display practically zero Poisson's ratios, resembling a "cork-like" characteristic that reduces lateral deformation under axial strain. The research also demonstrates the anisotropic mechanical response of ZIFs and demonstrates the axially dependent Young's and shear moduli characteristics. The research explores MOF mechanics and goes beyond these

elastic qualities to shed information on behaviors that exceed the elastic limit. This covers intermolecular rupture, fundamental yielding, irreversible plastic deformation, and cracking, and it offers essential insights into the mechanical behavior of MOFs. The study adds a great understanding of MOF mechanics by highlighting how crucial it is to take into account the mechanical and physical characteristics of MOFs in the context of practical applications.(M. Ryder & Tan, 2015).

2.5 Artificial Intelligence Applications in Predicting Mechanical Characteristics

In the field of AI-based prediction of mechanical properties of ZIFs, researchers have explored various algorithms and techniques. Studies have investigated the use of a combination of biologically inspired evolutionary algorithms and machine learning to tailor ZIFs for specific diffusivities, demonstrating the potential of AI in material design. Additionally, studies have compared various AI techniques—including linear regression, support vector regularized linear regression, support vector regression, multi-layer neural networks, random forest regression, and gradient boosting regression—to predict the mechanical properties of sheet metal during stamping processes, aiming to enhance predictive accuracy (Castel & Coudert, n.d.). Moreover, it has been demonstrated that alterations to ZIFs through terminal group substitutions greatly affect mechanical modulus; electron-withdrawing groups enhance stiffness, and charge distribution analyses explain the mechanism underlying the variations in elastic stiffness (Krokidas et al., n.d.).

(Verpoort et al., 2018) The paper presents an artificial neural network that models and validates material properties using composition-property and property-property correlations. It demonstrates the ability to handle incomplete data sets and treat graphical data as a unified entity. The framework has been tested and applied to case studies involving alloys and polymers, identifying twenty errors within a commercial materials database. The paper emphasizes the effectiveness of machine learning techniques in predicting previously unseen materials.

Machine learning offers a more accurate prediction of zeolite elastic behavior than traditional force field approaches. This approach extracts geometric features such as local geometry, porosity, and structural composition of zeolitic materials. The model reveals correlations between the elastic moduli of zeolite framework properties and

offers mechanistic insights into porous crystalline materials. Through the prediction of elastic response over a variety of theoretical zeolitic topologies, the approach exposes stability tendencies in porous materials. Analysis of the bulk and shear moduli distribution indicates that some hypothetical structures show reduced stiffness and shear resistance in comparison to existing zeolite frameworks.(D. Evans & Coudert, 2017).

2.6 Conclusions and Future Perspectives in ZIF Research

In conclusion, the bond structure, porosity, and mechanical properties of Zeolitic Imidazolate Frameworks are closely interconnected and play a crucial role in determining the overall performance and functionality of these materials. Large-scale ab initio calculations and machine learning have provided valuable insights into these properties, revealing the influence of bond structure on porosity, mechanical modulus, and adsorption properties.

However, it is important to note that although large-scale ab initio calculations have provided significant insights, further experimental studies are necessary to validate and confirm these findings to get good accuracy from the machine model. Additionally, more research is needed to explore the influence of different ligands and metal centers on the bond structure, porosity, and mechanical properties of ZIFs to make a large database. Furthermore, the development of new machine model algorithms and simulation techniques will enhance understanding of these materials and facilitate the design of ZIFs with tailored properties. Moreover, the application of ZIFs in various fields, such as gas adsorption, separation, catalysis, and electronics, highlights the need for further research in optimizing the bond structure, porosity, and mechanical properties to meet specific application requirements. Zeolitic Imidazolate Frameworks are at the forefront of scientific research and findings in this field.

CHAPTER 3

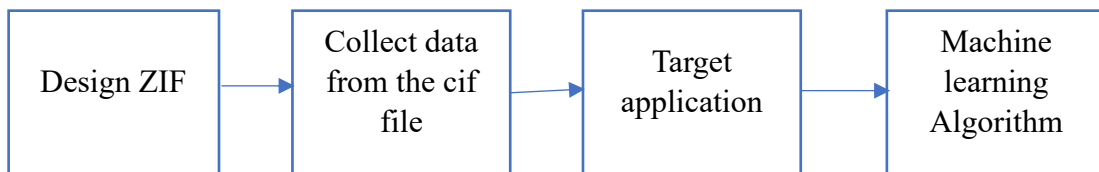
METHODOLOGY

The development of new materials through experimental methods alone is both costly and time-consuming, often requiring several years. However, advancements in the predictive capabilities of computer simulations have significantly expedited the material design and development process. The determination of mechanical properties is critical for the application of composite materials in various engineering disciplines. Recently, there has been considerable interest in utilizing artificial intelligence, particularly machine learning and deep learning, to accurately predict the mechanical properties of composite materials. This study demonstrates how machine learning, supported by multi-level simulations, can effectively predict the performance of Zeolite Imidazole Frameworks (ZIFs), representing a significant advancement in the field of porous materials science.

3.1 Flowchart of Methodology

Figure 3.1

Methodology Process Map

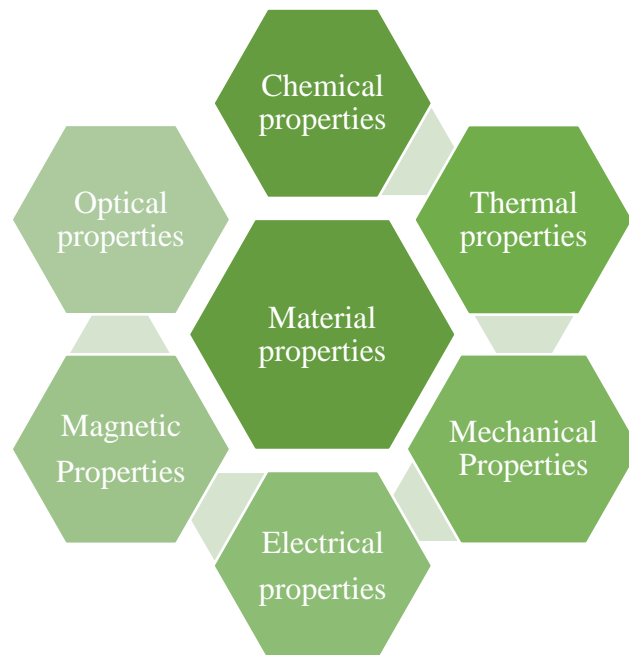


3.2 Specific Mechanical Properties

Scientists and engineers working with materials are constantly trying to get better at understanding what makes materials behave the way they do. They want to be able to predict how a material will perform and even improve its properties for specific uses. These properties cover a wide range, as shown in Figure 1, including how a material reacts to chemicals, heat, force, electricity, light, and magnetism. But especially important is being able to predict how a material will handle physical stress and strain. This includes things like strength, flexibility, and how easily it breaks. Knowing these properties is crucial for engineers to choose the right material for different projects (Song et al., 2023).

Figure 3.2

Basic Properties of Engineering Materials.



Elastic constants are fundamental parameters in material science and mechanics that describe a material's response to mechanical deformation. These constants provide essential information about a material's stiffness, strength, and ability to return to its original shape after deformation. They play a crucial role in understanding a material's behavior under various conditions and are vital for designing and analyzing structures and components in engineering and science.

There are several elastic constants, but the most common ones include:

Young's Modulus (E):

A measure of a material's resistance to elastic deformation, which refers to the temporary change in shape of a material when subjected to tensile or compressive loads known as Young's modulus. A higher value indicates stiffer material, as it requires more force to stretch or compress. This property is specific to each material and is crucial for engineers and designers when selecting materials for specific applications, such as structural components or flexible components.

Shear Modulus (G or μ):

Shear Modulus is a physical property of a material that describes its resistance to shear deformation or distortion. It is also known as the Modulus of Rigidity or the Elastic Shear Modulus. It is represented by the symbol G or μ (mu) and is measured in units of pressure like Pascals (Pa) or pounds per square inch (psi). The Shear Modulus is crucial for understanding how a material responds to shear forces, such as torsion or external stress. Materials with higher Shear Moduli are stronger and more rigid.

Bulk Modulus (K):

The Bulk Modulus (K) is a physical property of a material that measures its resistance to changes in volume under hydrostatic pressure. It measures the amount of pressure needed to compress a material by a certain amount. High Bulk Modulus materials are more resistant to compression and require more pressure, while low-modulus materials are easier to compress. Measured in pressure units like Pascals or psi, it is used in fields like materials science, engineering, and geology to understand material behavior under different conditions.

Poisson's Ratio (ν):

Poisson's Ratio is a material property that describes how a material deforms under stress. It is a dimensionless quantity that relates the lateral contraction of a material to its longitudinal extension under axial loading. It is defined as the negative ratio of transverse strain to longitudinal strain in a material under uniaxial stress. A value between 0 and 0.5 indicates incompressibility, while a negative value indicates expansion. Poisson's Ratio helps predict material behavior under different stress types and determines the elastic modulus, also known as Hooke's Law. (Burtch et al., 2018)

Elastic constants are parameters that describe a material's response to stress and strain. They are used by engineers and material scientists to select materials for specific applications. Researchers use elastic constants to study materials' properties, developing innovative materials with specific mechanical properties.

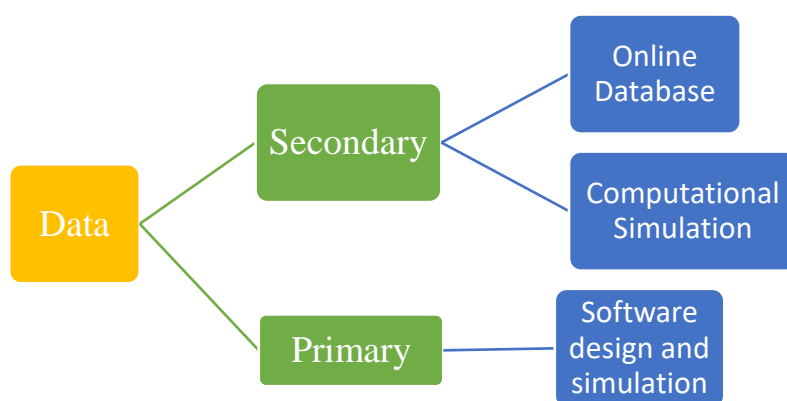
In the realm of material science, ZIFs have garnered significant interest due to their unique properties. However, accurately predicting their mechanical behavior, specifically their bulk and shear modulus, remains a challenge. To address this, researchers are focusing on building robust datasets that leverage quantitative data.

Larger data creation for MOFs would necessitate additional simulations, which would be computationally expensive(Lyu et al., 2020)(Jablonka et al., 2020). Quantitative structure-property relationships (QSPR) are a time-efficient and alternative method of correlating different chemical and structural attributes with a given performance parameter. By examining 137,953 hMOF (Fernandez et al., 2013), presented one of the earliest QSPR investigations and looked at how MOF structural characteristics affected their ability to store CH₄. They demonstrated how highly accurate it is to develop various regression models based on data from less than 10% of the available hMOFs to forecast CH₄ uptake for the remaining material set.

The approach involves meticulously collecting data on the composition, structure, and density of various ZIFs. This data can be obtained through a combination of experimental techniques like X-ray diffraction and gas sorption measurements. Additionally, computational simulations can be employed to calculate theoretical values for these properties. Together, this comprehensive dataset encompassing composition, structure, and density serves as a strong foundation for predicting the mechanical response of ZIFs.

Figure 3.3

Data Type Process Map



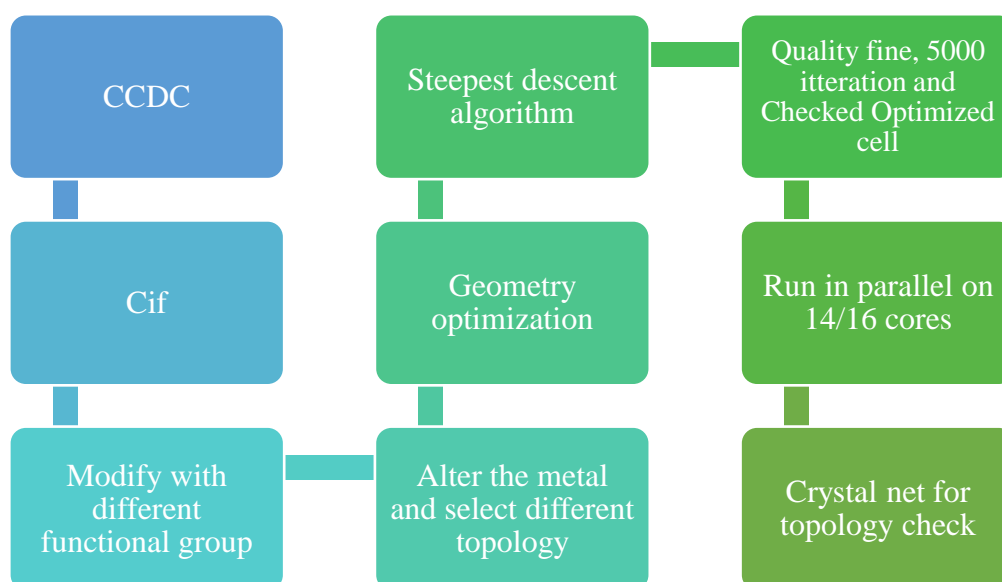
Furthermore, the dataset is enriched by incorporating information on the mechanical properties themselves. This can involve measuring the bulk and shear modulus of various ZIF samples using a machine-learning model. By incorporating these computationally determined values, the dataset becomes even more powerful for establishing predictive models. With a robust dataset that combines structural, local and porosity-related descriptor researchers utilized machine learning algorithms to identify patterns and relationships between the ZIF's properties and its bulk and shear modulus. This paves the way for more accurate predictions of these crucial mechanical properties for novel ZIF materials.

3.3 Collecting Data Through Designed ZIF Structure

Machine learning models are essential for handling diverse jobs and require high-quality data for optimal performance. However, challenges arise such as determining the appropriate amount of data, obtaining statistics, assessing input data quality, and improving it. These questions are crucial for designing mechanical materials using machine learning models. Information can be gathered from existing books or databases, or unprocessed datasets can be created through high-throughput experiments or simulations.

Figure 3.4

Crystal Structure Modification Process Flow



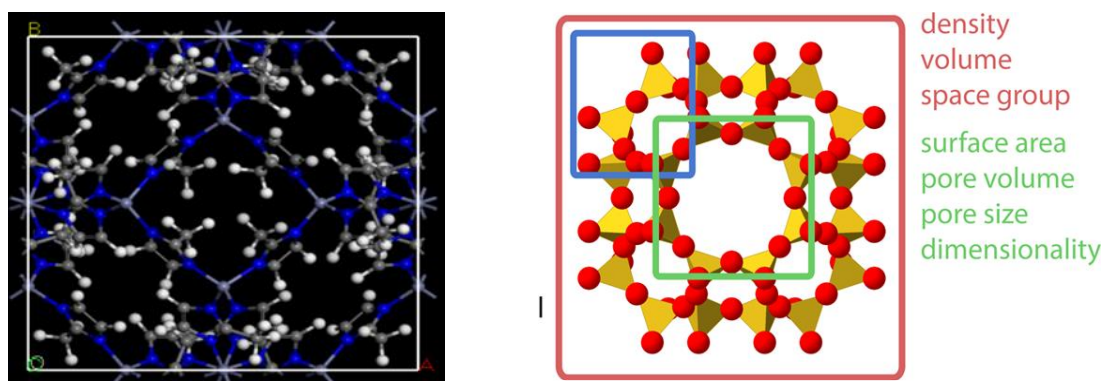
Start with an existing crystal structure represented in the Cambridge Crystallographic Data Centre (CCDC) format (.cif file). This initial structure serves as the starting point for modifications. Next, introduce different functional groups into the crystal structure to alter chemical properties, bonding interactions, and overall behavior. Replace metal atoms within the crystal lattice to impact material properties such as bulk and shear modulus. Choose a specific topology for the modified crystal, referring to the arrangement of atoms and bonds within the lattice. Finally, perform geometry optimization using computational methods to adjust atomic positions, minimize energy, and achieve stable configurations. Utilize the steepest descent optimization algorithm, iteratively adjusting atomic positions along the steepest energy gradient to reach a local minimum. Monitor the optimization quality to ensure convergence, energy stability, and reasonable atomic positions. Run the optimization for a specified number of iterations 5000 steps to ensure accurate results. Verify the optimized cell parameters (unit cell dimensions, angles) to ensure consistency with experimental data or desired properties. Adjust parallel computing on 14 or 16 CPU cores to speed up calculations by distributing tasks across multiple cores. Finally, assess the modified crystal's topology to confirm that the desired structural features, such as coordination environments and connectivity, align with expectations. By following this process, systematically modify crystal structures while considering functional groups, metals, and topology, ultimately achieving the desired material properties.

3.4 Computational Representation

The FORCITE module of Materials Studio is a computational tool used for simulating the behavior of materials at the molecular level. It is specifically designed for studying the mechanical properties of materials, such as their strength, elasticity, and deformation behavior. The FORCITE module uses a variety of computational techniques, including molecular dynamics simulations, quantum mechanical calculations, and force field methods, to model the performance of materials under unlike circumstances. It can simulate the behavior of materials under different temperatures, pressures, and strain rates, allowing researchers to study the effects of these variables on the mechanical properties of materials.

Figure 3.5

Computational Representation of Crystal Structure and Selective Descriptor



One of the key advantages of the FORCITE module is its ability to predict the mechanical properties of materials without the need for complex and time-consuming experiments. By inputting the molecular structure of a material into the FORCITE module, researchers can quickly generate predictions of its mechanical properties, such as its Young's modulus, shear modulus, and Poisson's ratio. The FORCITE module is particularly useful for studying ZIF, which are a class of porous materials composed of metal ions or clusters linked by organic ligands. ZIF have a wide range of potential applications, including gas storage, catalysis, and drug delivery, but their mechanical stability is a key factor in determining their suitability for these applications. By using the FORCITE module to study the mechanical properties of ZIF, it is possible to identify key structural features that influence their mechanical stability. This information can then be used to design new ZIF with improved mechanical properties or to optimize existing MOFs for specific applications. Overall, the FORCITE module of Materials Studio is a powerful tool for studying the mechanical properties of materials at the molecular level and has important applications in materials science, chemistry, and engineering.

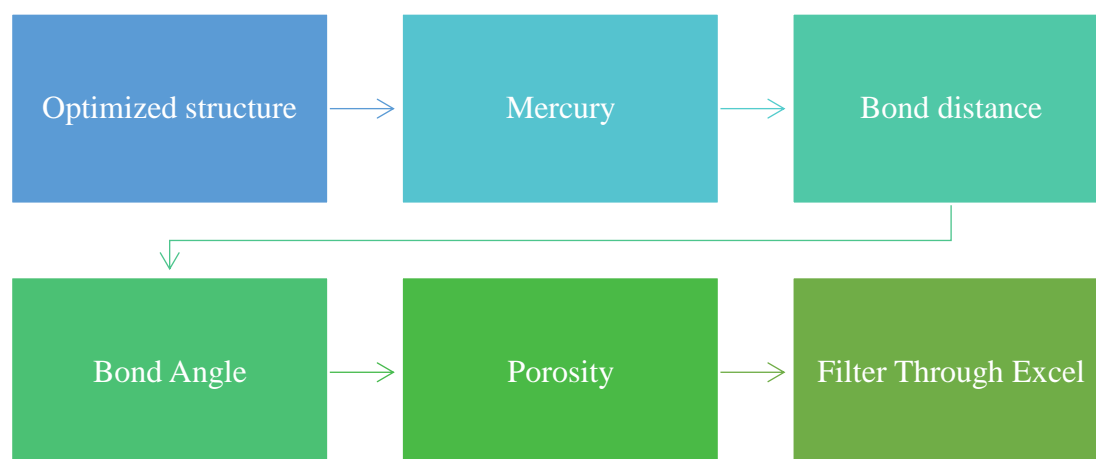
3.5 Data Preprocessing

Data preprocessing and augmentation approaches are necessary to improve the quality of datasets used in machine learning models, which require structured data inputs.

Eliminating unnecessary data points that could negatively impact model performance is also essential.

Figure 3.6

Data Processing Process Map



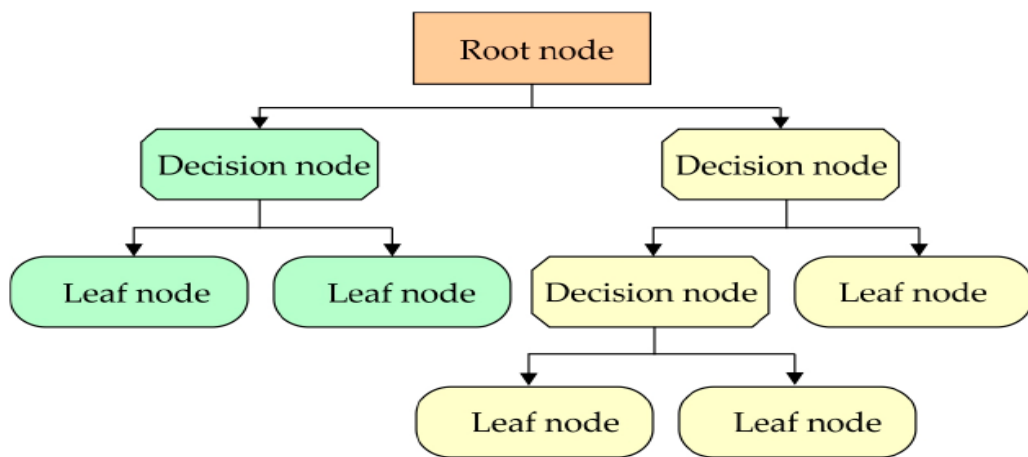
Zeolitic frameworks consist of a three-dimensional network of corner-sharing SiO₄ tetrahedra. Consequently, the local geometry of each atomic environment is typically characterized by straightforward parameters such as Si–O bond lengths and Si–O–Si bond angles. In contrast, for Zeolitic imidazole frameworks, the relevant parameters are the N-metal distances and N-metal-N bond angles. Numerous studies, including earlier research on structure-property relationships in zeolitic frameworks (Wragg et al., 2008), have demonstrated that these two parameters are crucial for understanding the physical and chemical properties. Previous research has demonstrated that ad hoc geometrical descriptors—developed based on chemical intuition and understanding of the systems—can be effectively utilized in supervised machine learning to predict mechanical properties. (D. Evans & Coudert, 2017; Gaillac et al., 2020). For each optimized zeolite structure, the distributions of bond distances, angles, and porosity were computed using the Mercury software provided free of charge by the CCDC. Statistical features of these distributions, such as various means, variances, maxima, minima, and average values, were then utilized as descriptors.

3.6 Gradient-Boosting Regression Algorithm (GBR)

A decision tree, a popular non-parametric supervised machine learning technique, serves both classification and regression tasks. These models consist of a root node, branches, and leaf nodes (depicted in Figure 5). The root node represents input data, while each branch signifies a potential decision. Ultimately, the leaves of the tree yield the algorithm's output.

Figure 3.7

General Schematic of Decision Tree Models



The researchers have determined a method to establish a linear relationship between the mechanical properties of the composite materials using the decision tree approach. Qi et al. (Qi et al., 2019) used a decision tree model to predict the mechanical properties of carbon-fiber-reinforced plastic. (Kosicka et al., 2022) used a decision tree model to predict the mechanical potential of polymers with alumina modifiers. However, overfitting affects the prediction performance greatly in decision trees in this area domain. The concept of the random forest was introduced to improve the prediction performance of the decision tree. Random forest regression is an example of an ensemble learning technique for regression versions. The ensemble in a random forest which is a number 'k' of decision trees which are selected at random for the maximum number of cycles in order to give a final prediction from the specified dataset. It works on the principle of ensemble learning and is a combination of weak learners (often decision trees), and combines their outputs to create a strong predictive model. GBR: Each tree is built primarily based on the mistakes made by the collective previous

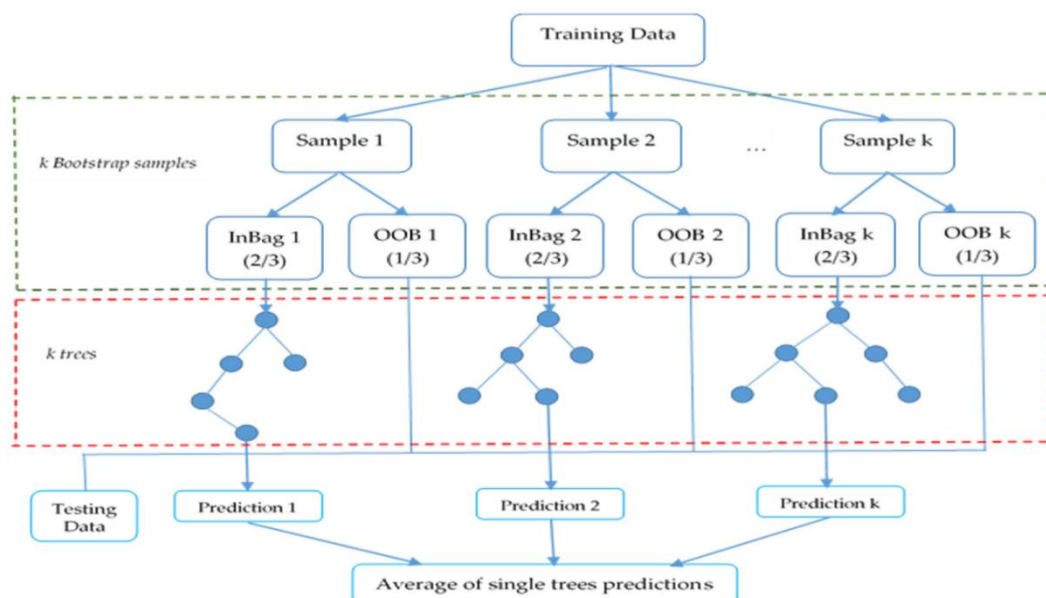
ensemble (previous tree), and hence trees are built in a sequential manner. In the context of GBR, decision trees are often used as base learners. The algorithm fits a tree to the data, calculates the residuals (differences between predicted and actual values), and then fits a new tree to these residuals. This process is repeated iteratively, and each new tree contributes to the overall model. (Pathan et al., 2019) used a gradient-boosting regression technique to forecast the unidirectional fiber composites' macroscopic elastic stiffness and yield strengths.

3.7 Machine Learning Method and GBR Model

The use of artificial intelligence (AI) techniques to forecast material qualities has grown significantly during the past few decades. This growth can be attributed to the greater accessibility of material data from numerical simulations and experimental observations. As a result, ML, a branch of AI, has made incredible strides and found wide use in the research of material properties. The primary idea behind utilizing ML to predict qualities is to examine and identify the nonlinear correlations between those properties and the factors associated with them using already available data. The knowledge of experimental properties of materials starts from a database, a list of entries data set, where each entry corresponds to a certain material.

Figure 3.8

GBR Model



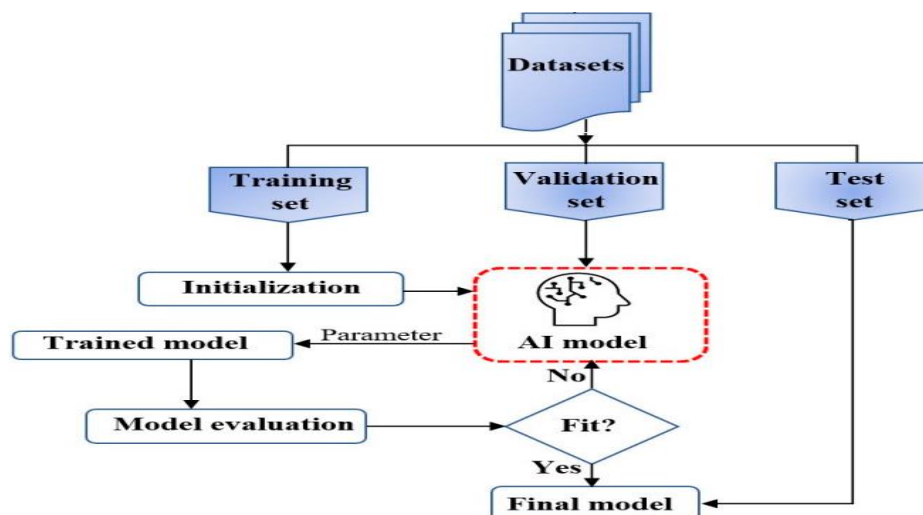
The problem with feeding raw data into an ML model is that it would be unnecessary or challenging to use ML-based methods to solve the problem if the data were either too simple to collect or too complex to obtain. For example, if an existing method can traverse the full design space at a reasonable cost, there is no need for ML, and it is more likely that the datasets that were gathered only cover a tiny section of the design space. Another possibility is that the accumulated databases of images or texts make sense to people but not to computers. In those situations, the raw data must typically be preprocessed before being fed into the machine learning model highlighting the significance of utilizing the researchers' domain expertise to obtain representative data and carry out data preprocessing properly for better results from the ML model.

3.8 Process of Prediction

In AI-based predictions of material properties, the raw experimental or simulated material data is consistently divided into three datasets: training, validation, and testing. The Artificial Intelligence Model is Trained using the Training Data The model uses this dataset to learn patterns and relationships during the training phase. At the same time, the validation dataset is used to keep a check on how well the model is performing and whether it may have started overfitting.

Figure 3.9

Standard Prediction Workflow for AI-Based Methods



When a model overfits, it becomes excessively dependent on the training set and cannot adapt well to new data. It is possible to optimize the model's hyperparameters by evaluating the model's performance on the validation dataset. Hyperparameters act as control variables that affect the learning process and the behavior of the model. After training and fine-tuning, the model can generate predictions on new input data, known as the testing dataset. This separate dataset enables the assessment of the model's predictive accuracy on previously unseen instances.

CHAPTER 4

RESULT AND DISCUSSION

4.1 Design of MOF

Here in this study total of 126 MOF crystal subsets was designed with the seven imidazole-based ligands (2-methylimidazole, 2-ethyl imidazole, 2-nitroimidazole, 2-methyl-4-nitroimidazole, Benzimidazole, Imidazole-2-carbaldehyde, and 3-Methyl-1,2,4-triazole) with three individual metals as well as the composition of these metals (Zn, Cu, Co, ZnCu, CoZn and CuCo) and specially focused on SOD, CAG and DFT topology.

4.2 Design of ZIF With Three Metals and Their Composition with Seven Ligands

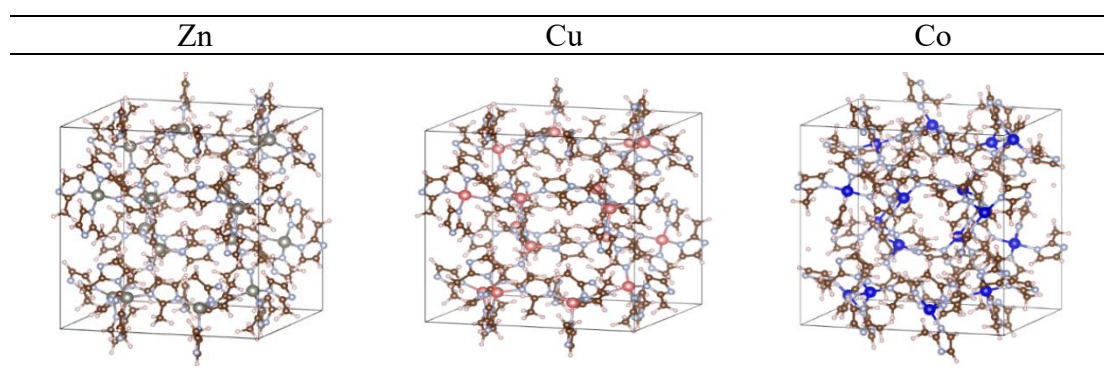
Here's a breakdown of the connectivity, impact, symmetry, and space group for each linker in ZIFs with Zn, Cu, and Co metal:

4.2.1 2-Methylimidazole (Hmim) with Zn, Cu, and Co

In ZIF structure, Zn (II) ions act as nodes, connecting with four nitrogen atoms from the organic linkers. These nitrogen atoms typically come from the imidazole ring of the linker molecule. The bonding involves nitrogen donating its lone pair of electrons to a vacant orbital on the Zn (II) ion, forming a coordinate covalent bond.

The methyl group (CH₃) on the Hmim molecule doesn't directly participate in the bonding with Zn. The Zn-N bonds might have slightly different lengths and angles depending on the specific ZIF structure. These Zn-Hmim linkages act as building blocks, connecting into a porous, three-dimensional network that defines the ZIF framework.

When it comes to Cu metal, there are ZIFs (Zeolitic Imidazolate Frameworks) built with copper (Cu) and imidazole linkers, 2-methylimidazole (Hmim) doesn't typically form a stable ZIF structure with Cu. It has partially filled d-orbitals that can participate in bonding. Imidazole, lacking readily available lone pairs on all its nitrogen atoms, might not offer the optimal bonding environment for Cu (II) compared to other linkers.

Table 4.1*Connectivity of Three Metals with 2-Methylimidazole Ligand*

In a hypothetical scenario where Cu-Hmim ZIF exists, the most likely bonding would involve the nitrogen atom from the imidazole ring donating its lone pair to a vacant d-orbital on Cu (II). The coordination geometry around Cu (II) would depend on the number of Hmim linkers coordinating and the influence of other factors like solvent molecules. It could be tetrahedral, square planar, or a more distorted geometry. Similar to Zn, Co (II) can form stable ZIFs with Hmim. The connectivity would involve the nitrogen atoms from Hmim donating lone pairs to Co (II) ions, likely forming a tetrahedral or octahedral geometry around Co depending on the specific ZIF structure.

All 3 crystal structures contain the space group Pbc_a (61) where P indicates a primitive unit cell. A primitive unit cell is the smallest possible repeating unit that defines the crystal structure. In simpler terms, it's the basic building block that forms the entire crystal when stacked in a specific way. b, c, a these represent the crystallographic axes a, b, and c. These axes define the edges of the unit cell. This space group represents the Orthorhombic crystal system. This means the unit cell has three unequal edges, all perpendicular to each other. Hmim is the most common linker for ZIFs due to its optimal size and lack of steric hindrance. It offers good thermal and chemical stability. Based on the topology it represents different cages.

4.2.2 2-Ethylimidazole (EtHim) with Zn, Cu and Co

The connection between EtHim and Zn in a ZIF is very similar to that of Hmim and Zn. The primary connection involves the lone pair of electrons on a nitrogen atom in the imidazole ring of EtHim donating to a vacant orbital on the Zn (II) ion. This forms a

coordinated covalent bond between nitrogen and zinc. Each Zn (II) ion is typically tetrahedrally coordinated by four nitrogen atoms from four separate EtHim molecules.

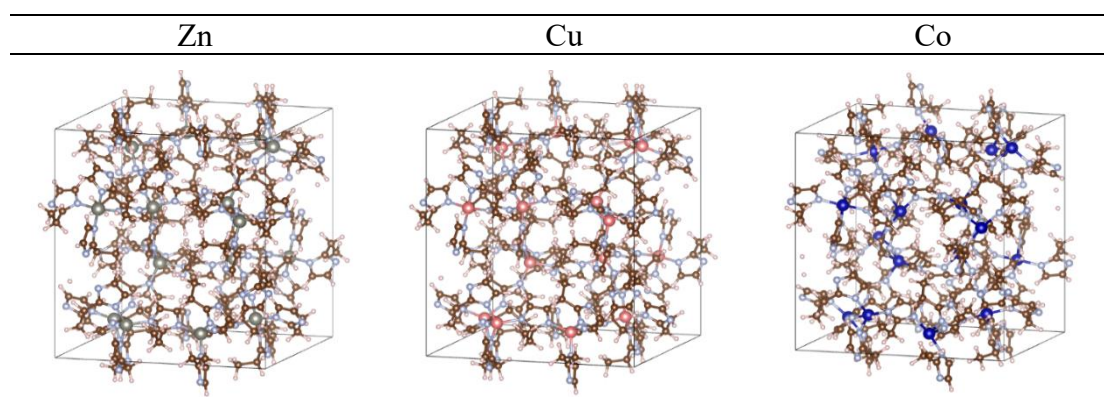
The presence of the ethyl group (CH_2CH_3) in EtHim compared to the methyl group (CH_3) in Hmim has minimal impact on the direct Zn-N bonding. The ethyl group is bulkier than methyl but isn't directly involved in coordinating with the metal center. Overall, the presence of the ethyl group doesn't significantly alter the fundamental Zn-N connectivity in EtHim-based ZIFs. However, it can introduce subtle changes in pore size and packing efficiency compared to ZIFs built with Hmim.

The thing about 2-ethylimidazole (EtHim) and Copper (Cu) in a ZIF structure similar to 2-methylimidazole (Hmim), Cu doesn't typically form a very stable ZIF with EtHim due to limitations in their interaction. The connection between EtHim and Co in a ZIF shares similarities with the Zn-EtHim system. The primary interaction involves the lone pair of electrons on a nitrogen atom in the imidazole ring of EtHim donating to a vacant orbital on the Co (II) ion. This forms a coordinate covalent bond between the nitrogen and cobalt.

Co (II) can exhibit various coordination geometries depending on the number of ligands and other factors. Likely geometries in a Co-EtHim ZIF include tetrahedral (with four EtHim linkers) or octahedral (with six EtHim linkers). Similar to Zn-EtHim ZIF, the ethyl group (CH_2CH_3) on EtHim has minimal influence on the direct Co-N bonding. It doesn't directly participate in coordinating with the metal center.

Table 4.2

Connectivity of Three Metals with 2-Ethyl Imidazole Ligand



The slightly larger size of the ethyl group compared to methyl (in Hmim) could lead to a small decrease in pore size compared to a Co-ZIF with Hmim. The increased steric bulk of the ethyl group might influence how EtHim linkers pack around the Co centers, potentially affecting the overall packing efficiency of the ZIF framework.

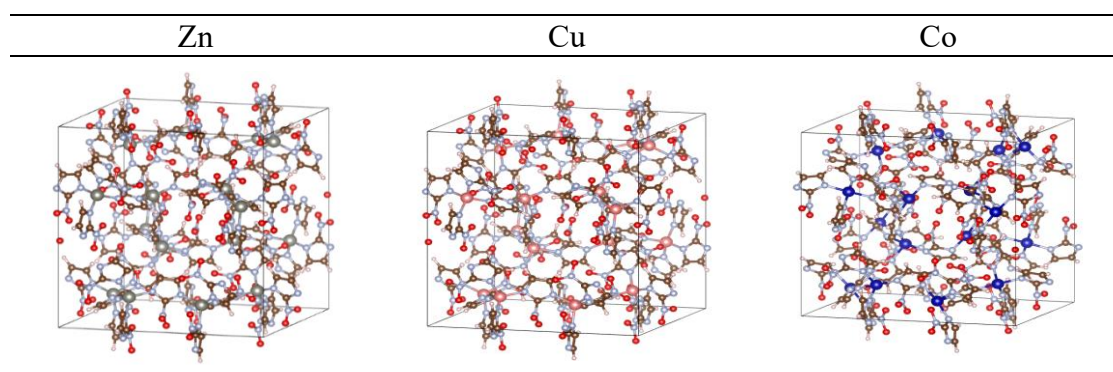
Both Zn and Co can form ZIFs with EtHim through nitrogen atom donation from the imidazole ring. The ethyl group's influence on connectivity is minimal in both cases. The specific coordination geometry around the metal center might differ between Co-EtHim and Zn-EtHim ZIFs due to the different electronic configurations of Zn (II) and Co (II). Overall, EtHim can connect with Co (II) to form a ZIF structure. The ethyl group has a minor effect on the direct metal-nitrogen bonding but could influence pore size and packing efficiency.

4.2.3 2-Nitroimidazole (NIz) with Zn, Cu and Co

The nitro group (NO₂) can participate in hydrogen bonding with neighboring linkers or guest molecules, potentially affecting pore chemistry and stability. The primary connection between NIz and Zn in a ZIF involves the lone pair of electrons on a nitrogen atom in the imidazole ring donating to a vacant orbital on the Zn (II) ion. This forms a coordinated covalent bond similar to other imidazole-based ZIFs. The presence of the nitro group (NO₂) on the imidazole ring introduces an additional functionality that influences the ZIF structure and properties.

The nitro group doesn't directly participate in bonding with Zn (II). The oxygen atoms in the nitro group can act as hydrogen bond acceptors. This allows NIz to form hydrogen bonds with neighboring NIz linkers, guest molecules containing hydrogen bond donors. Hydrogen bonding interactions between NIz linkers can influence how they pack around the Zn centers, potentially affecting the overall pore size and arrangement within the ZIF framework.

The Zn (II) ion remains tetrahedrally coordinated, with the nitrogen atom from the imidazole ring of each NIz molecule forming the primary bond. The nitro group doesn't directly affect the Zn-N bond but can introduce hydrogen bonding interactions that influence the ZIF structure.

Table 4.3*Connectivity of Three Metals with 2-Nitroimidazole Ligand*

Similar to other ZIFs, Zn (II) is typically tetrahedrally coordinated by four nitrogen atoms. In a NIZ-Zn ZIF, three of these nitrogen's would come from the imidazole rings of separate NIZ linkers, while the fourth nitrogen could come from another NIZ or potentially from a solvent molecule coordinated to Zn (II). 2-nitroimidazole connects to Zn through the imidazole nitrogen, forming a ZIF structure. The nitro group introduces hydrogen bonding possibilities that can influence the packing, pore properties due to its larger size, and potentially the stability of the ZIF through hydrogen bonding.

Here's the thing about 2-nitroimidazole (NIZ) and Copper (Cu) in a ZIF structure similar to what was discussed previously for Cu with other imidazole linkers, Cu-NIZ ZIFs are not very common due to limitations in their interaction. Cu (II) has partially filled d-orbitals that favor specific geometries and orbital overlap for strong bonding. The arrangement of atoms in NIZ, with its two nitrogens' might not provide the optimal electron configuration for Cu (II) compared to other linkers. The nitro group's oxygen atoms are potential electron donors. This could introduce competition with the imidazole nitrogen for bonding with Cu (II) d-orbitals, potentially weakening the overall framework.

Similar to other imidazole-based ZIFs, the primary connection between NIZ and Co involves the lone pair of electrons on a nitrogen atom in the imidazole ring donating to a vacant orbital on the Co (II) ion. This forms a coordinate covalent bond, linking the NIZ molecule to the central Co (II) center. The nitro group can act as a hydrogen bond

acceptor, potentially forming interactions with neighboring NIz linkers, guest molecules, or solvent molecules within the ZIF pores. These hydrogen bonds can influence framework stability and porosity.

The nitro group is bulkier than a hydrogen atom (present in Hmim or EtHim). This can influence how NIz linkers pack around Co (II) ions, potentially affecting pore size and accessibility. While less likely to be the primary interaction, the oxygen atoms in the nitro group might weakly coordinate with Co (II) depending on the overall coordination geometry and electronic configuration.

Co (II) exhibits various coordination geometries depending on the number of ligands and other factors. In a Co-NIz ZIF, tetrahedral is common with four NIz molecules coordinating through their imidazole nitrogen. Both Zn (II) and Co (II) can form ZIFs with NIz through nitrogen atom donation from the imidazole ring. The nitro group's influence on core connectivity is likely minimal in both cases. NIz can connect with Co (II) to form a ZIF structure. The presence of the nitro group adds complexity compared to simpler linkers. Hydrogen bonding capabilities, steric effects, and potential weak interaction with the nitro group can influence the stability, porosity, and functionalities of the Co-NIz ZIF.

4.2.4 2-Methyl-4-nitroimidazole (MNIz) with Zn, Cu and Co

Similar to 2-nitroimidazole, the primary connection between MNIz and Zn involves the single pair of electrons on a nitrogen atom in the imidazole ring donating to a vacant orbital on the Zn (II) ion. This forms a coordinate covalent bond, linking the MNIz molecule to the central Zn (II) center. MNIz has two functional groups that can influence the ZIF structure and properties. The Methyl group is positioned at the second position of the imidazole ring and has minimal impact on the direct Zn-N bonding while nitro groups are located at the fourth position. The nitro group can act as a hydrogen bond acceptor, potentially forming interactions with neighboring MNIz linkers, guest molecules, or solvent molecules within the ZIF pores.

These hydrogen bonds can influence framework stability and porosity. The nitro group is bulkier than a hydrogen atom (present in Hmim or EtHim). This can influence how MNIz linkers pack around Zn (II) ions, potentially affecting pore size and accessibility.

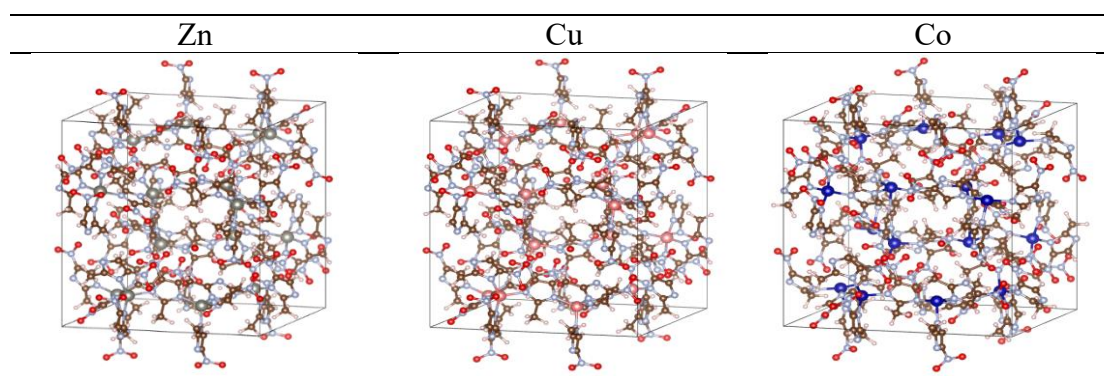
The presence of both the methyl and nitro groups adds complexity compared to simpler imidazole linkers like Hmim or EtHim. While the core Zn-N bonding remains similar, the steric effects of the nitro group and its potential for hydrogen bonding can influence the stability, porosity, and potential functionalities of the resulting Zn-MNIZ ZIF.

2-Methyl-4-nitroimidazole (MNIZ) and Copper (Cu) in a ZIF structure similar to what was discussed previously for Cu with other functionalized imidazole. Cu (II) has partially filled d-orbitals that favor specific geometries and orbital overlap for strong bonding. The imidazole ring, even with the combined effects of the methyl and nitro groups, might not offer the optimal electronic configuration for Cu (II) compared to other linkers. The nitro group's oxygen atoms are potential binding sites. However, strong coordination between Cu (II) and the nitro group might compete with the desired coordination of MNIZ's imidazole nitrogen to Cu (II), leading to an unstable framework. The methyl and nitro groups can create steric hindrance around the Cu (II) center, further complicating the formation of a stable and well-defined coordination geometry.

Here it can explore the connectivity and geometry of 2-methyl-4-nitroimidazole (MNIZ) with Cobalt (Co) in a Zeolitic Imidazole Framework (ZIF) Similar to other imidazole-based ZIFs, the primary connection between MNIZ and Co involves the single pair of electrons on a nitrogen atom in the imidazole ring donating to a vacant orbital on the Co (II) ion. This forms a coordinate covalent bond, linking the MNIZ molecule to the central Co (II) center.

Table 4.4

Connectivity of Three Metals with 2-Methyl-4-Nitroimidazole Ligand



The nitro group can act as a hydrogen bond acceptor, potentially forming interactions with neighboring MNiZ linkers, guest molecules, or solvent molecules within the ZIF pores. These hydrogen bonds can influence framework stability and porosity. The nitro group is bulkier than a hydrogen atom (present in Hmim or EtHim). This can influence how MNiZ linkers pack around Co (II) ions, potentially affecting pore size and accessibility. While less likely to be the primary interaction, the oxygen atoms in the nitro group might weakly coordinate with Co (II) depending on the overall coordination geometry and electronic configuration.

Both Zn (II) and Co (II) can form ZIFs with MNiZ through nitrogen atom donation from the imidazole ring. The methyl group's influence on core connectivity is minimal in both cases. Zn (II) typically prefers tetrahedral geometry, while Co (II) can exhibit both tetrahedral and octahedral geometries. The final geometry in the ZIF might differ depending on the metal used. The possibility of weak coordination between the nitro group and Co (II) might influence the overall framework stability and electronic properties compared to Zn-MNiZ ZIF.

However, MNiZ can connect with Co (II) to form a ZIF structure. The existence of the methyl and nitro groups adds complexity compared to simpler linkers. Hydrogen bonding capabilities, steric effects, and potential weak interaction with the nitro group can influence the stability, porosity, and functionalities of the Co-MNiZ ZIF.

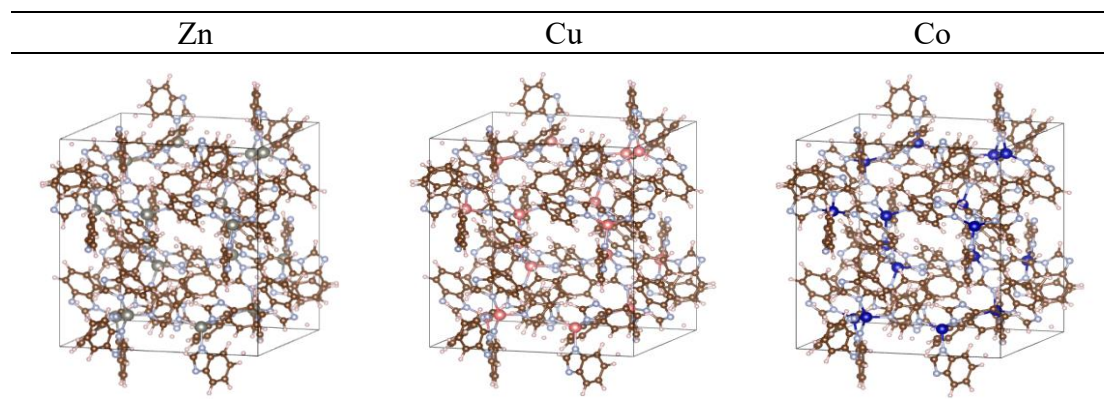
4.2.5 Benzimidazole (BIm) with Zn, Cu and Co

This linker is larger than the previous ones due to the fused benzene ring. It can play a pivotal role in the formation of larger pores but might also affect the stability of the ZIF framework due to steric hindrance unlike typical imidazole linkers (like Hmim or EtHim), benzimidazole (BIm) doesn't have a direct available nitrogen atom on the aromatic ring for coordination with the metal center. However, BIm can still form ZIFs with Zn through a different mechanism. During ZIF synthesis, one of the ring nitrogens in BIm loses a proton (H⁺), becoming negatively charged. This deprotonated nitrogen then donates its lone pair of electrons to a vacant orbital on Zn (II), forming a coordinate covalent bond. Zn (II) typically prefers a tetrahedral coordination geometry. In a Zn-BIm ZIF, the four coordination sites around Zn (II) would likely be occupied by

nitrogen atoms from deprotonated BIm molecules. Each Zn (II) center would bind to the deprotonated nitrogen atom of four separate BIm linkers.

Table 4.5

Connectivity of Three Metals with Benzimidazole Ligand



The Zn-BIm ZIF would have a different structure compared to ZIFs with imidazole linkers like Hmim or EtHim. The connection points would be on the aromatic ring instead of the imidazole nitrogen. This can influence the pore size, shape, and overall properties of the ZIF. Both BIm and Hmim can form ZIFs with Zn. However, the connectivity mechanism differs. Hmim uses a lone pair directly on its imidazole nitrogen, while BIm relies on deprotonation and N-metalation. Hmim connects through the imidazole nitrogen, while BIm connects through a deprotonated aromatic nitrogen. The different connection points might lead to variations in pore size and shape between BIm-Zn and Hmim-Zn ZIFs. Due to its larger size compared to other linkers, benzimidazole can lead to the formation of larger pores. However, the increased steric bulk might affect framework stability.

Benzimidazole (BIm) and Copper (Cu) in a ZIF structure Cu-BIm ZIFs are not very common. BIm lacks readily available nitrogen atoms on the aromatic ring for strong coordination with Cu (II). Unlike Zn (II) which can form a bond with the deprotonated nitrogen in BIm, Cu (II) prefers stronger interactions often involving multiple nitrogen atoms nearby. Cu (II) has partially filled d-orbitals that favor specific geometries and orbital overlap for optimal bonding. The arrangement of nitrogen atoms in BIm might not provide the ideal electronic configuration for stable Cu-BIm coordination. In a

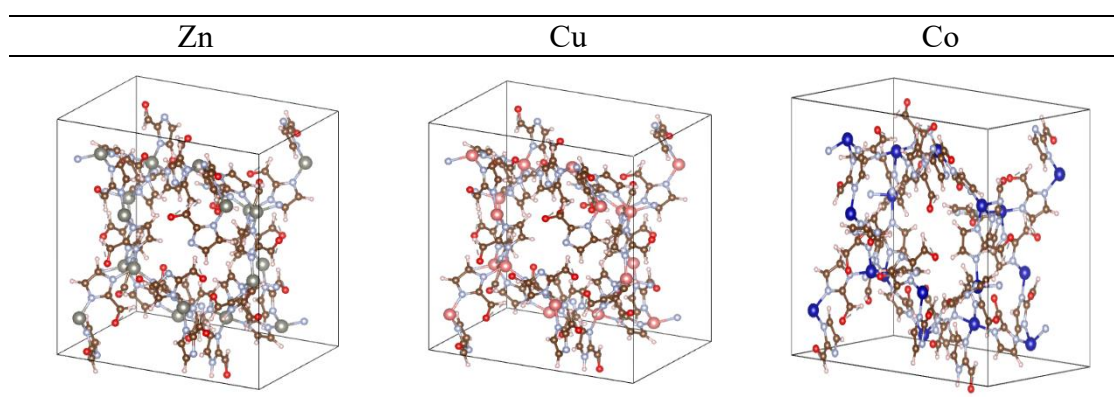
hypothetical scenario where a Cu-BIm ZIF exists, the most likely interaction would involve deprotonation of BIm similar to Zn-BIm ZIF. However, the resulting bond between Cu (II) and the deprotonated nitrogen might be weaker than in Zn-BIm due to Cu (II)'s preference for stronger interactions.

Core Connectivity is similar to Zn-BIm ZIFs, cobalt can potentially form ZIFs with BIm through deprotonation and N-metalation. Co (II) exhibits various coordination geometries depending on the number of ligands and other factors. Tetrahedral is a possibility with four deprotonated BIm molecules coordinating through their N1 nitrogen atoms. Both Zn (II) and Co (II) can form ZIFs with BIm through deprotonation and N-metalation of the aromatic ring nitrogen.

4.2.6 Imidazole-2-carbaldehyde (IC) with Zn, Cu and Co

Imidazole-2-carbaldehyde (IC) with Zinc (Zn) when building ZIFs offers two potential coordination sites for Zn (II). Nitrogen atom (N1) in the imidazole ring is similar to other imidazole linkers (like Hmim or EtHim), the lone pair of electrons on N1 can donate to a vacant orbital on Zn (II), forming a coordinate covalent bond. The oxygen atom (O) from the aldehyde group (CHO) has lone pairs that can potentially coordinate with Zn (II). However, the competition between these sites and the overall stability of the ZIF depends on several factors.

The N1 nitrogen in the imidazole ring is typically more acidic than the oxygen atom in the aldehyde group. This means deprotonation (loss of a proton) of N1 is more likely, favoring N1 coordination. Zn (II) generally prefers coordination with nitrogen atoms due to stronger interaction compared to oxygen. Zn (II) typically prefers a tetrahedral coordination geometry. The presence of the aldehyde group in IC introduces the possibility of hydrogen bonding, steric effects, and potential weak secondary interactions with Zn (II). These can influence the overall ZIF properties compared to the simpler Hmim linker.

Table 4.6*Connectivity of Three Metals with Imidazole-2-Carbaldehyde Ligand*

The aldehyde group can act as a hydrogen bond donor, potentially forming interactions with guest molecules or solvent molecules within the ZIF pores. These hydrogen bonds can influence framework stability and potentially introduce specific functionalities. The aldehyde group is bulkier than a hydrogen atom (present in Hmim or EtHim). This can influence how IC linkers pack around Zn (II) ions, potentially affecting pore size and accessibility. While less likely to be the primary connection, the oxygen atom in the aldehyde group might weakly coordinate with Zn (II) under specific conditions. This could influence the overall framework stability or introduce additional functionalities depending on the guest molecules incorporated.

IC can connect with Zn (II) to form a ZIF structure. The N1 nitrogen atom in the imidazole ring is the most likely coordination site. The presence of the aldehyde group can introduce hydrogen bonding capabilities, steric effects, and potential secondary interactions, influencing the ZIF's stability, porosity, and potential functionalities.

While IC can connect with Zn to form a ZIF, Cu-IC ZIFs are not very common for a few reasons. IC offers two potential binding sites the nitrogen atom (N1) in the imidazole ring and the oxygen atom (O) from the aldehyde group (CHO). While N1 is generally preferred, strong coordination between Cu (II) and oxygen might compete with the desired N1-Cu (II) bond, leading to framework instability. Even if a Cu-IC ZIF could be formed, it might be less stable than ZIFs with linkers offering stronger and more well-defined coordination environments for Cu (II). While Cu can potentially interact with IC, the competition between coordination sites and the preference of Cu

(II) for specific bonding geometries make Cu-IC ZIFs challenging to synthesize and less common than other ZIF structures.

Similar to Zn-IC ZIFs, IC offers two potential coordination sites for Co (II). Nitrogen atom (N1) in the imidazole ring has a lone pair of electrons on N1 that can donate to a vacant orbital on Co (II), forming a coordinate covalent bond. The oxygen atom has lone pairs that can potentially coordinate with Co (II). The N1 nitrogen is generally more acidic than the aldehyde oxygen. Deprotonation (loss of a proton) of N1 is more likely, favoring N1 coordination. Co(II) exhibits some flexibility in coordination geometry and can interact with various donor atoms. However, nitrogen atoms often offer stronger interactions compared to oxygen.

Co (II) can exhibit various coordination geometries depending on the number of ligands and other factors. This is a very common possibility, with four IC molecules coordinating through their N1 nitrogen atoms. The d-orbital electronic configuration of Co (II) allows for good orbital overlap with the lone pairs on the nitrogen in a tetrahedral arrangement, leading to a stable bonding geometry. IC can connect with Co (II) to form a ZIF structure. The N1 nitrogen atom in the imidazole ring is the most likely coordination site. The presence of the aldehyde group can introduce hydrogen bonding capabilities, steric effects, and potential secondary interactions, influencing the ZIF's stability, porosity, and potential functionalities.

4.2.7 3-Methyl-1,2,4-triazole (3-MTZ) with Zn, Cu and Co

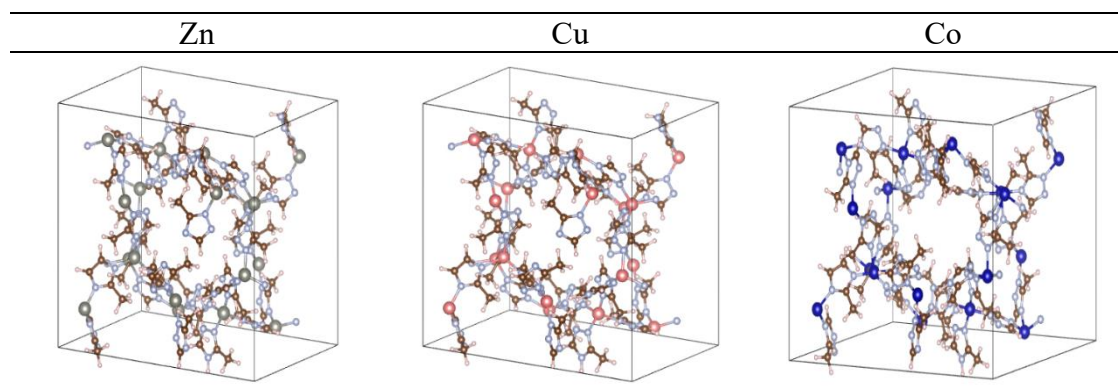
In the case of ZIFs with Zn metal and 3-MTZ ligands, the connectivity arises from the coordination bonds between Zn ions and 3-MTZ molecules. The 3-MTZ ligand acts as a bridge, connecting adjacent Zn ions to form a three-dimensional network. The resulting structure is porous, with channels and cavities that can host guest molecules.

The 3-MTZ ligand coordinates with the Zn metal center through its nitrogen and carbon atoms. Specifically, the nitrogen atom of the triazole ring (the 1,2,4-triazole moiety) binds to the Zn ion, forming a Zn-N bond. Additionally, the carbon atoms of the triazole ring and the methyl group (from 3-MTZ) participate in π -bonding interactions with the Zn ion. Overall, the synchronized geometry around the Zn center is typically octahedral, with the 3-MTZ ligand occupying multiple coordination sites. The porous structure

allows for gas adsorption, separation, and catalysis. The specific ligand (in this case, 3-MTZ) influences the pore size, surface area, and guest molecule interactions.

Table 4.7

Connectivity of Three Metals with 3-Methyl-1,2,4-Triazole Ligand



Regarding copper (Cu) metal and 3-Methyl-1,2,4-triazole (3-MTZ) ligands to form ZIFs materials, the connectivity arises from coordination bonds between Cu ions and 3-MTZ molecules. The 3-MTZ ligand acts as a bridge, connecting adjacent Cu ions to form a three-dimensional network. The resulting structure is porous, with channels and cavities that can host guest molecules.

The 3-MTZ ligand coordinates with the Cu metal center through its nitrogen and carbon atoms. Specifically, the nitrogen atom of the triazole ring (the 1,2,4-triazole moiety) binds to the Cu ion, forming a Cu-N bond. Additionally, the carbon atoms of the triazole ring and the methyl group (from 3-MTZ) participate in π -bonding interactions with the Cu ion. The coordination geometry around the Cu center is typically octahedral, with the 3-MTZ ligand occupying multiple coordination sites. This octahedral geometry results from the arrangement of ligands around the central Cu ion, where the Cu ion is surrounded by six ligands (three from 3-MTZ and three water molecules in hydrated forms), forming a distorted octahedron.

When building a ZIF with Co metal and 3-MTZ ligands, coordination bonds are formed between Co ions and 3-MTZ molecules. The 3-MTZ ligand acts as a bridge, connecting adjacent Co ions to create a three-dimensional network. The resulting structure is porous, with channels and cavities that can host guest molecules.

The 3-MTZ ligand coordinates with the Co metal center through its nitrogen and carbon atoms. Specifically, the nitrogen atom of the triazole ring binds to the Co ion, forming a Co-N bond. Additionally, the carbon atoms of the triazole ring and the methyl group participate in π -bonding interactions with the Co ion. Overall, the synchronized geometry around the Co center is typically octahedral, with the 3-MTZ ligand occupying multiple coordination sites. This octahedral geometry results from the arrangement of ligands around the central Co ion, with six ligands (three from 3-MTZ and three water molecules in hydrated forms) surrounding the Co ion and forming a distorted octahedron.

4.3 Model Accuracy

This study used a technique called gradient boosting regressor (GBR) to create the predictive model. GBR is a tool available in the Python scikit-learn package, a popular library for machine learning in Python. Gradient boosting is a machine learning technique that builds predictive models in a stepwise manner by combining multiple weak models, like decision trees, to create a strong predictive model. GBR is known for its accuracy and effectiveness in various fields, including web search ranking. In this study, GBR was chosen over other methods like support vector machines because it is considered robust, interpretable, and suitable for the small dataset used in this research. Well-established selection criteria and cross-validation techniques were rigorously applied to ensure the accuracy and reliability of the predictive model.

Regression trees involve optimizing arbitrary loss functions during the training process. Regression trees are a type of decision tree used for regression tasks. In this context, the regression trees are being used to predict the elastic response of zeolites based on geometric features. The model was built gradually, with each step optimizing the loss function to improve accuracy. By training regression trees in this way, the model could effectively learn the relationships between the geometric features of zeolites and their elastic moduli.

The process involves creating a regression tree at each stage based on the negative gradient of the loss function. The negative gradient guides the construction of the tree, which functions as a decision-making model to predict outcomes based on input features. By fitting the regression tree to the negative gradient, the model aims to

minimize errors in predicting the target variable. This iterative process refines the model's predictions and improves accuracy over successive stages.

Here, 5-fold cross-validation was employed, a common technique in ML, to estimate the performance of the model. The 5-fold cross-validation technique entails splitting the data into five parts, using four parts for training the model and the remaining part for testing it. This process helps determine the model's ability to generalize to new data. To ensure robustness, the cross-validation was performed 100 times, offering a detailed evaluation of the model's accuracy across various iterations. Hyperparameters, listed in the table, were selected to maximize prediction accuracy and flexibility while minimizing overfitting.

Table 4.8

Hyperparameters of the Model

Parameter	Value
Estimators	1000
Learning rate	0.01
Maximum depth	3
Minimum samples per leaf	3
Random state	42

The table provided outlines the hyperparameters utilized to train the Gradient Boosting Regressor model, which is an ML approach employed in the study. The hyperparameters include the number of estimators, learning rate, minimum samples for splitting, maximum depth, and other parameters that influence the model's performance.

4.3.1 Evaluation of RMSE Value for Shear Modulus (G)

In this work, the machine learning model's accuracy was tested using cross-validation against the training set. The results showed excellent accuracy and low variance, indicating the model's reliability. The figure below illustrates the comparison among the model results and the MD training set for the 126-imidazole zeolite framework. The plot in Figure demonstrates how well the machine learning model performed in

predicting the mechanical properties of the ZIFs. The high accuracy and low variance of the model's predictions represent that it effectively estimates the elastic response of zeolites based on geometric features

The average RMSE across all folds is 2.96. This value is a general measure of the model's predictive performance and represents the typical magnitude of prediction errors observed across the different cross-validation folds. It indicates a balanced view of the model's performance, averaging out the variations seen in individual folds.

Figure 4.1

Evaluating GBR Predictions Against Cross-Validated MD Training Data.

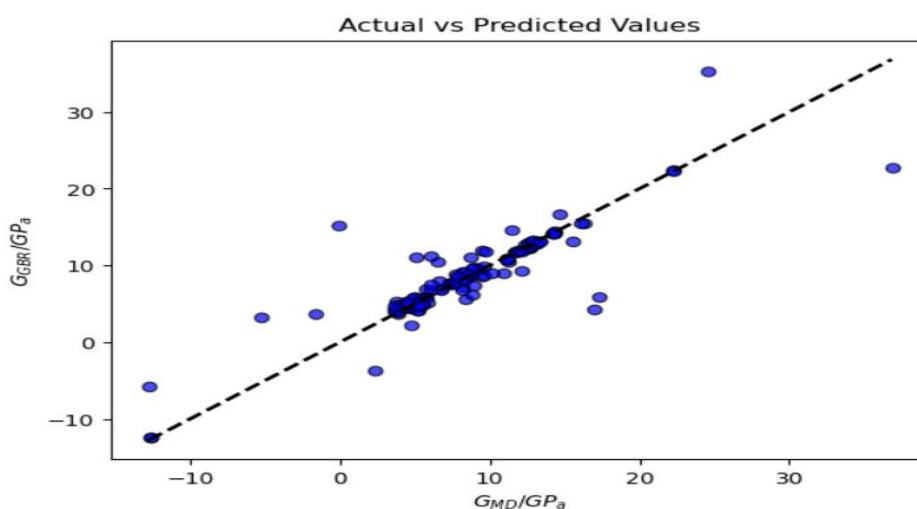
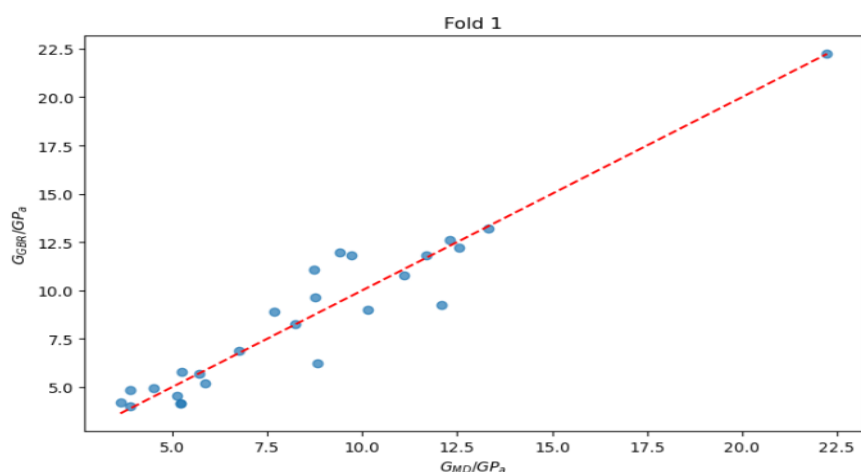


Figure 4.2

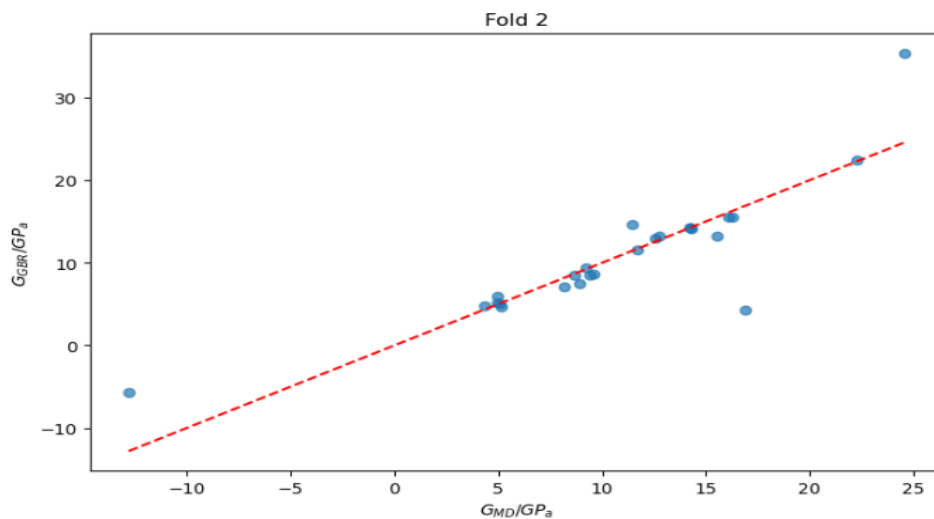
Best-Fitted Line for Shear Modulus G (Fold-1).



The lowest Root Mean Squared Error (RMSE) observed in this fold is 1.24. This indicates that the model performed exceptionally well on this specific subset of the data, suggesting that the training and test sets in Fold 1 were particularly well-suited for accurate predictions by the model.

Figure 4.3

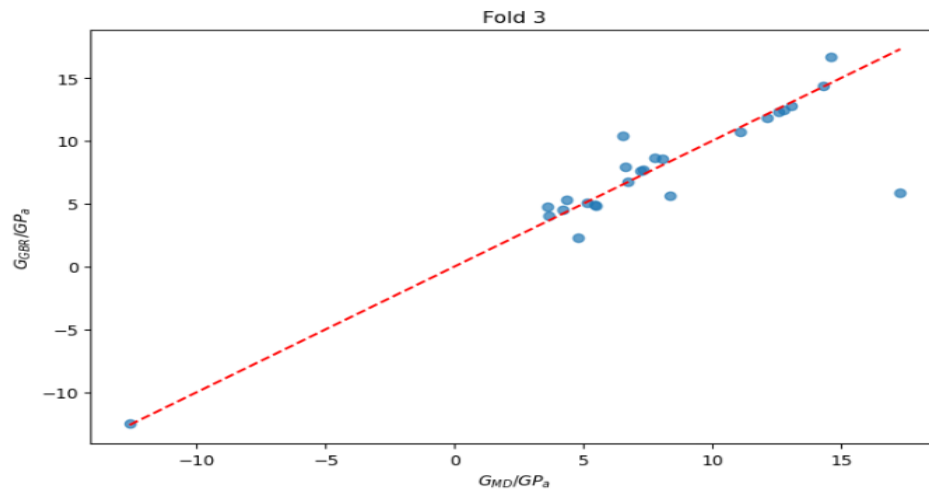
Best-Fitted Line for Shear Modulus G (Fold-2).



In contrast, Fold 2 exhibits the highest RMSE value of 3.74. This significant increase in error suggests that the model encountered substantial difficulties in accurately predicting outcomes within this fold. The discrepancy may be due to greater variability or complexity in the test data for Fold 2, which the model struggled to generalize effectively.

Figure 4.4

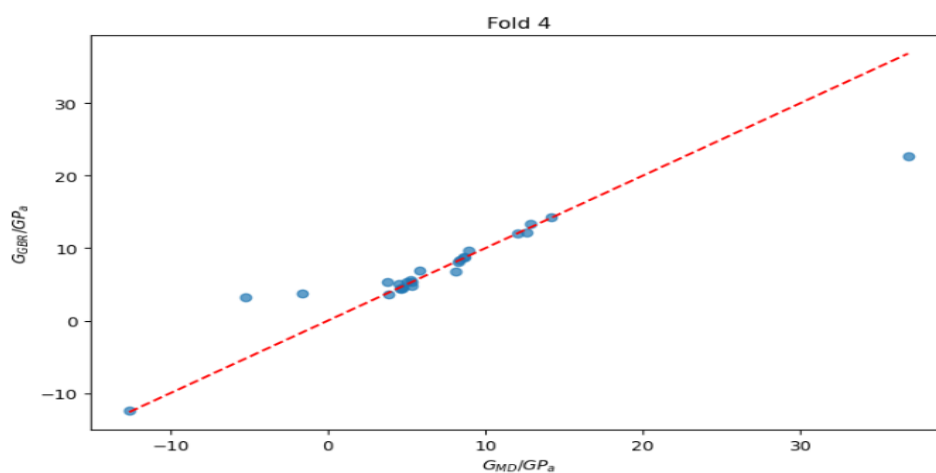
Best-Fitted Line for Shear Modulus G (Fold-3).



The RMSE values for Folds 3, 4, and 5 are 2.61, 3.52, and 3.71, respectively. These values fall within a moderate performance range, indicating varying levels of prediction accuracy across these folds. Fold 3 is closer to the lower end of the error spectrum with an RMSE of 2.61, suggesting relatively better performance than Folds 4 and 5.

Figure 4.5

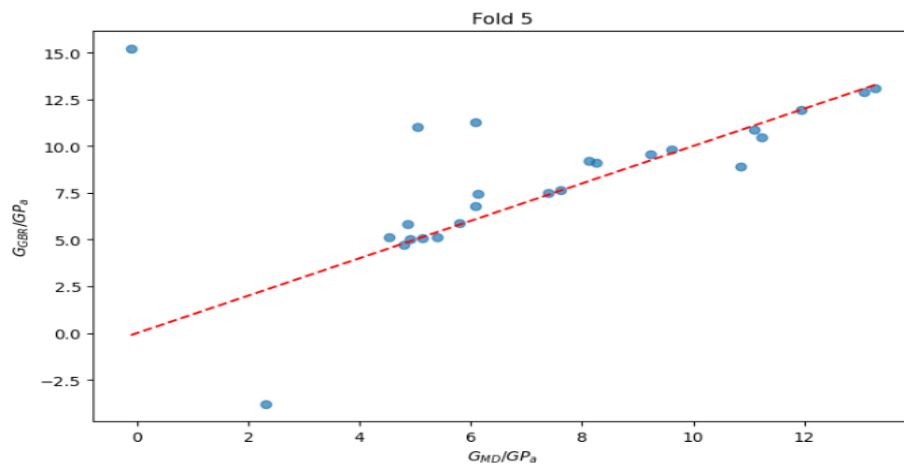
Best-Fitted Line for Shear Modulus G (Fold-4).



Fold 4 and Fold 5, with RMSE values of 3.52 and 3.71 respectively, are positioned toward the higher end of the error distribution, indicating that the model faced challenges in these folds similar to those encountered in Fold 2.

Figure 4.6

Best-Fitted Line for Shear Modulus G (Fold-5).

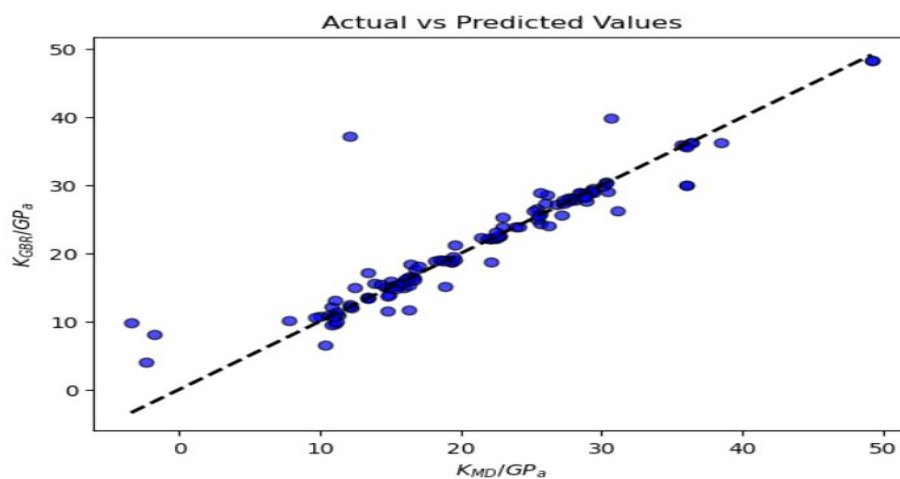


In summary, understanding the variation in RMSE across folds provides valuable insights into the model's robustness and its ability to generalize to unobserved data. The lower RMSE in Fold 1 highlights the model's potential for high accuracy under favorable conditions, while the higher errors in Folds 2, 4, and 5 indicate areas where the model may need improvement or further tuning. Researchers and practitioners can use these results to inform model selection and further improvements, ensuring that the predictive model is both reliable and effective across diverse datasets.

4.3.2 Evaluation of RMSE Value for Bulk Modulus (K)

Figure 4.7

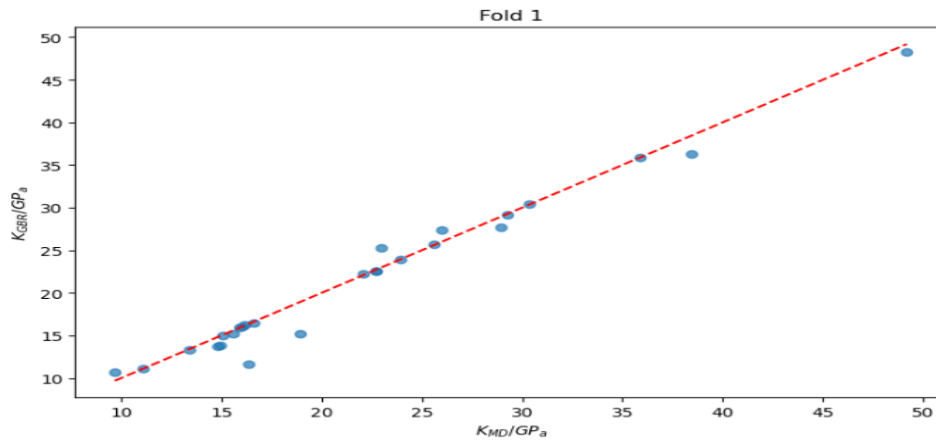
Evaluating GBR Predictions Against Cross-Validated MD Training Data for K.



The average RMSE across all folds is 2.80, which provides a general measure of the model's predictive performance. This average value indicates that, on average, the model's predictions are within 2.80 units of the actual values across all folds.

Figure 4.8

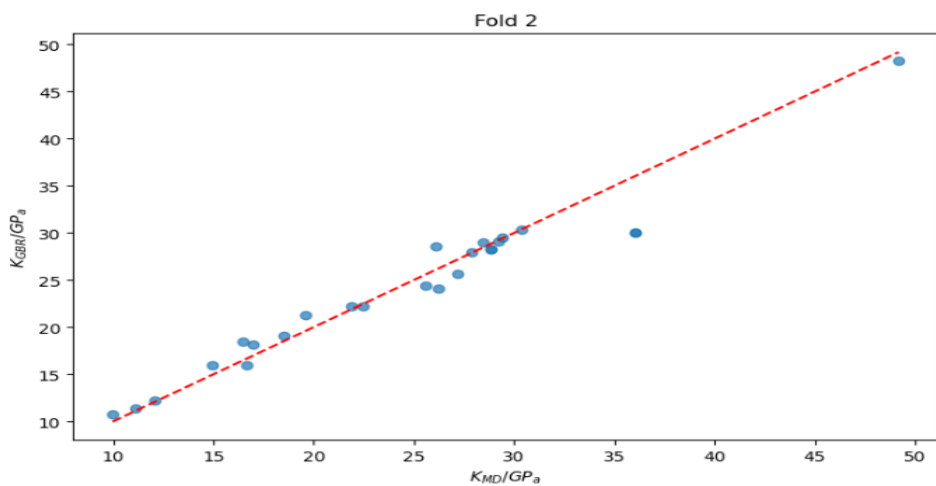
Best-Fitted Line for Bulk Modulus K (Fold-1).



The RMSE of 1.44 is the lowest among all folds, indicating the model performed very well on this subset of data. This suggests that the data distribution in Fold 1 was more conducive to accurate predictions by the model.

Figure 4.9

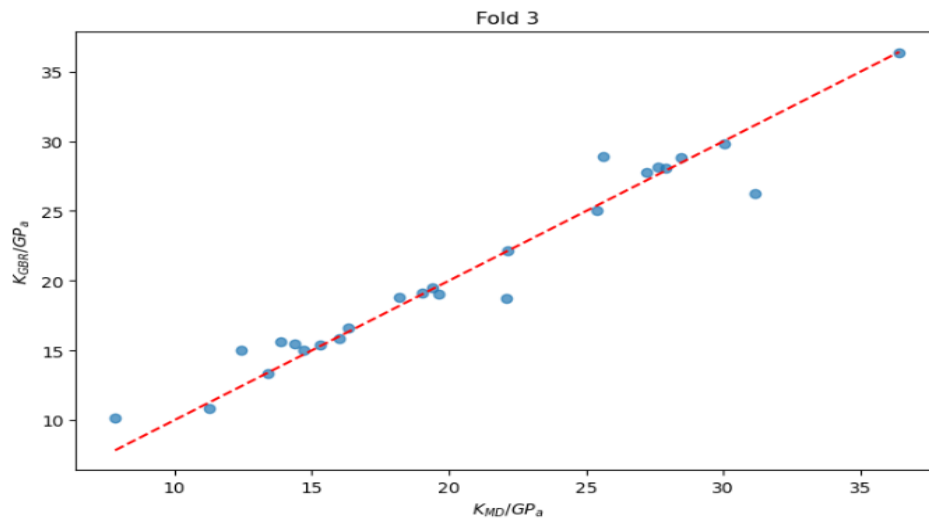
Best-Fitted Line for Bulk Modulus K (Fold-2).



With an RMSE of 1.99, the performance in Fold 2 is slightly lower than in Fold 1 but still relatively good. The data in Fold 2 posed more challenges to the model, but it still maintained reasonable predictive accuracy.

Figure 4.10

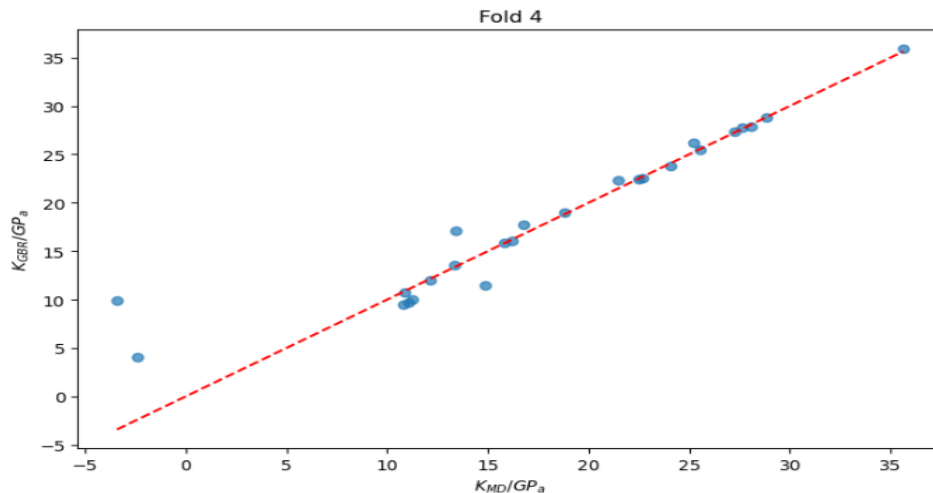
Best-Fitted Line for Bulk Modulus K (Fold-3).



The RMSE of 1.61 is closer to the RMSE in Fold 1, indicating similar model performance. The model effectively captured the underlying patterns in the data for this fold.

Figure 4.11

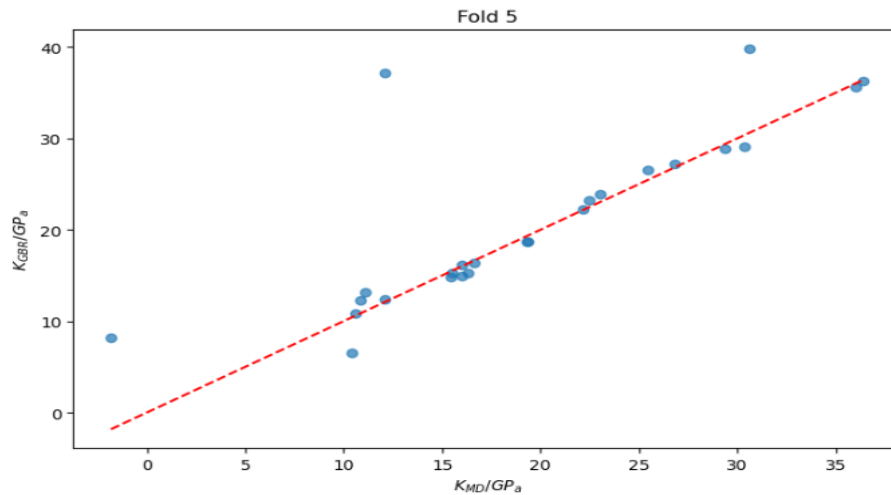
Best-Fitted Line for Bulk Modulus K (Fold-4).



An RMSE of 3.17 shows a noticeable increase in prediction error. The data in Fold 4 might have been more complex or had a different distribution, leading to a higher error rate.

Figure 4.12

Best-Fitted Line for Bulk Modulus K (Fold-5).



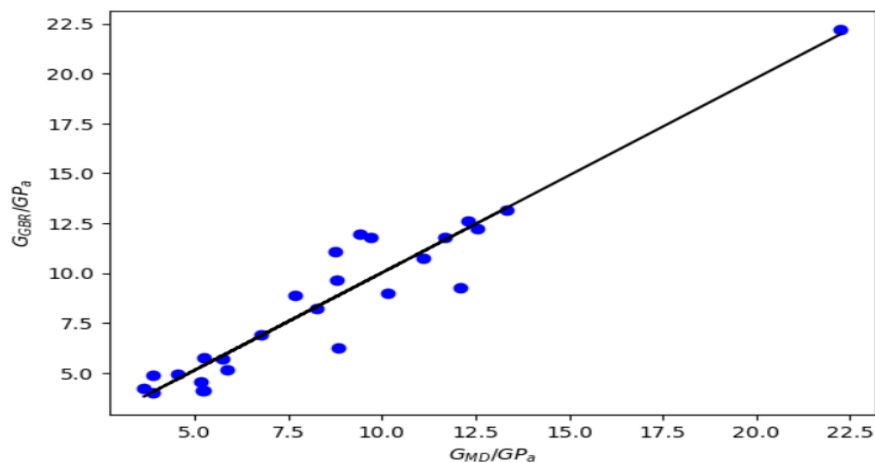
With the highest RMSE of 5.80, Fold 5 represents the most challenging subset for the model. This significant increase in error suggests that the model struggled to generalize well to the data in this fold.

Understanding the RMSE values for each fold highlights the variability in model performance across different subsets of the data. The lower RMSE in folds 1, 2, and 3 demonstrates the model's potential for high accuracy under certain conditions. In comparison, the higher RMSE in folds 4 and 5 indicates areas where the model may need improvement or further tuning. The average RMSE value of 2.80 is a useful benchmark for the model's overall performance, providing insights into its generalization ability and robustness.

4.4 Without Validation the Test Data

Figure 4.13

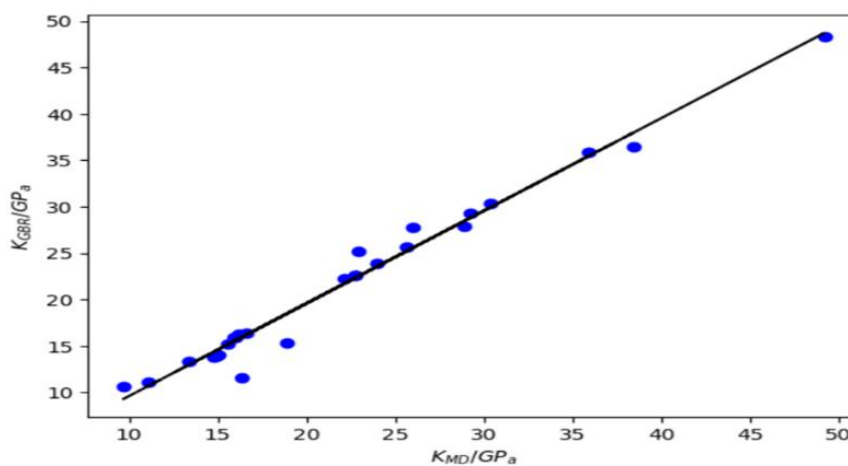
Best-Fitted Line of Test Data Set for Shear Modulus (K) For Fold.



Without cross-validation, the RMSE value obtained was 1.24 for predicting the shear modulus of ZIFs. The training and test data were divided into 80% and 20% respectively. Thus, the training data was 100 from the 126 zeolitic imidazole frameworks and 26 data used for the test.

Figure 4.14

Best-Fitted Line of Test Data Set for Shear Modulus (K) for Fold.



Similar to the shear modulus the model was fed with 100 data while 26 were used for the test data and the gained RMSE value for bulk modulus (K) obtained 1.44 which

represents the good performance of the model in terms of forecasting the elastic moduli of ZIFs.

4.5 Model Feature

In a machine learning model, descriptors refer to the features or characteristics of the data that are used to make predictions or classifications. Not all descriptors have the same level of importance or influence on the model's performance. Some descriptors may have a stronger correlation or relationship with the target variable, while others may have little to no impact. Certain descriptors may provide more valuable information for accurate predictions, while others may be less relevant or misleading.

After training a machine learning model, it is possible to interpret the model to understand which descriptors or features are most significant for assembly forecasts. By analyzing the model's internal workings, such as the weights assigned to each descriptor or the feature importance scores, we can identify the crucial features that have the weightiest effect on the model's predictions. This interpretation helps in understanding the underlying relationships between the descriptors and the target variable, providing insights into which features are driving the predictions and why.

Feature selection is the process of selecting the most related features (or variables) that subsidize the most to the prediction task. In the context of the GBR model, feature selection is important because it helps to identify which geometric features of zeolites are most important for predicting their elastic response. By using regression trees, the GBR model automatically determines which features are most informative and includes them in the model, while disregarding less important features.

Intrinsic feature selection has several advantages in the context of guessing the mechanical properties of zeolite imidazole frameworks. Firstly, it reduces the complexity of the model by excluding irrelevant or redundant features, which can help to prevent overfitting. By automatically selecting the most important features, the GBR model with regression trees can avoid overfitting and generalize well to new imidazole zeolite samples. Secondly, intrinsic feature selection improves the interpretability of the model by focusing on the most meaningful features. By identifying the key geometric features that are strongly correlated with the elastic response of imidazole-based

zeolites, academics can expansion valuable insights into the underlying mechanics of zeolitic frameworks. These insights can then be used to guide further research and development of zeolite materials with desired mechanical properties.

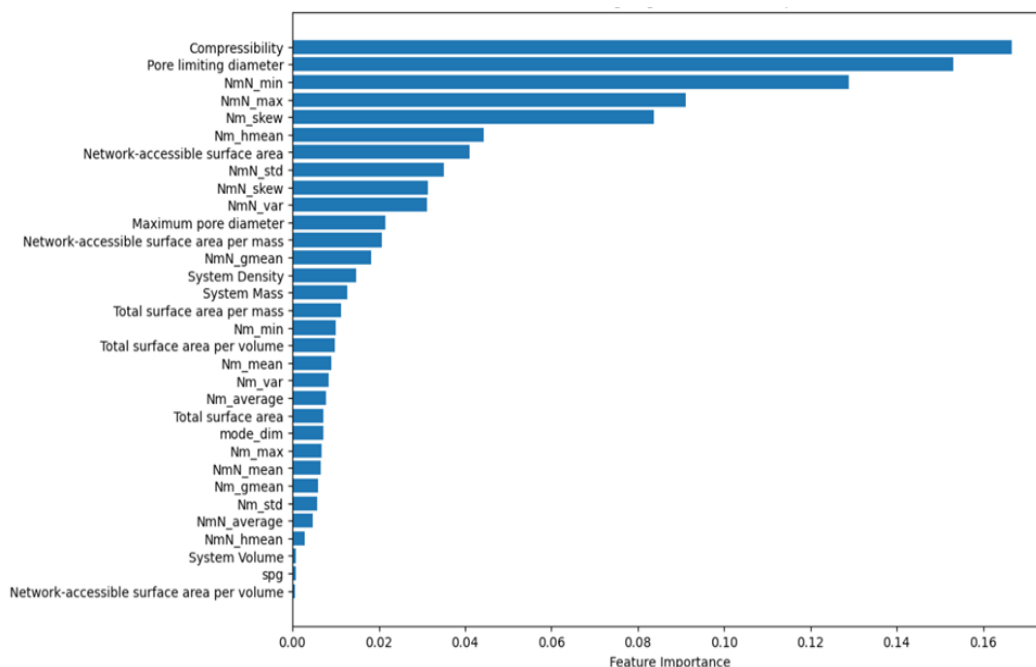
4.5.1 Descriptors and Their Importance to Predict Shear Modulus Accurately

Local descriptors refer to specific parameters or characteristics of a zeolite's local geometry, structure, and porosity. These local descriptors play a pivotal role in guessing the mechanical properties of zeolites using ML.

Parameters related to the porosity showed the largest weight in the model to predict the shear modulus. Compressibility refers to how much a material can be compressed under pressure, which is directly related to its mechanical stability and rigidity.

Figure 4.15

Relative Importance of The Descriptors Used to Produce the GBR Model for G.



Compressibility, defined as the extent to which a material can be compacted under pressure, is a fundamental descriptor in evaluating the mechanical properties of ZIFs. Lower compressibility signifies enhanced rigidity and mechanical stability, which are critical attributes for applications necessitating structural integrity, such as high-pressure gas storage and structural components. Similarly, the pore-limiting diameter,

which is the maximum size of pores within the ZIF structure, plays a pivotal role in determining gas sorption, diffusion, and accessibility. Larger pore sizes facilitate the adsorption of guest molecules, thereby enhancing the effectiveness of ZIFs in applications like gas storage and separation processes.

In addition, the maximum pore diameter, representing the size of the most expansive cavity within the ZIF framework, significantly influences the adsorption capacity and selectivity. This characteristic is particularly crucial for applications that require the selective adsorption of large molecules. Moreover, the network-accessible surface area per volume, which quantifies the surface area available to guest molecules relative to the framework volume, directly correlates with the adsorption capacity and catalytic activity of ZIFs. A higher network-accessible surface area per volume is essential for optimizing the efficiency of ZIFs in catalytic and adsorption processes. Furthermore, system density, defined as the mass per unit volume of the ZIF, affects its mechanical stability and packing efficiency. A higher density often correlates with increased structural robustness, vital for maintaining integrity under mechanical stress.

Total surface area per volume and network-accessible volume are also significant descriptors influencing the performance of ZIFs. The total surface area per volume, indicating the overall surface area relative to the framework volume, suggests a greater potential for adsorption performance, which is vital for applications involving gas storage and separation. The network-accessible volume, or the volume within the ZIF framework accessible to guest molecules, enhances the material's capacity for gas storage and adsorption applications. The system mass, or the total mass of the ZIF system, affects mechanical properties and stability, with heavier systems exhibiting greater mechanical stability, important for applications requiring structural integrity. Lastly, the total surface area, encompassing the overall surface area of the ZIF, enhances adsorption capacity and catalytic activity, crucial for optimizing the material's performance in gas adsorption and catalytic applications. These descriptors collectively play pivotal roles in determining the mechanical stability, adsorption properties, and overall performance of ZIFs, guiding engineers in designing frameworks optimized for specific applications by ensuring desired properties such as mechanical robustness, adsorption capacity, and selectivity. The relationship between these descriptors and

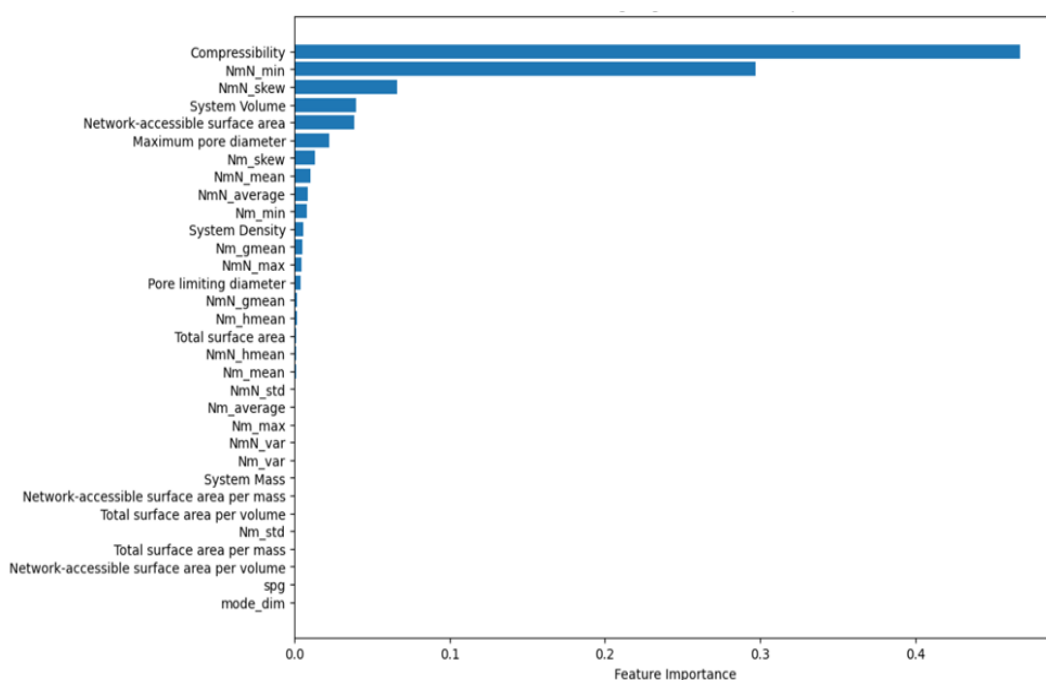
their importance is essential for advancing the development and application of ZIFs in various fields.

4.5.2 Descriptors and Their Importance to Predict Bulk Modulus Accurately

The compressibility index is a vital descriptor in evaluating a framework's mechanical response to external pressure. A higher compressibility index signifies greater flexibility within the material, which directly impacts its bulk modulus, a measure of the material's resistance to uniform compression. Additionally, system volume is a crucial factor, as larger volumes tend to result in lower bulk moduli. This relationship occurs because larger volumes allow more deformation under pressure, thereby reducing the material's overall stiffness. Moreover, the network-accessible surface area significantly influences the framework's mechanical properties by affecting interactions with guest molecules. This descriptor determines how well the framework can interact with and accommodate guest molecules, thereby influencing its structural integrity and mechanical stability.

Figure 4.16

Relative Importance of The Descriptors Used to Produce the GBR Model for Bulk Modulus (K).



The maximum pore diameter is another important descriptor affecting the bulk modulus. Larger pores within the framework can lead to reduced stiffness, as the material becomes more deformable under pressure. This reduction in stiffness can negatively impact the bulk modulus, making the material less resistant to uniform compression. Understanding these relationships is crucial for predicting the bulk modulus of ZIFs, as it allows for the design of frameworks with tailored mechanical properties for specific applications.

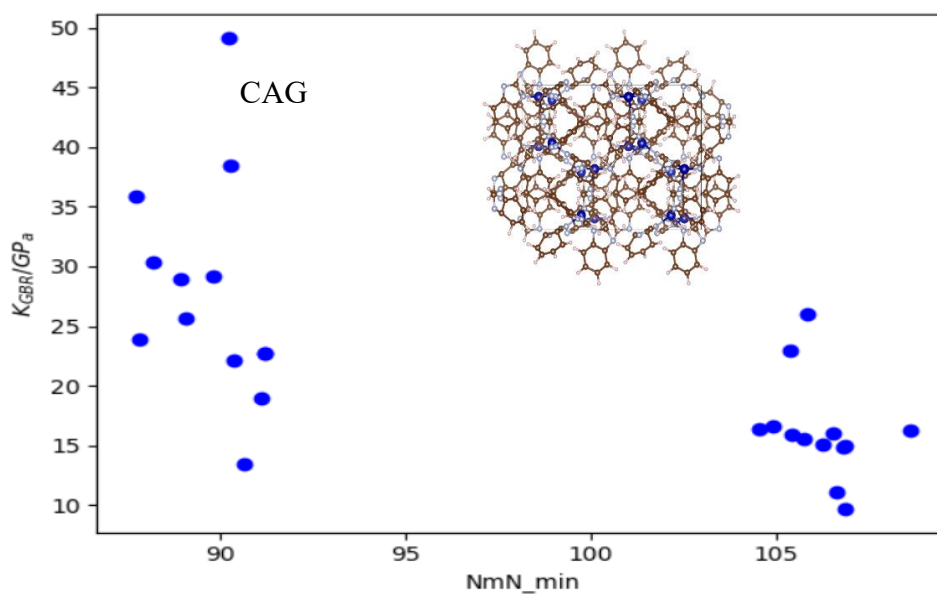
ML models play a pivotal role in guessing the bulk modulus by analyzing various descriptors to discern patterns and determine feature importance. These models, including techniques such as linear regression, support vector regression, and neural networks, are employed to effectively learn the intricate relationships between descriptors and the bulk modulus. The success of these regression models relies heavily on high-quality training data with accurately labeled bulk modulus values. This ensures that the models capture underlying trends and generalize well to unseen ZIFs, enabling accurate predictions of their mechanical properties. Through the application of machine learning, researchers can optimize the design and functionality of ZIFs for a wide range of industrial applications.

4.5.3 Correlation Between K and $N-M-N$ Min in The MD Training Set

There is a robust connection between the minimum value of the $N-M-N$ angles and the K of the zeolitic imidazole frameworks. The correlation suggests that zeolitic imidazole frameworks with mostly linear $N-M-N$ angles for tetrahedral geometry, such as those found in the CAG framework, tend to be very stiff materials with large bulk moduli for Benzimidazole CuCo. In an ideal zeolitic structure, the angle is typically around 109.5 degrees, representing tetrahedral geometry. Any deviation from this ideal angle, such as the 90.24-degree angle observed in this study, indicates a more rigid and strained structure. The smaller $N-m-N$ angle (90.24 degrees) suggests a more condensed and less flexible arrangement of atoms in the ZIF framework. This condensed structure makes it harder to compress the material, resulting in a higher bulk modulus (k) of 49.1836 GPa. Due to different ligands and their connection distinct angle distortion happens.

Figure 4.17

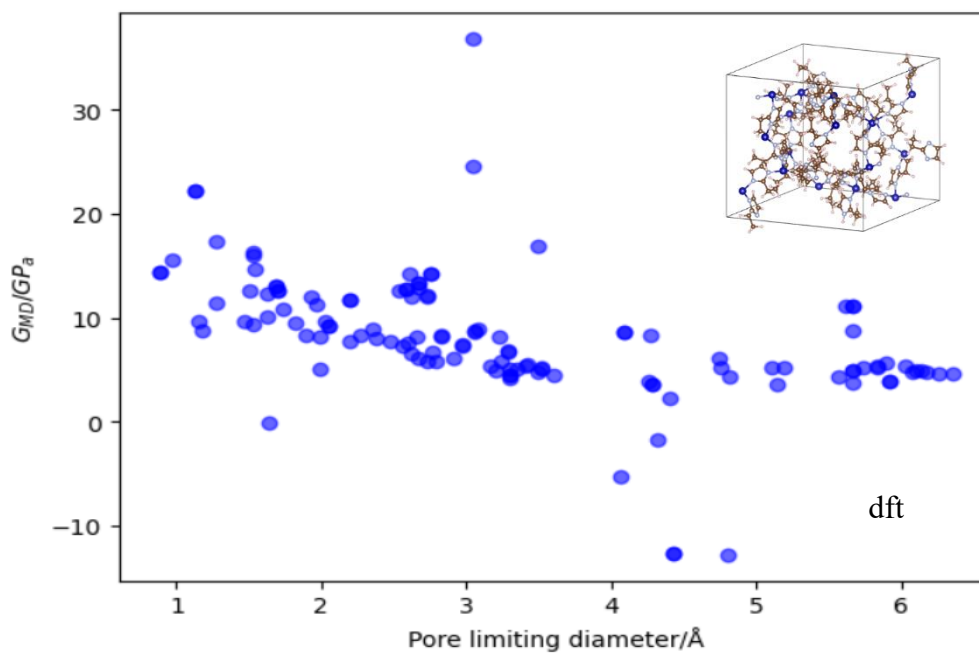
Correlation Between K and $N-M-N$ Min



4.5.4 Correlation Between G and Pore Limiting Diameter in The MD Training Set

Figure 4.18

Correlation Between G and Pore Limiting Diameter



"Porosity descriptor" and a " Pore limiting diameter (PLD)" are important factors in predicting the shear modulus (G) of zeolite structures. A porosity descriptor is a characteristic that describes the amount of space or pores within a zeolite structure. It provides information about the porosity or voids present in the material. The pore-limiting diameter refers to the maximum size of pores within a ZIF. It is measured in terms of its diameter, which represents the maximum distance between two points on the surface of the cavity.

It can be found in this study that zeolitic imidazole framework with PLD, such as the dft structure, which has a cage greater than 4.5 Å (angstroms) in diameter, show really low shear modulus values of -12.80 GPa for 2-ethyl imidazole where the metal was Co. However, a negative shear modulus implies that the material responds in the opposite direction to the applied shear stress.

4.6 Discussion

In this work, the RMSE value from the cross-validation of the MD training set and GBR model predictions for K of 126 pure zeolite imidazole framework obtained 2.80, and for shear modulus (G) 2.96 which represents a good performance of the model compared to (D. Evans & Coudert, 2017) this paper. They showed a good performance in terms of RMSE value for 121 pure silica zeolites but I observed from their code they used all data for cross-validation which represents a good performance. Normally cross-validation should have the test and train data. (Ducamp & Coudert, 2022) The authors of this paper predict the thermal properties of the zeolite through ML and the result showed an average RMSE value of $4.28 \cdot 10^{-6} \text{ k}^{-1}$ and they consider it is reasonable for the small data set. In a comparison, in this study can claim the model performance is quite well for this small data set of 126 zeolite imidazole framework.

Parameters related to the N-M-N angles also have a significant weight in the model. N-M-N angles refer to the angles formed between Nitrogen (N) and metal (M=Co, Cu, Zn) atoms in the zeolite framework. The specific angles at which these atoms are arranged affect zeolites' overall stability and mechanical properties. This study achieved accurate predictions of the bulk and shear moduli by incorporating these parameters into the ML model.

The results of the analysis of feature importances are consistent with the findings of a previous study conducted in 2004 by Monson and co-workers. The previous study focused on five different types of silica zeolites: SOD, LTA, CHA, MOR, and MFI (Astala et al., 2004). Here, in this study it has been demonstrated that the N–M–N bond angles, volume per unit for metal and nitrogen, and space group collectively influence the bulk modulus (K) of ZIFs. N–M–N angles and volume per unit for metal and nitrogen are similarly essential for forecasting G, but porosity and other N–M bond lengths are significant additional descriptors.

Zeolite structures with larger cavities or pores tend to have lower shear modulus values. This is because larger voids allow for more flexibility and easier deformation of the material under shear stress. On the other hand, zeolitic imidazole framework structures with smaller or fewer pores have higher shear modulus values, indicating greater rigidity and resistance to deformation. There is a specific type of zeolite α -cristobalite shown that the Si–O–Si angles have a significant impact on its elastic properties. This suggests that the same principle may apply to other zeolites as well, indicating a general relationship between Si–O–Si angles and the resulting mechanical properties of zeolite frameworks (Yeganeh-Haeri et al., 1992).

In this study, a few negative shear moduli were observed from the molecular dynamics calculation which can be counted as a metamaterial in terms of application in the field of engineering and industry. (Shaaf & El Dhaba, 2019) Explained well how the shear modulus of metamaterials can change based on material size and microstructure topology, defining conditions for zero, negative, or positive shear modulus values.

Examining the local geometry, structure, and porosity of zeolites enables the determination of their influence on the material's properties. The correlation between these characteristic features and the properties of zeolites offers an unparalleled level of understanding compared to previous methods.

CHAPTER 5

CONCLUSION

In this research study, 126 porous zeolite imidazole structures were systematically optimized using molecular dynamics simulations. These optimized structures served as the training dataset for a machine-learning model. The 1st objective of this study was to build the primary data set by utilizing the Avogadro, forcite module, and mercury software and 2nd objective was to train the machine model for predicting the elastic properties of zeolites, including both the bulk modulus and shear modulus. By leveraging computational simulations and machine learning techniques, aimed to enhance the understanding of zeolite elastic properties and contribute to the field of materials science and industry.

Upon determining the optimal hyperparameters for the gradient-boosting regression models, the accuracy of models constructed using various types of structure descriptors was compared. These included geometric descriptors (based on N–M distances and N–M–N angles), porosity-related descriptors, and structural descriptors. Through the training of machine learning models, acquired valuable insights into the intricate structure-property correlations within ZIFs. Notably, the investigation of geometric descriptors revealed that angle descriptions hold greater significance than distances for these frameworks. Indeed, angles emerged as the pivotal parameter during model training. The angle between the N-M-N showed the highest feature importance in bulk modulus while the porosity descriptor played a pivotal role in measuring the shear modulus.

By integrating computational simulations with machine learning techniques, this research sheds light on the elastic properties of ZIFs. It emphasizes the critical role of accurately labeled training data and the thoughtful selection of relevant material descriptors for successful machine learning models. Furthermore, this work contributes to the broader field of materials science, opening new avenues for designing novel ZIF-based materials with tailored properties.

5.1 Future Suggestion

Building upon the findings of this research, several promising avenues can be explored to enhance our understanding and practical application of ZIFs:

1. **Expanded Dataset:** To gain a more comprehensive understanding of how variations in ligands and metal centers influence mechanical properties, we should expand the dataset to include a wider variety of ZIF structures. This expansion would involve synthesizing new ZIF structures and conducting extensive molecular dynamics simulations.
2. **Refined Machine Learning Models:** Exploring advanced algorithms, such as deep learning and ensemble methods, could further refine our predictive models. Additionally, incorporating electronic properties and surface chemistry descriptors would provide a holistic view of the factors influencing mechanical behavior.
3. **Experimental Validation:** Collaborating with experimental researchers to synthesize selected ZIF structures and measure their mechanical properties is essential for validating the accuracy and reliability of our machine-learning models. Their feedback will help refine the models and enhance their predictive capabilities.
4. **Beyond Elastic Properties:** We should extend our predictive models to explore other physical properties of ZIFs, including thermal stability, adsorption capacity, and catalytic activity. By doing so, we can design ZIF tailored for specific applications in gas separation, catalysis, and electronics

REFERENCES

- A. Tiba, A., V. Tivanski, A., & R. MacGillivray, L. (2019). Size-Dependent Mechanical Properties of a Metal–Organic Framework: Increase in Flexibility of ZIF-8 by Crystal Downsizing. *Nano Letters*, *19*(9), 6140–6143. <https://doi.org/10.1021/acs.nanolett.9b02125>
- Acuna-Yeomans, E., Gutierrez-Sevillano, J. J., Calero, S., & Dubbeldam, D. (2023). Evaluation of ZIF-8 flexible force fields for structural and mechanical properties. *Microporous and Mesoporous Materials*, *348*. <https://doi.org/10.1016/j.micromeso.2022.112406>
- Bennett, T. D., Tan, J. C., Mosga Ch, S. A., Galvelis, R., Mellot-Draznieks, C., Reisner, B. A., Thirumurugan, A., Allan, D. R., & Cheetham, A. K. (2010). Mechanical properties of dense zeolitic imidazolate frameworks (ZIFs): A high-pressure X-ray diffraction, nanoindentation and computational study of the zinc framework Zn(Im)₂, and its Lithium-Boron Analogue, LiB(Im)₄. *Chemistry - A European Journal*, *16*(35), 10684–10690. <https://doi.org/10.1002/chem.201001415>
- Bennett, T. D., Tan, J. C., Yue, Y., Baxter, E., Ducati, C., Terrill, N. J., Yeung, H. H. M., Zhou, Z., Chen, W., Henke, S., Cheetham, A. K., & Greaves, G. N. (2015). Hybrid glasses from strong and fragile metal-organic framework liquids. *Nature Communications*, *6*. <https://doi.org/10.1038/ncomms9079>
- Bennett, T. D., Yue, Y., Li, P., Qiao, A., Tao, H., Greaves, N. G., Richards, T., Lampronti, G. I., Redfern, S. A. T., Blanc, F., Farha, O. K., Hupp, J. T., Cheetham, A. K., & Keen, D. A. (2016). Melt-Quenched Glasses of Metal–Organic Frameworks. *Journal of the American Chemical Society*, *138*(10). <https://doi.org/10.1021/jacs.5b13220>
- Burtch, N. C., Heinen, J., Bennett, T. D., Dubbeldam, D., & Allendorf, M. D. (2018). Mechanical Properties in Metal–Organic Frameworks: Emerging Opportunities and Challenges for Device Functionality and Technological Applications. In *Advanced Materials* (Vol. 30, Issue 37). Wiley-VCH Verlag. <https://doi.org/10.1002/adma.201704124>
- Castel, N., & Coudert, F.-X. (n.d.). *Computation of Finite Temperature Mechanical Properties of ZIF Glasses by Molecular Dynamics*.
- Chen, C. X., Qiu, Q. F., Pan, M., Cao, C. C., Zhu, N. X., Wang, H. P., Jiang, J. J., Wei, Z. W., & Su, C. Y. (2018). Tunability of fluorescent metal-organic frameworks through dynamic spacer installation with multivariate fluorophores. *Chemical Communications*, *54*(97). <https://doi.org/10.1039/c8cc07441k>
- D. Evans, J., & Coudert, F.-X. (2017). Predicting the Mechanical Properties of Zeolite Frameworks by Machine Learning. *Chemistry of Materials*, *29*(18), 7833–7839. <https://doi.org/10.1021/acs.chemmater.7b02532>

- Ducamp, M., & Coudert, F. X. (2022). Prediction of Thermal Properties of Zeolites through Machine Learning. *Journal of Physical Chemistry C*, 126(3). <https://doi.org/10.1021/acs.jpcc.1c09737>
- Ethiraj, J., Palla, S., & Reinsch, H. (2020). Insights into high pressure gas adsorption properties of ZIF-67: Experimental and theoretical studies. *Microporous and Mesoporous Materials*, 294, 109867. <https://doi.org/10.1016/j.micromeso.2019.109867>
- Fan, Q., Yan, Z., Zhou, H., Yao, Y., Wang, Z., Gao, Y., Wang, Y., Lu, S., Liu, M., & Ji, W. (2023). Near-infrared multiphoton absorption and third harmonic generation with CsPbBr₃ quantum dots embedded in micro-particles of metal-organic frameworks. *Journal of Materials Chemistry C*, 11(17). <https://doi.org/10.1039/d3tc00306j>
- Fernandez, M., Woo, T. K., Wilmer, C. E., & Snurr, R. Q. (2013). Large-scale quantitative structure-property relationship (QSPR) analysis of methane storage in metal-organic frameworks. *Journal of Physical Chemistry C*, 117(15). <https://doi.org/10.1021/jp4006422>
- Furukawa, H., Cordova, K. E., O’Keeffe, M., & Yaghi, O. M. (2013). The chemistry and applications of metal-organic frameworks. In *Science* (Vol. 341, Issue 6149). <https://doi.org/10.1126/science.1230444>
- Gaillac, R., Chibani, S., & Coudert, F. X. (2020). Speeding up Discovery of Auxetic Zeolite Frameworks by Machine Learning. *Chemistry of Materials*, 32(6). <https://doi.org/10.1021/acs.chemmater.0c00434>
- Gao, H., Wei, W., Dong, L., Feng, G., Jiang, X., Wu, R., Lin, Z., & Li, W. (2017). Enhanced framework rigidity of a zeolitic metal-azolate via ligand substitution. *Crystals*, 7(4). <https://doi.org/10.3390/cryst7040099>
- Gascon, J., Corma, A., Kapteijn, F., & Llabrés I Xamena, F. X. (2014). Metal organic framework catalysis: Quo vadis? In *ACS Catalysis* (Vol. 4, Issue 2). <https://doi.org/10.1021/cs400959k>
- Gómez-Gualdrón, D. A., Colón, Y. J., Zhang, X., Wang, T. C., Chen, Y. S., Hupp, J. T., Yildirim, T., Farha, O. K., Zhang, J., & Snurr, R. Q. (2016). Evaluating topologically diverse metal-organic frameworks for cryo-adsorbed hydrogen storage. *Energy and Environmental Science*, 9(10), 3279–3289. <https://doi.org/10.1039/c6ee02104b>
- H. Baur, W., & X. Fischer, R. (2019). The Floppiness of It All: Bond Lengths Change with Atomic Displacement Parameters and the Flexibility of Various Coordination Tetrahedra in Zeolitic Frameworks. An Empirical Structural Study of Bond Lengths and Angles. *Chemistry of Materials*, 31(7), 2401–2420. <https://doi.org/10.1021/acs.chemmater.8b04919>
- Imawaka, K., Sugita, M., Takewaki, T., & Tanaka, S. (2019). Mechanochemical synthesis of bimetallic CoZn-ZIFs with sodalite structure. *Polyhedron*, 158. <https://doi.org/10.1016/j.poly.2018.11.018>
- Jablonka, K. M., Ongari, D., Moosavi, S. M., & Smit, B. (2020). Big-Data Science in Porous Materials: Materials Genomics and Machine Learning. In *Chemical Reviews* (Vol. 120, Issue 16). <https://doi.org/10.1021/acs.chemrev.0c00004>

- Ke, Q., Duan, Y., Ji, Y., Zhao, D., Zhang, H., Duan, C., Li, L., & Wei, Y. (2021). Identical Composition and Distinct Performance: How ZIF-8 Polymorphs' Structures Affect the Adsorption/Separation of Ethane and Ethene. *Journal of Chemical & Engineering Data*, 66(9), 3483–3492. <https://doi.org/10.1021/acs.jced.1c00322>
- Kosicka, E., Krzyzak, A., Dorobek, M., & Borowiec, M. (2022). Prediction of Selected Mechanical Properties of Polymer Composites with Alumina Modifiers. *Materials*, 15(3). <https://doi.org/10.3390/ma15030882>
- Krokidas, P., Kainourgiakis, M., Steriotis, T., & Giannakopoulos, G. (n.d.). *Inverse Design of ZIFs through Artificial Intelligence Methods*.
- Li, H., Chen, W., Liu, B., Yang, M., Huang, Z., Sun, C., Deng, C., Cao, D., & Chen, G. (2023). A purely green approach to low-cost mass production of zeolitic imidazolate frameworks. *Green Energy and Environment*, 8(3). <https://doi.org/10.1016/j.gee.2021.09.003>
- Li, M., Duan, Y., Wei, J., Lin, H., Feng, Q., Tuo, Y., Chen, Z., Lv, J., Li, M., & Wu, Q. (2022). One-step synthesis of ZIF-8 and anchoring it on SCB for rapid and high-capacity capture of mercury from aqueous solution. *Journal of Environmental Chemical Engineering*, 10(6). <https://doi.org/10.1016/j.jece.2022.108852>
- Liu, B., Vellingiri, K., Jo, S. H., Kumar, P., Ok, Y. S., & Kim, K. H. (2018). Recent advances in controlled modification of the size and morphology of metal-organic frameworks. In *Nano Research* (Vol. 11, Issue 9). <https://doi.org/10.1007/s12274-018-2039-3>
- Lyu, H., Ji, Z., Wuttke, S., & Yaghi, O. M. (2020). Digital Reticular Chemistry. In *Chem* (Vol. 6, Issue 9). <https://doi.org/10.1016/j.chempr.2020.08.008>
- Miller, S. R., Heurtaux, D., Baati, T., Horcajada, P., Grenèche, J. M., & Serre, C. (2010). Biodegradable therapeutic MOFs for the delivery of bioactive molecules. *Chemical Communications*, 46(25). <https://doi.org/10.1039/c001181a>
- Moosavi, S. M., G. Boyd, P., Sarkisov, L., & Smit, B. (2018). Improving the Mechanical Stability of Metal–Organic Frameworks Using Chemical Caryatids. *ACS Central Science*, 4(7), 832–839. <https://doi.org/10.1021/acscentsci.8b00157>
- Möslein, A. F., Donà, L., Civalleri, B., & Tan, J.-C. (n.d.). *Defects in ZIF-8 crystallization and their impact on mechanical properties*.
- Ortiz, A. U., Boutin, A., Fuchs, A. H., & Coudert, F. X. (2013). Investigating the pressure-induced amorphization of zeolitic imidazolate framework ZIF-8: Mechanical instability due to shear mode softening. *Journal of Physical Chemistry Letters*, 4(11), 1861–1865. <https://doi.org/10.1021/jz400880p>
- Pathan, M. V., Ponnusami, S. A., Pathan, J., Pitongsawat, R., Erice, B., Petrinic, N., & Tagarielli, V. L. (2019). Predictions of the mechanical properties of unidirectional fibre composites by supervised machine learning. *Scientific Reports*, 9(1). <https://doi.org/10.1038/s41598-019-50144-w>

- Pérez-Miana, M., Reséndiz-Ordóñez, J. U., & Coronas, J. (2021). Solventless synthesis of ZIF-L and ZIF-8 with hydraulic press and high temperature. *Microporous and Mesoporous Materials*, 328. <https://doi.org/10.1016/j.micromeso.2021.111487>
- Qi, Z., Zhang, N., Liu, Y., & Chen, W. (2019). Prediction of mechanical properties of carbon fiber based on cross-scale FEM and machine learning. *Composite Structures*, 212. <https://doi.org/10.1016/j.compstruct.2019.01.042>
- Redfern, L. R., & Farha, O. K. (2019). Mechanical properties of metal-organic frameworks. In *Chemical Science* (Vol. 10, Issue 46, pp. 10666–10679). Royal Society of Chemistry. <https://doi.org/10.1039/c9sc04249k>
- Ryder, M. R., Civalleri, B., & Tan, J. C. (2016). Isoreticular zirconium-based metal-organic frameworks: Discovering mechanical trends and elastic anomalies controlling chemical structure stability. *Physical Chemistry Chemical Physics*, 18(13). <https://doi.org/10.1039/c6cp00864j>
- Ryder, M. R., & Tan, J. C. (2016a). Explaining the mechanical mechanisms of zeolitic metal-organic frameworks: Revealing auxeticity and anomalous elasticity. *Dalton Transactions*, 45(10), 4154–4161. <https://doi.org/10.1039/c5dt03514g>
- Ryder, M. R., & Tan, J. C. (2016b). Explaining the mechanical mechanisms of zeolitic metal-organic frameworks: Revealing auxeticity and anomalous elasticity. *Dalton Transactions*, 45(10), 4154–4161. <https://doi.org/10.1039/c5dt03514g>
- Ryder, M., & Tan, J.-C. (2015). Explaining the Mechanical Mechanisms of Zeolitic Metal-Organic Frameworks: Revealing Auxeticity and Anomalous Elasticity. *Dalton Trans.*, 45. <https://doi.org/10.1039/C5DT03514G>
- Shaht, M., & El Dhaba, A. R. (2019). On the equivalent shear modulus of composite metamaterials. *Composites Part B: Engineering*, 172. <https://doi.org/10.1016/j.compositesb.2019.05.056>
- Shi, Z., Hartati, S., Arramel, A., & Li, N. (2023). Unraveling the bond structure, porosity, and mechanical properties amorphous ZIF-4 and its topological equivalents: Large scale ab initio calculations. *APL Materials*, 11(2). <https://doi.org/10.1063/5.0139208>
- Song, L., Wang, D., Liu, X., Yin, A., & Long, Z. (2023). Prediction of mechanical properties of composite materials using multimodal fusion learning. *Sensors and Actuators A: Physical*, 358, 114433. <https://doi.org/10.1016/J.SNA.2023.114433>
- Su, Z., Miao, Y. R., Mao, S. M., Zhang, G. H., Dillon, S., Miller, J. T., & Suslick, K. S. (2015). Compression-induced deformation of individual metal-organic framework microcrystals. *Journal of the American Chemical Society*, 137(5). <https://doi.org/10.1021/ja5113436>
- Tan, J. C., Bennett, T. D., & Cheetham, A. K. (2010). *Chemical structure, network topology, and porosity effects on the mechanical properties of Zeolitic Imidazolate Frameworks*. 107(22).

<https://doi.org/10.1073/pnas.1003205107/-/DCSupplemental>

- Tan, J. C., & Cheetham, A. K. (2011). Mechanical properties of hybrid inorganic–organic framework materials: Establishing fundamental structure–property relationships. *Chemical Society Reviews*, *40*(2). <https://doi.org/10.1039/c0cs00163e>
- Tan, J. C., Civalleri, B., Erba, A., & Albanese, E. (2015). Quantum mechanical predictions to elucidate the anisotropic elastic properties of zeolitic imidazolate frameworks: ZIF-4 vs. ZIF-zni. *CrystEngComm*, *17*(2).
<https://doi.org/10.1039/c4ce01564a>
- Tan, J. C., Civalleri, B., Lin, C. C., Valenzano, L., Galvelis, R., Chen, P. F., Bennett, T. D., Mellot-Draznieks, C., Zicovich-Wilson, C. M., & Cheetham, A. K. (2012). Exceptionally low shear modulus in a prototypical imidazole-based metal-organic framework. *Physical Review Letters*, *108*(9).
<https://doi.org/10.1103/PhysRevLett.108.095502>
- Tian, T., Velazquez-Garcia, J., Bennett, T. D., & Fairen-Jimenez, D. (2015). Mechanically and chemically robust ZIF-8 monoliths with high volumetric adsorption capacity. *Journal of Materials Chemistry A*, *3*(6), 2999–3005.
<https://doi.org/10.1039/c4ta05116e>
- Tian, Y. Q., Zhao, Y. M., Chen, Z. X., Zhang, G. N., Weng, L. H., & Zhao, D. Y. (2007). Design and generation of extended zeolitic metal-organic frameworks (ZMOFs): Synthesis and crystal structures of zinc(II) imidazolate polymers with zeolitic topologies. *Chemistry - A European Journal*, *13*(15).
<https://doi.org/10.1002/chem.200700181>
- Verpoort, P. C., MacDonald, P., & Conduit, G. J. (2018). Materials data validation and imputation with an artificial neural network. *Computational Materials Science*, *147*, 176–185. <https://doi.org/10.1016/j.commatsci.2018.02.002>
- Wang, H., Xia, J., Pan, L., Ngoc Ha, M., Yang, Y., & Wang, X. (2020). Lithium-ion storage behavior of ZIFs polyhedral carbons with topological structure. *Chemical Engineering Science*, *221*. <https://doi.org/10.1016/j.ces.2020.115708>
- Wang, W., & Yuan, D. (2014). Mesoporous carbon originated from non-permanent porous MOFs for gas storage and CO₂/CH₄ separation. *Scientific Reports*, *4*. <https://doi.org/10.1038/srep05711>
- Widmer, R. N., Lampronti, G. I., Chibani, S., Wilson, C. W., Anzellini, S., Farsang, S., Kleppe, A. K., Casati, N. P. M., Macleod, S. G., Redfern, S. A. T., Coudert, F. X., & Bennett, T. D. (2019). Rich Polymorphism of a Metal-Organic Framework in Pressure-Temperature Space. *Journal of the American Chemical Society*, *141*(23). <https://doi.org/10.1021/jacs.9b03234>
- Wragg, D. S., Morris, R. E., & Burton, A. W. (2008). Pure silica zeolite-type frameworks: A structural analysis. *Chemistry of Materials*, *20*(4).

<https://doi.org/10.1021/cm071824j>

Wu, H., Zhou, W., & Yildirim, T. (2007). Hydrogen storage in a prototypical zeolitic imidazolate framework-8. *Journal of the American Chemical Society*, 129(17). <https://doi.org/10.1021/ja0691932>

Yeganeh-Haeri, A., Weidner, D. J., & Parise, J. B. (1992). Elasticity of α -cristobalite: A silicon dioxide with a negative poisson's ratio. *Science*, 257(5070). <https://doi.org/10.1126/science.257.5070.650>

Yin, X., Li, Z., Wang, S., Chu, N., Yang, J., & Wang, J. (2015). Hydrothermal synthesis of hierarchical zeolite T aggregates using tetramethylammonium hydroxide as single template. *Microporous and Mesoporous Materials*, 201(C).

<https://doi.org/10.1016/j.micromeso.2014.09.018>

Yu, Z., Ye, S., Sun, Y., Zhao, H., & Feng, X. Q. (2021). Deep learning method for predicting the mechanical properties of aluminum alloys with small data sets. *Materials Today Communications*, 28.

<https://doi.org/10.1016/j.mtcomm.2021.102570>

Zhang, Z., Zhao, Y., Gong, Q., Lib, Z., & Li, J. (2013). MOFs for CO₂ capture and separation from flue gas mixtures: The effect of multifunctional sites on their adsorption capacity and selectivity. *Chemical Communications*, 49(7). <https://doi.org/10.1039/c2cc35561b>

Zheng, B., Sant, M., Demontis, P., & B. Suffritti, G. (2012). Force Field for Molecular Dynamics Computations in Flexible ZIF-8 Framework. *The Journal of Physical Chemistry C*, 116(1), 933–938. <https://doi.org/10.1039/C5DT03514G>

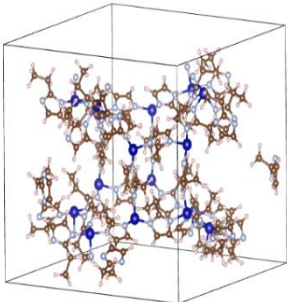
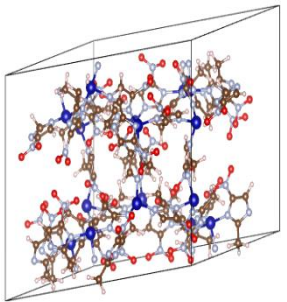
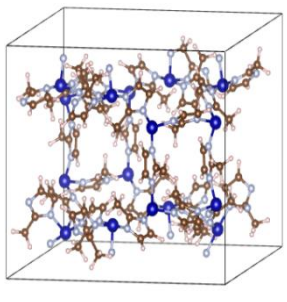
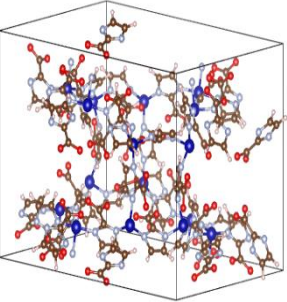
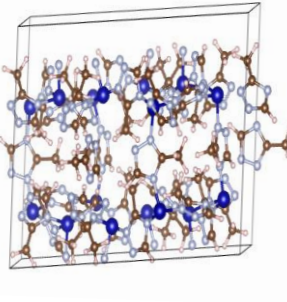
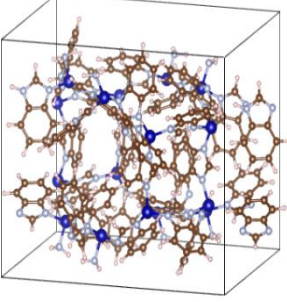
Zheng, B., Zhu, Y., Fu, F., Wang, L. L., Wang, J., & Du, H. (2017). Theoretical prediction of the mechanical properties of zeolitic imidazolate frameworks (ZIFs). *RSC Advances*, 7(66), 41499–41503. <https://doi.org/10.1039/c7ra07242b>

APPENDICES

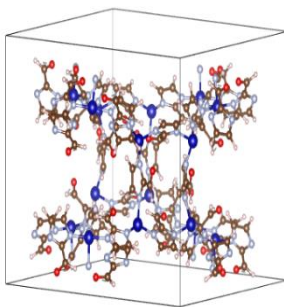
APPENDIX A
SEVEN LIGANDS, THREE TOPOLOGY AND THREE METALS
WITH THEIR COMPOSITION

Table A1 CAG topology with 7 ligands and 3 metals with their composition

CAG topology with 7 ligands and Co metal

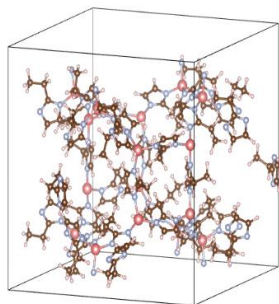
2-ethylimidazole_cag_Co	2-methyl-4-nitroimidazole_cag_Co
	
2-methylimidazole_cag_Co	2-nitroimidazole_cag_Co
	
3-Methyl-1,2,4-triazole_cag_Co	Benzimidazole_cag_Co
	

Imidazole-2-carbaldehyde_cag_Co

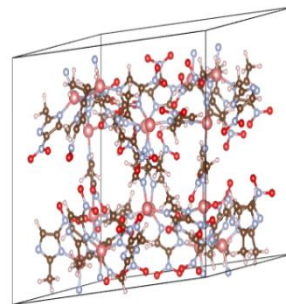


CAG topology with 7 ligands and Cu metal

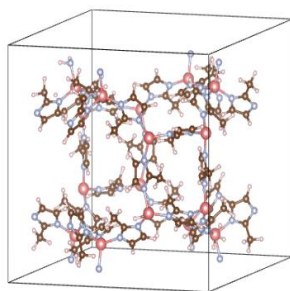
2-ethylimidazole_cag_Cu



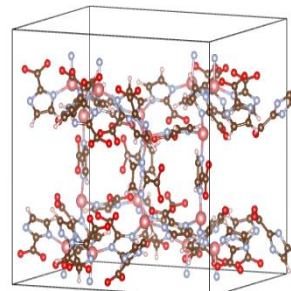
2-methyl-4-nitroimidazole_cag_Cu



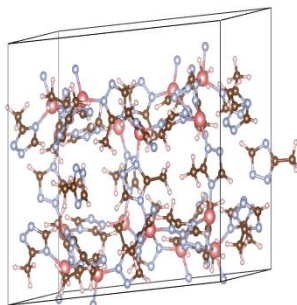
2-methylimidazole_cag_Cu



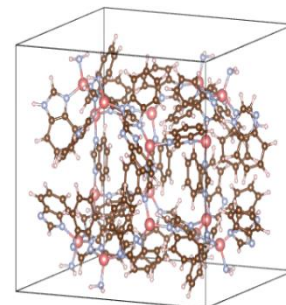
2-nitroimidazole_cag_Cu



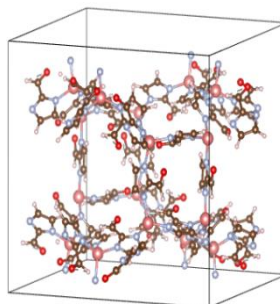
3-Methyl-1,2,4-triazole_cag_Cu



Benzimidazole_cag_Cu

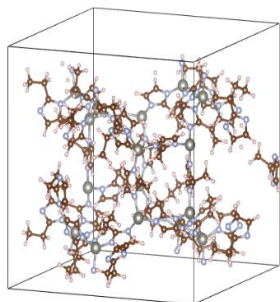


Imidazole-2-carbaldehyde_cag_Cu

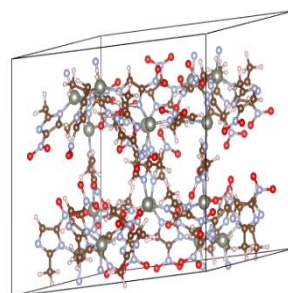


CAG topology with 7 ligands and Zn metal

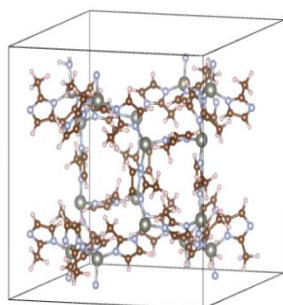
2-ethylimidazole_cag_Zn



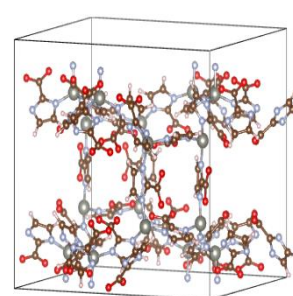
2-methyl-4-nitroimidazole_cag_Zn



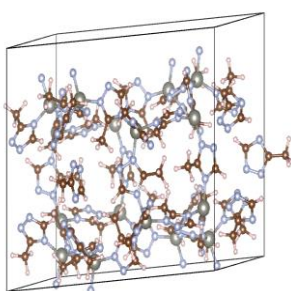
2-methylimidazole_cag_Zn



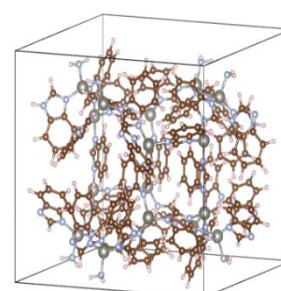
2-nitroimidazole_cag_Zn



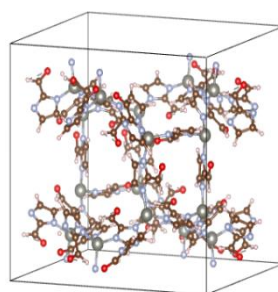
3-Methyl-1,2,4-triazole_cag_Zn



Benzimidazole_cag_Zn

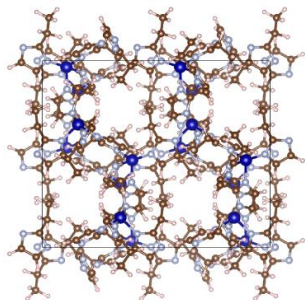


Imidazole-2-carbaldehyde_cag_Zn

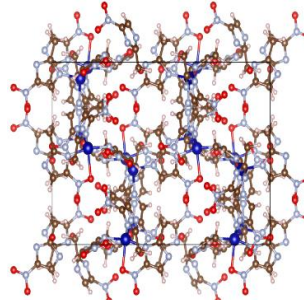


CAG topology with 7 ligands and CoZn metal

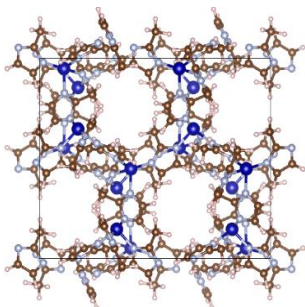
2-ethylimidazole_cag_CoZn



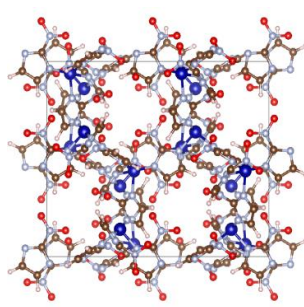
2-methyl-4-nitroimidazole_cag_CoZn



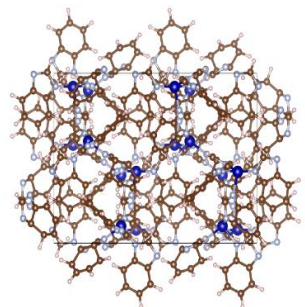
2-methylimidazole_cag_CoZn



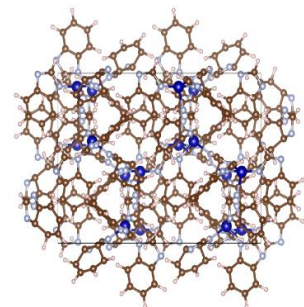
2-nitroimidazole_cag_CoZn



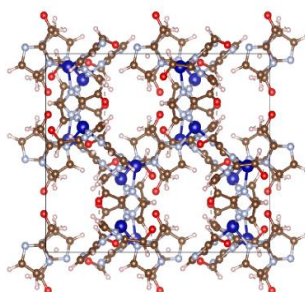
3-Methyl-1,2,4-triazole_cag_CoZn



Benzimidazole_cag_CoZn

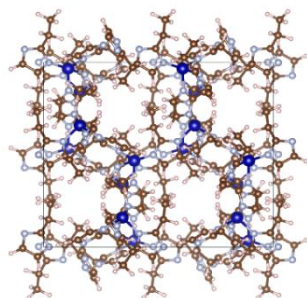


Imidazole-2-carbaldehyde_cag_CoZn

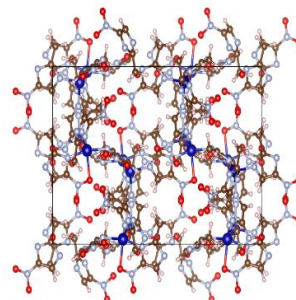


CAG topology with 7 ligands and CuCo metal

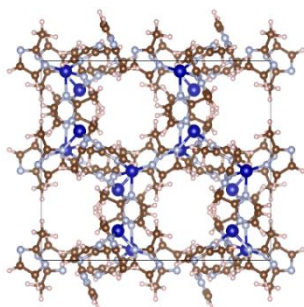
2-ethylimidazole_cag_CuCo



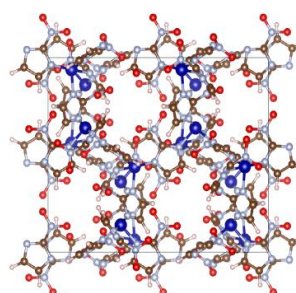
2-methyl-4-nitroimidazole_cag_CuCo



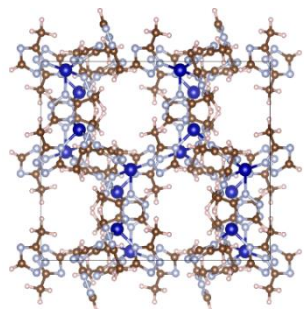
2-methylimidazole_cag_CuCo



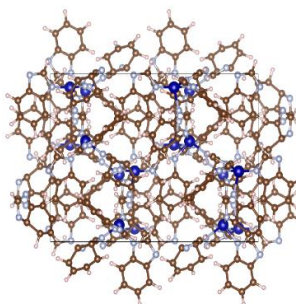
2-nitroimidazole_cag_CuCo



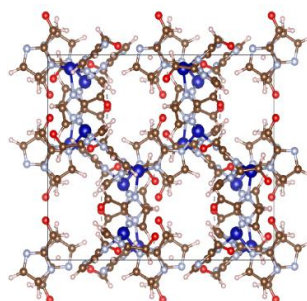
3-Methyl-1,2,4-triazole_cag_CuCo



Benzimidazole_cag_CuCo

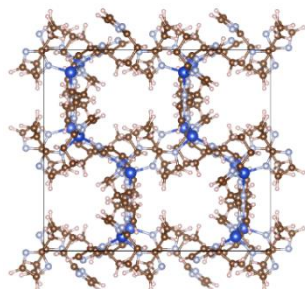


Imidazole-2-carbaldehyde_cag_CuCo

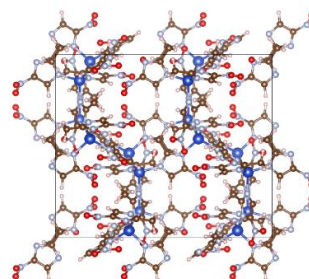


CAG topology with 7 ligands and ZnCu metal

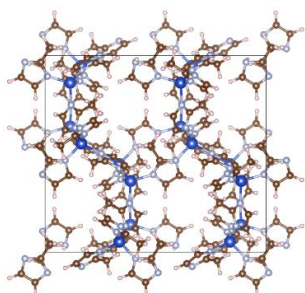
2-ethylimidazole_cag_ZnCu



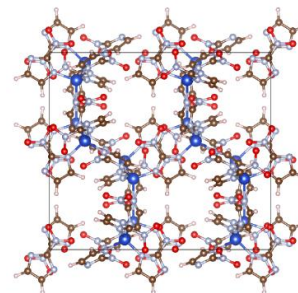
2-methyl-4-nitroimidazole_cag_ZnCu



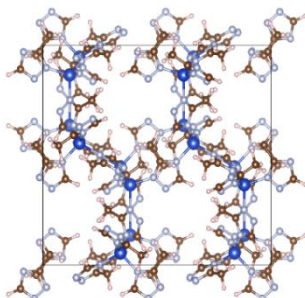
2-methylimidazole_cag_ZnCu



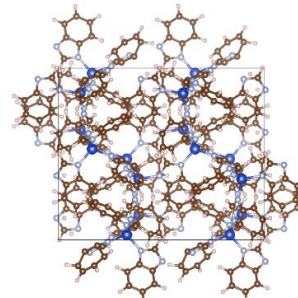
2-nitroimidazole_cag_ZnCu



3-Methyl-1,2,4-triazole_cag_ZnCu



Benzimidazole_cag_ZnCu



Imidazole-2-carbaldehyde_cag_ZnCu

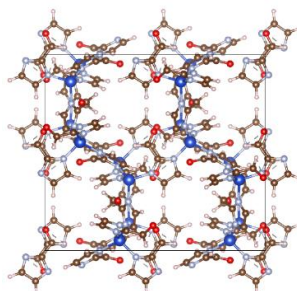
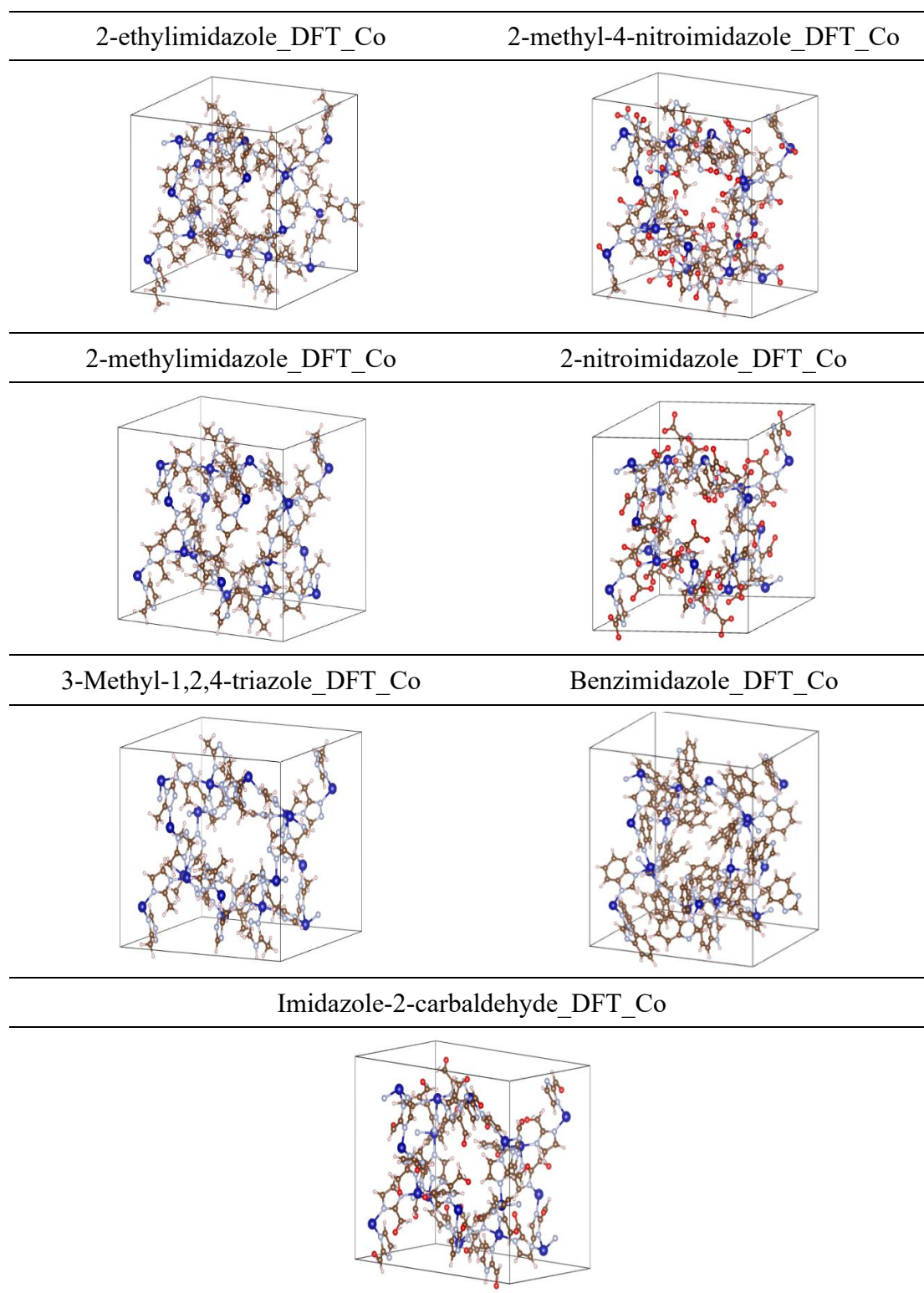


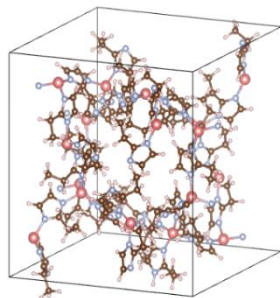
Table A2 DFT topology with 7 ligands and 3 metals with their composition

DFT topology with 7 ligands and Co metal

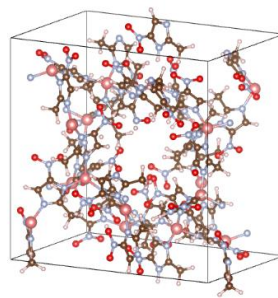


DFT topology with 7 ligands and Cu metal

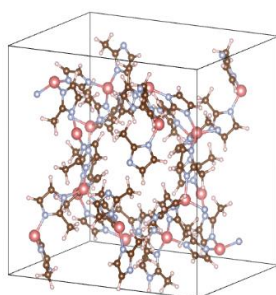
2-ethylimidazole_DFT_Cu



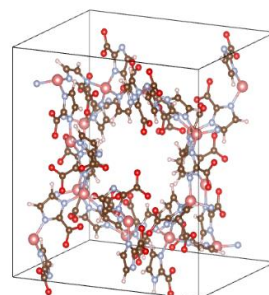
2-methyl-4-nitroimidazole_DFT_Cu



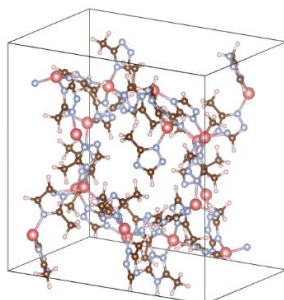
2-methylimidazole_DFT_Cu



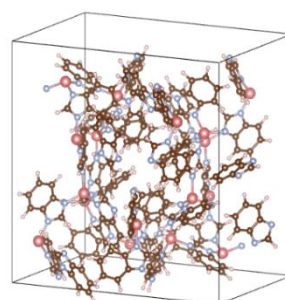
2-nitroimidazole_DFT_Cu



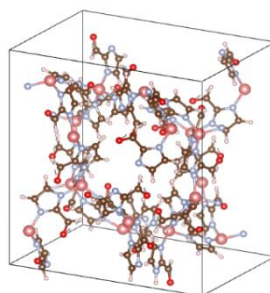
3-Methyl-1,2,4-triazole_DFT_Cu



Benzimidazole_DFT_Cu

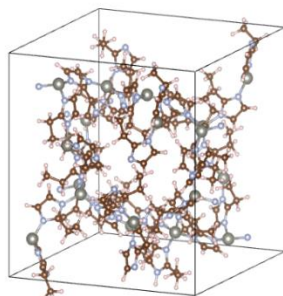


Imidazole-2-carbaldehyde_DFT_Cu

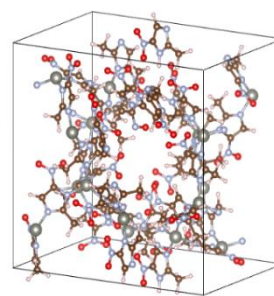


DFT topology with 7 ligands and Zn metal

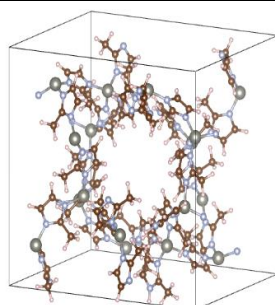
2-ethylimidazole_DFT_Zn



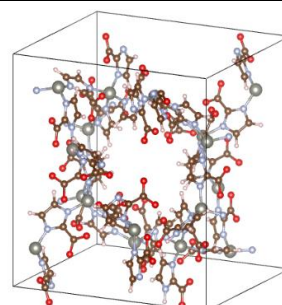
2-methyl-4-nitroimidazole_DFT_Zn



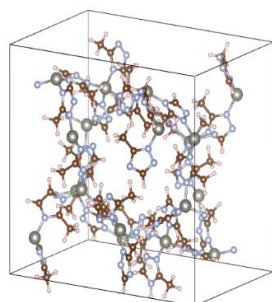
2-methylimidazole_DFT_Zn



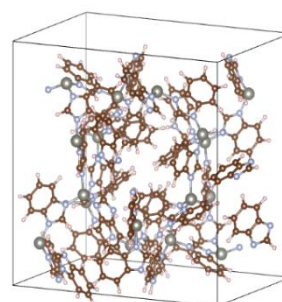
2-nitroimidazole_DFT_Zn



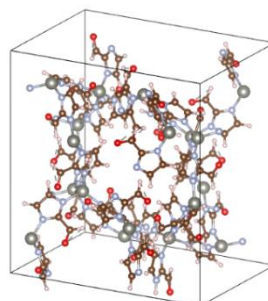
3-Methyl-1,2,4-triazole_DFT_Zn



Benzimidazole_DFT_Zn

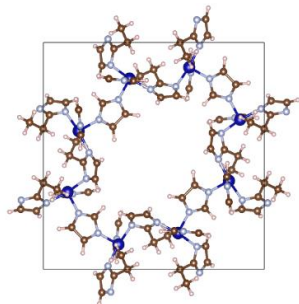


Imidazole-2-carbaldehyde_DFT_Zn

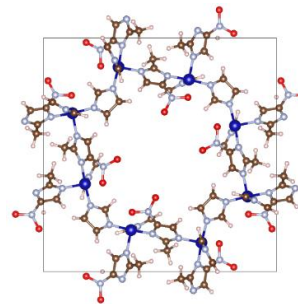


DFT topology with 7 ligands and CoZn metal

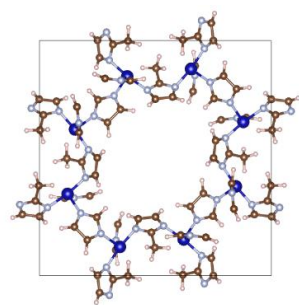
2-ethylimidazole_DFT_CoZn



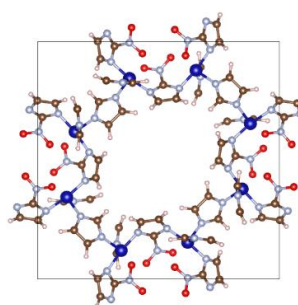
2-methyl-4-nitroimidazole_DFT_CoZn



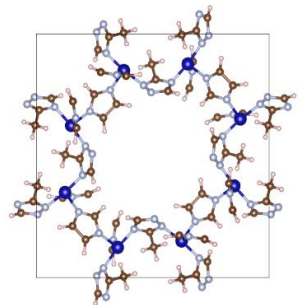
2-methylimidazole_DFT_CoZn



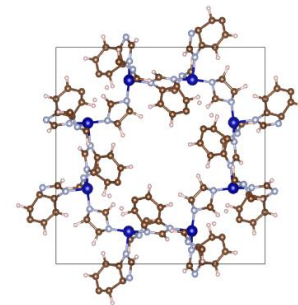
2-nitroimidazole_DFT_CoZn



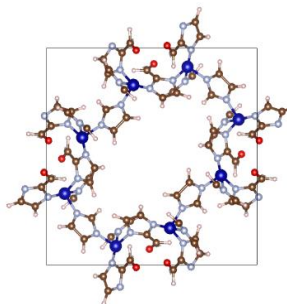
3-Methyl-1,2,4-triazole_DFT_CoZn



Benzimidazole_DFT_CoZn

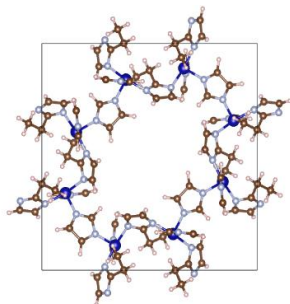


Imidazole-2-carbaldehyde_DFT_CoZn

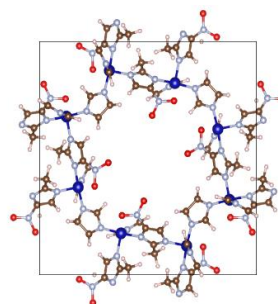


DFT topology with 7 ligands and CuCo metal

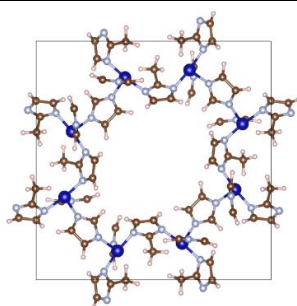
2-ethylimidazole_DFT_CuCo



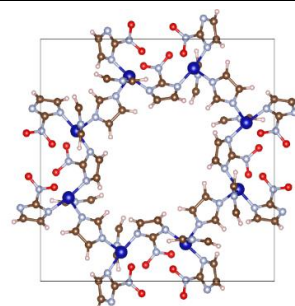
2-methyl-4-nitroimidazole_DFT_CuCo



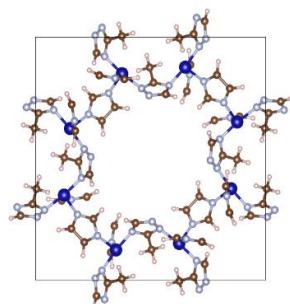
2-methylimidazole_DFT_CuCo



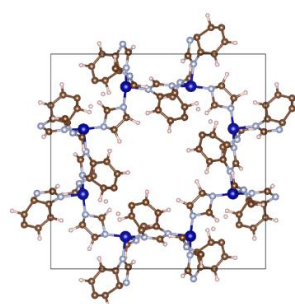
2-nitroimidazole_DFT_CuCo



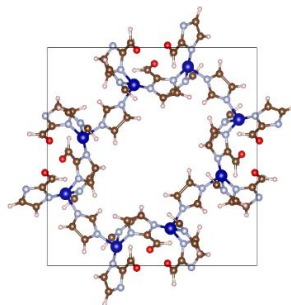
3-Methyl-1,2,4-triazole_DFT_CuCo



Benzimidazole_DFT_CuCo

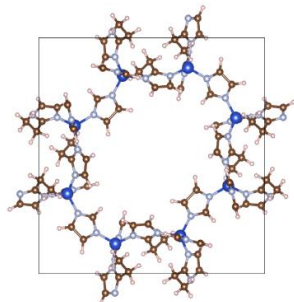


Imidazole-2-carbaldehyde_DFT_CuCo

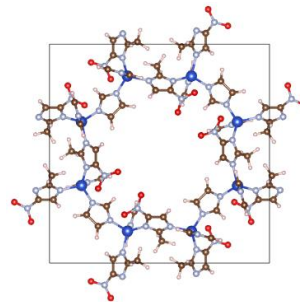


DFT topology with 7 ligands and ZnCu metal

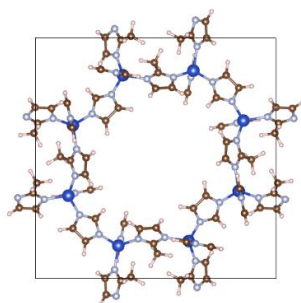
2-ethylimidazole_DFT_ZnCu



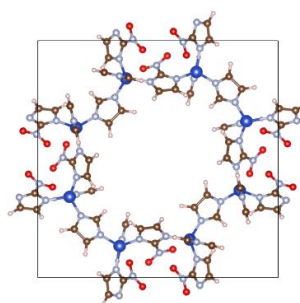
2-methyl-4-nitroimidazole_DFT_ZnCu



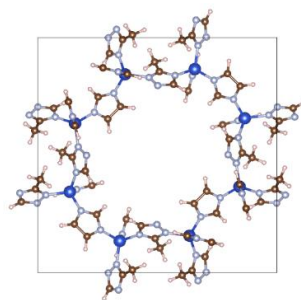
2-methylimidazole_DFT_ZnCu



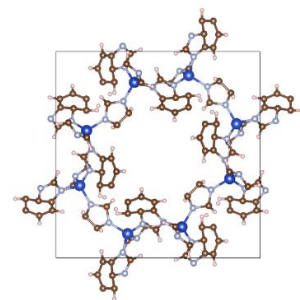
2-nitroimidazole_DFT_ZnCu



3-Methyl-1,2,4-triazole_DFT_ZnCu



Benzimidazole_DFT_ZnCu



Imidazole-2-carbaldehyde_DFT_ZnCu

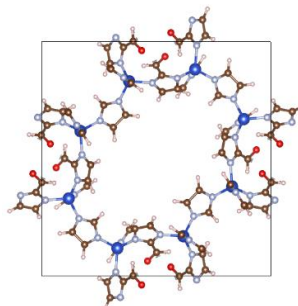
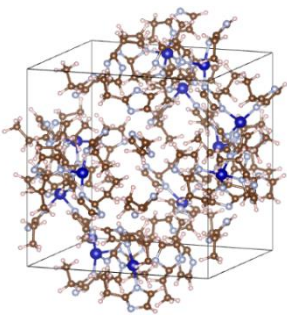
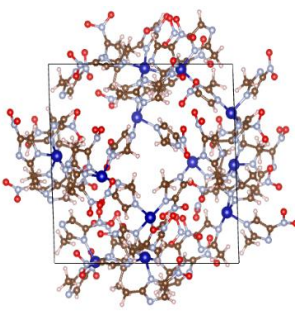
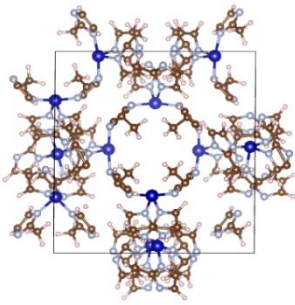
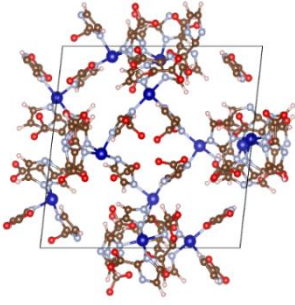
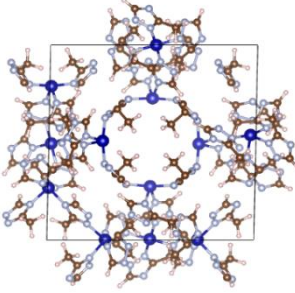
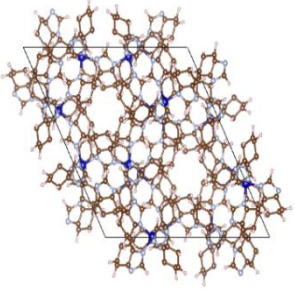
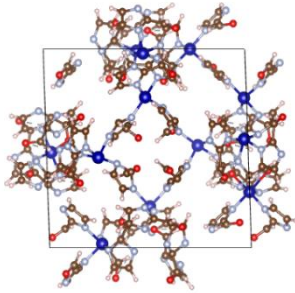


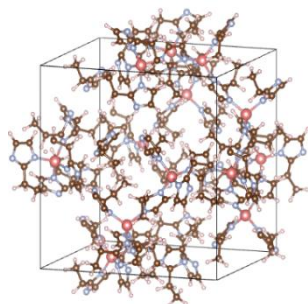
Table A3 SOD topology with 7 ligands and 3 metals with their composition

SOD topology with 7 ligands and Co metal

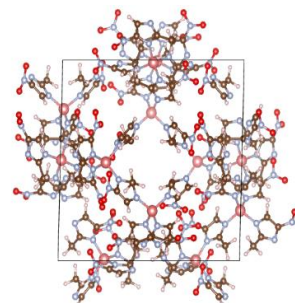
2-ethylimidazole_SOD_Co	2-methyl-4-nitroimidazole_SOD_Co
	
2-methylimidazole_SOD_Co	2-nitroimidazole_SOD_Co
	
3-Methyl-1,2,4-triazole_SOD_Co	Benzimidazole_SOD_Co
	
Imidazole-2-carbaldehyde_SOD_Co	
	

SOD topology with 7 ligands and Cu metal

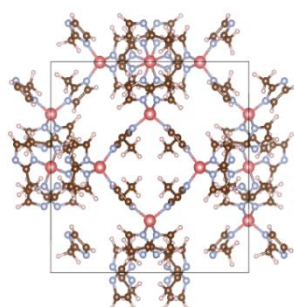
2-ethylimidazole_SOD_Cu



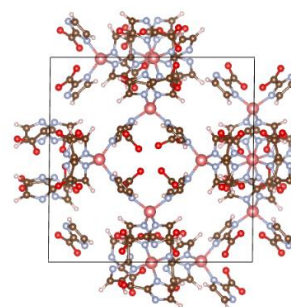
2-methyl-4-nitroimidazole_SOD_Cu



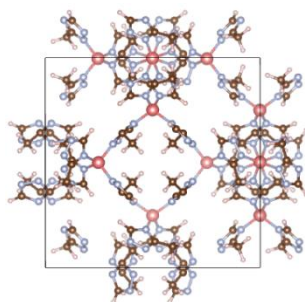
2-methylimidazole_SOD_Cu



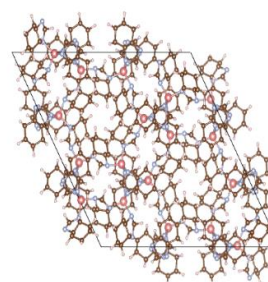
2-nitroimidazole_SOD_Cu



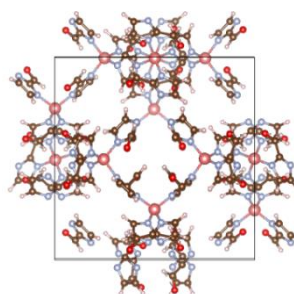
3-Methyl-1,2,4-triazole_SOD_Cu



Benzimidazole_SOD_Cu

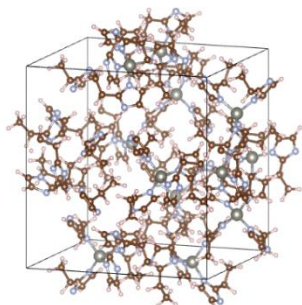


Imidazole-2-carbaldehyde_SOD_Cu

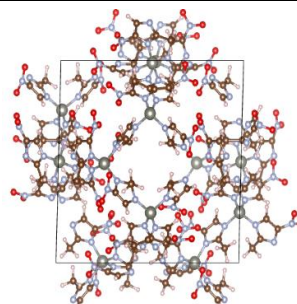


SOD topology with 7 ligands and Zn metal

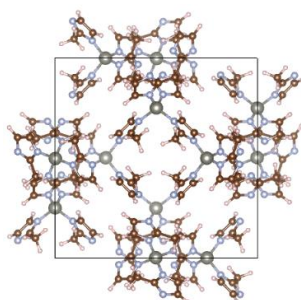
2-ethylimidazole_SOD_Zn



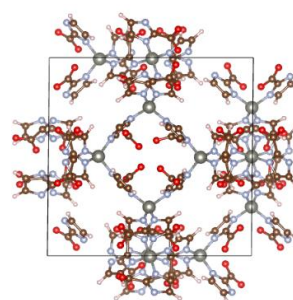
2-methyl-4-nitroimidazole_SOD_Zn



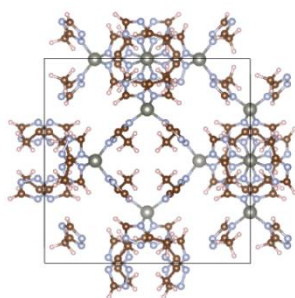
2-methylimidazole_SOD_Zn



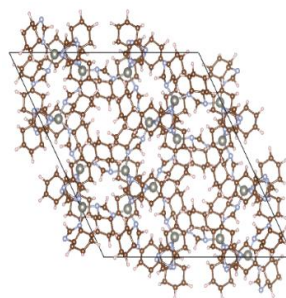
2-nitroimidazole_SOD_Zn



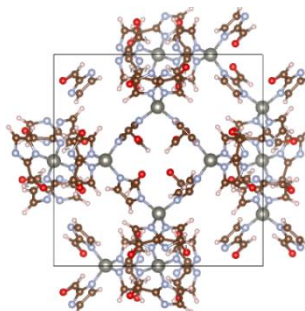
3-Methyl-1,2,4-triazole_SOD_Zn



Benzimidazole_SOD_Zn

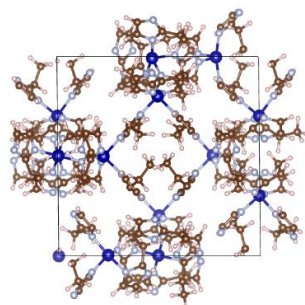


Imidazole-2-carbaldehyde_SOD_Zn

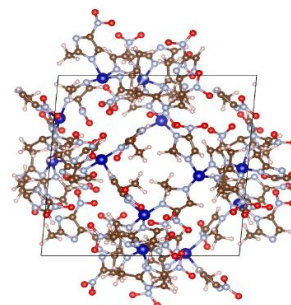


SOD topology with 7 ligands and CoZn metal

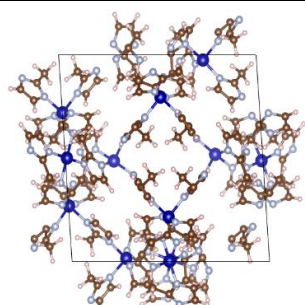
2-ethylimidazole_SOD_CoZn



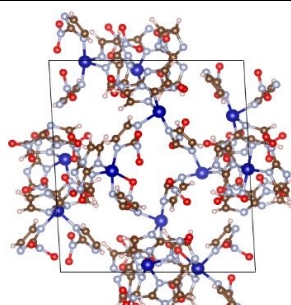
2-methyl-4-nitroimidazole_SOD_CoZn



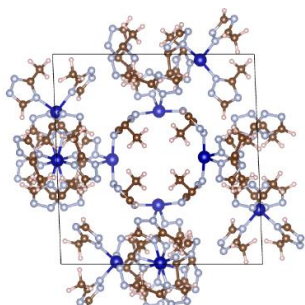
2-methylimidazole_SOD_CoZn



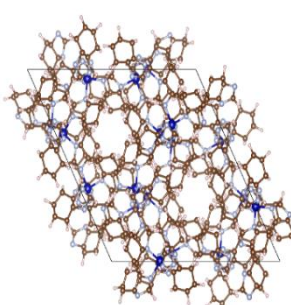
2-nitroimidazole_SOD_CoZn



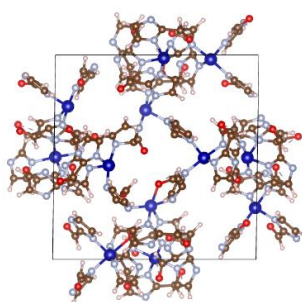
3-Methyl-1,2,4-triazole_SOD_CoZn



Benzimidazole_SOD_CoZn

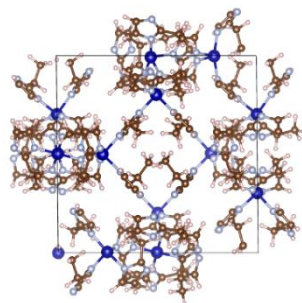


Imidazole-2-carbaldehyde_SOD_CoZn

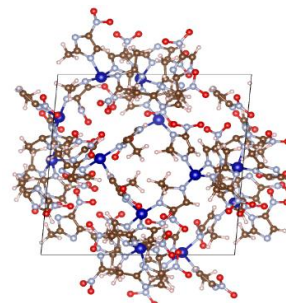


SOD topology with 7 ligands and CuCo metal

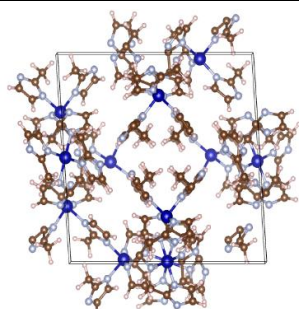
2-ethylimidazole_SOD_CuCo



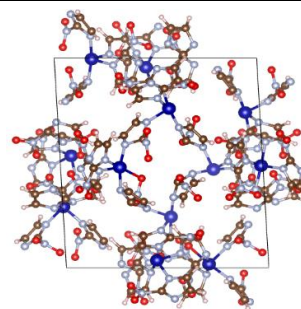
2-methyl-4-nitroimidazole_SOD_CuCo



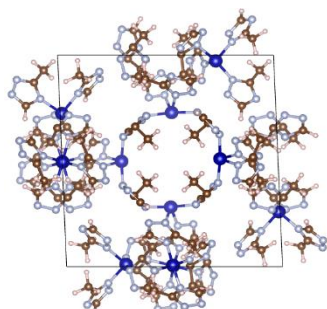
2-methylimidazole_SOD_CuCo



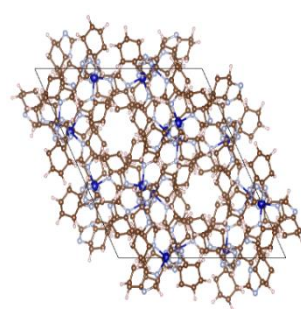
2-nitroimidazole_SOD_CuCo



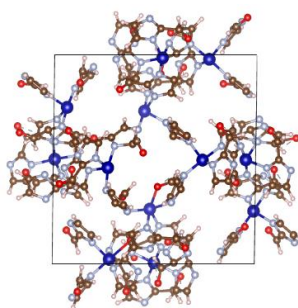
3-Methyl-1,2,4-triazole_SOD_CuCo



Benzimidazole_SOD_CuCo

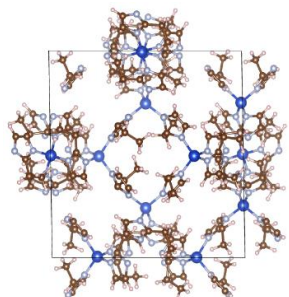


Imidazole-2-carbaldehyde_SOD_CuCo

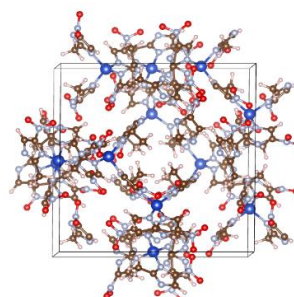


SOD topology with 7 ligands and ZnCu metal

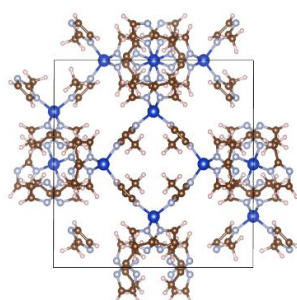
2-ethylimidazole_SOD_ZnCu



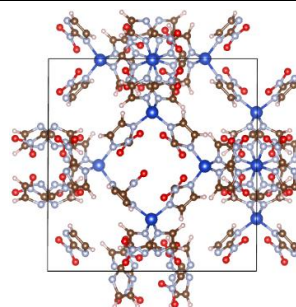
2-methyl-4-nitroimidazole_SOD_ZnCu



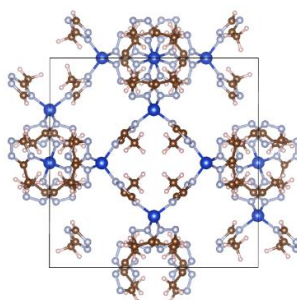
2-methylimidazole_SOD_ZnCu



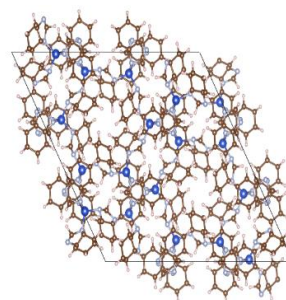
2-nitroimidazole_SOD_ZnCu



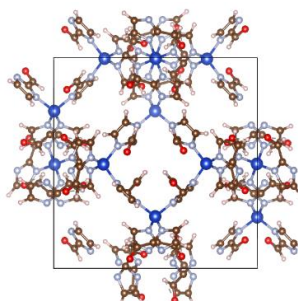
3-Methyl-1,2,4-triazole_SOD_ZnCu



Benzimidazole_SOD_ZnCu



Imidazole-2-carbaldehyde_SOD_ZnCu



APPENDIX B
GITHUB LINK FOR THE MACHINE MODEL

<https://github.com/sarmin-khan/ZIF-Mechanical-Properties>